

Optogenetic approaches  
for determining the  
temporal role of  
morphogen inputs on  
target gene expression

Thesis by  
James Mitchell McGehee

In Partial Fulfillment of the Requirements for  
the degree of  
Doctor of Philosophy

CALIFORNIA INSTITUTE OF TECHNOLOGY  
Pasadena, California

2023  
(Defended 1 May 2023)

© 2023

James Mitchell McGehee  
ORCID: 0000-0002-9353-1235

All rights reserved

## ACKNOWLEDGEMENTS

I would like to thank my advisor and mentor, Angela Stathopoulos, for giving me the opportunity to explore transcription factor dynamics and guiding me throughout my PhD. I would also like to thank my committee, Marianne Bronner, Lea Goentoro, Kai Zinn, and Justin Bois for their advice and feedback during my PhD. I would like to thank Jihyun Irizarry for helping train me and working together on many projects. Without her contributions this work would have taken much longer. In addition, I'd like to thank our collaborators David Stein, who provided valuable insight in to starting these projects, and Mounia Lagha and Virginia Pimmett for their helpful discussions, expertise in quantification, and complementary assays. Finally, I'd like to thank Leslie Dunipace for technical support, and all past and present members of the Stathopoulos lab for helpful discussions and feedback.

## ABSTRACT

The Dorsal transcription factor and morphogen is important for patterning the Dorsal-Ventral axis of *Drosophila melanogaster* and while it has been extensively studied, the temporal dynamics of Dorsal are not well understood. There are many processes that contribute to Dorsal nuclear concentration levels, including Toll signaling and Cactus degradation, interactions with other proteins, shuttling of Dorsal to the ventral side, DNA binding, and nuclear spacing. Dorsal nuclear levels are known to activate or repress target gene expression in a concentration or threshold dependent manner. To test how Dorsal dynamics and changes to the Dorsal gradient over time affect target gene expression, we added two optogenetic tags to Dorsal at the endogenous locus to control Dorsal nuclear levels: Blue Light Inducible Degradation (BLID) and Light Inducible Nuclear Export System (LEXY). We found that upon degradation of Dorsal using blue light and BLID that a downstream ratchet was able to maintain the expression of high threshold target genes. Using blue light and LEXY to export Dorsal, we identified an important window where Dorsal activity is required to allow activation of high threshold target genes at later stages. In comparing BLID and LEXY in conjunction with mutations to a nuclear export sequence, we also identified how rapid nuclear import and export of Dorsal is sufficient for low threshold target gene expression but actively disrupts high threshold target gene expression. We conclude that not only are final concentration levels, but also the dynamics leading to those levels are important for proper gene expression.

## PUBLISHED CONTENT AND CONTRIBUTIONS

Stevens LM, Kim G, Koromila T, Steele JW, McGehee J, Stathopoulos A, Stein DS. Light-dependent N-end rule-mediated disruption of protein function in *Saccharomyces cerevisiae* and *Drosophila melanogaster*. *PLoS Genet*. 2021 May 17;17(5):e1009544. doi: 10.1371/journal.pgen.1009544.

J.M. assisted in fly crosses, stained embryos, assisted with live imaging, data validation and processing, and provided comments and edits to the manuscript.

Irizarry J, McGehee J, Kim G, Stein D, Stathopoulos A. Twist-dependent ratchet functioning downstream from Dorsal revealed using a light-inducible degen. *Genes Dev*. 2020 Jul 1;34(13-14):965-972. doi: 10.1101/gad.338194.120. Epub 2020 May 28.

J.M. participated in the conception of the project, generated the mutant lines, tested the lines by antibody staining and in situ, analyzed the data, and participated in writing the manuscript.

## TABLE OF CONTENTS

Acknowledgements .....	iii
Abstract.....	iv
Published Content and Contributions .....	v
Table of Contents .....	vi
List of Illustrations and/or Tables .....	viii
Abbreviations .....	ix
Chapter I: Introduction: Mechanisms for Controlling Dorsal Nuclear Levels ..	1
Abstract .....	1
An Introduction to formation of the Dorsal gradient.....	1
1. Post-translational modification of Dorsal.....	5
2. Shuttling .....	9
3. DNA Binding.....	11
4. Nuclear Spacing.....	13
Summary and unanswered questions regarding the control of nuclear Dorsal levels.....	15
References .....	18
Chapter II: Light-dependent N-end rule-mediated disruption of protein function in <i>Saccharomyces cerevisiae</i> and <i>Drosophila melanogaster</i> .....	25
Abstract .....	25
Author Summary.....	26
Introduction .....	27
Results .....	31
a. Ura3p.....	32
b. yEmRFP .....	36
c. Cdc28p .....	37
The PND directs light-dependent protein degradation.....	38
The PND and the B-LID domain direct blue light-dependent protein loss-of-function and degradation in <i>Drosophila</i> embryos .....	41
Discussion .....	51
Materials and Methods.....	57
References .....	74
Figures and Legends .....	84
Chapter III: Twist-dependent ratchet functioning downstream from Dorsal revealed using a light-inducible degron .....	106
Abstract .....	106
Introduction .....	106
Results .....	107
Discussion .....	117
Materials and Methods.....	120
Acknowledgements .....	124

References .....	124
Figures .....	128
Chapter IV: A subset of target genes requires Dorsal transcription factor nuclear retention .....	136
Summary .....	136
Results and Discussion.....	137
Acknowledgements .....	146
Author contributions .....	147
Declaration of interests .....	147
Figures and Legends .....	148
Star Methods .....	157
References .....	166
Chapter V: Discussion.....	170
The role of phosphorylation of Dorsal.....	170
The role of Dorsal at nc13.....	171
The role of enhancers in Dorsal mediate transcription.....	171
Modeling the Dorsal gradient and downstream genetic circuit.....	173
Optogenetics as a useful tool for dissecting gene regulatory networks ...	175
References .....	176
Appendix A: Supplementary materials for Chapter 2 .....	178
Appendix B: Supplementary materials for Chapter 3 .....	182
Appendix C: Supplementary materials for Chapter 4 .....	206

## LIST OF ILLUSTRATIONS AND/OR TABLES

<i>Number</i>	<i>Page</i>
1. Chapter 1, Figure 1.....	7
2. Chapter 1, Figure 2.....	14
3. Chapter 2, Figure 1 .....	84
4. Chapter 2, Figure 2 .....	87
5. Chapter 2, Figure 3 .....	90
6. Chapter 2, Figure 4 .....	92
7. Chapter 2, Figure 5 .....	94
8. Chapter 2, Figure 6 .....	96
9. Chapter 2, Figure 7 .....	98
10. Chapter 2, Figure 8 .....	100
11. Chapter 2, Figure 9 .....	101
12. Chapter 2, Figure 10 .....	103
13. Chapter 2, Table 1.....	105
14. Chapter 2, Table 2.....	105
15. Chapter 3, Figure 1 .....	128
16. Chapter 3, Figure 2 .....	130
17. Chapter 3, Figure 3 .....	132
18. Chapter 3, Figure 4 .....	134
19. Chapter 4, Figure 1 .....	148
20. Chapter 4, Figure 2 .....	150
21. Chapter 4, Figure 3 .....	152
22. Chapter 4, Figure 4 .....	154
23. Appendix B, Figures.....	189
24. Appendix C, Figures.....	208

## ABBREVIATIONS

**AP.** Anterior-posterior

**DL or *dl*.** Dorsal

**DV.** Dorsal-Ventral.

***sna*.** Snail

***sog*.** Short gastrulation

***twi*.** Twist

***vnd*.** Ventral nervous system defective.

***zen*.** Zerknullt

*Chapter 1***INTRODUCTION: MECHANISMS FOR CONTROLLING DORSAL NUCLEAR LEVELS****ABSTRACT**

Formation of the Dorsal gradient is important for the proper establishment of gene expression patterns along the Dorsal-Ventral axis during embryogenesis in *Drosophila melanogaster*. While Toll signaling likely provides the majority of the information necessary for Dorsal to form a gradient, there are a number of additional mechanisms that could factor into achieving correct nuclear levels of Dorsal. This includes post-translational modification, shuttling, DNA binding, and nuclear spacing. Post-translational modification could regulate nuclear Dorsal through phosphorylation of import and export. Shuttling, or the facilitated diffusion of Dorsal through its interaction with its cytoplasmic inhibitor Cactus, could regulate nuclear Dorsal levels by delivering more Dorsal to the ventral side of the embryo. DNA binding could affect the observed export rate of Dorsal if less Dorsal is available for export because it is bound to DNA. Nuclear spacing could result in higher Dorsal by leaving fewer nuclei to uptake Dorsal in the ventral domain. These mechanisms are not mutually exclusive and need not be occurring independently. This review covers how each of these mechanisms may be involved in determining Dorsal nuclear levels.

**AN INTRODUCTION TO FORMATION OF THE DORSAL GRADIENT**

Over the course of embryogenesis, gene regulation and differentiation must occur to properly pattern an embryo, giving rise to the tissues that ultimately make up an organism. In

*Drosophila melanogaster*, or the fruit fly, the embryo is patterned along the Anterior-Posterior (AP) axis and the Dorsal-Ventral (DV) axis by two morphogens, Bicoid (Driever and Nüsslein-Volhard, 1988a, 1988b) and Dorsal (Nüsslein-Volhard et al., 1980; Anderson and Nüsslein-Volhard, 1984), respectively. While Bicoid forms a mRNA gradient from anterior to posterior that gives rise to a gradient of Bicoid along the AP axis (Driever and Nüsslein-Volhard, 1988a), Dorsal protein forms a nuclear concentration gradient where Dorsal nuclear levels are highest on the ventral side of the embryo and lowest on the dorsal side (Steward et al., 1988; Roth et al., 1989; Steward, 1989). This concentration gradient is achieved through Toll signaling (Steward et al., 1988; Roth et al., 1989; Steward, 1989).

Toll signaling occurs during the early stages of embryogenesis, stage 3-5 (Anderson et al., 1985; Hashimoto et al., 1988, 1991). During this period of time, the *Drosophila* embryo is a syncytium, where nuclei are not separated by cell membranes. Due to the rapid nuclear divisions during these early stages, time is measured by nuclear cycle (nc). The Dorsal nuclear concentration gradient is observed to form during nc10-nc14, culminating in gastrulation (DeLotto et al., 2007; Reeves et al., 2012). For Toll signaling to properly occur, the ligand Spaetzle must be processed by a cascade of proteases (Dissing et al., 2001; LeMosy et al., 2001). In order for this cascade to properly proceed, correct distribution of Gurken, an EGFR ligand, must occur during oogenesis (Price et al., 1989; Schejter and Shilo, 1989; Neuman-Silberberg and Schüpbach, 1993, 1996). This signaling event correctly patterns the gene pipe to the ventral side of the oocyte, such that the correct modification of the vitelline membrane occurs (Sen et al., 1998; Zhang et al., 2009b). This modification is necessary for the protease cascade that ultimately processes Spaetzle (Zhang et al., 2009a).

It is believed that Spaetzle diffusion in the perivitelline space causes graded activation of Toll (Morisato, 2001).

Toll is a receptor and mediates signaling through the adaptor proteins Weckle, Myd88, Tube, and the kinase Pelle (Edwards et al., 1997; Yang and Steward, 1997; Charatsi et al., 2003; Chen et al., 2006; Moncrieffe et al., 2008). While Weckle's role in the signaling complex is not completely known, it is believed it forms a complex with Myd88 and Tube upon Toll activation that also recruits Pelle kinase to the membrane (Edwards et al., 1997; Chen et al., 2006). This complex is able to interact with Dorsal and Dorsal's inhibitor, Cactus. Cactus binds Dorsal and is thought to keep Dorsal cytoplasmically localized (Roth et al., 1991). Upon Toll signaling, Cactus is phosphorylated and degraded, freeing Dorsal to enter the nucleus (Belvin et al., 1995). Pelle kinase is known to phosphorylate itself (Shen and Manley, 1998, 2002; Towb et al., 2001), Tube (Grosshans et al., 1994; Towb et al., 2001), and Toll (Shen and Manley, 1998), and may also act to phosphorylate Cactus (Grosshans et al., 1994; Reach et al., 1996; Daigneault et al., 2013). However, in embryos that lack Cactus, a shallow Dorsal gradient still forms and is Toll dependent (Roth et al., 1991; Bergmann et al., 1996). This suggests that either there are other factors involved, or that Toll directly regulates Dorsal, potentially through phosphorylation.

Regardless of the exact mechanism, once activated, Dorsal forms a nuclear concentration gradient which controls target gene expression (Roth et al., 1989; Stathopoulos et al., 2002). Specifically, Dorsal acts as a transcription factor, activating and repressing target gene expression in a concentration dependent manner (Reeves et al., 2012). High levels of Dorsal

on the ventral side are known to be required for expression of genes in the presumptive mesoderm, such as *snail* (*sna*) and *twist* (*twi*). Intermediate levels of Dorsal activate genes in the lateral region, including short gastrulation (*sog*), ventral neuroblasts defective (*vnd*), intermediate neuroblasts defective (*ind*), and *brinker* (*brk*) (Reeves et al., 2012). These target genes are repressed by *sna* (Ip et al., 1992a) or other transcription factors. In addition to its role as an activator, these intermediate and low levels of Dorsal are able to repress genes that should only be expressed in the dorsal region, such as *zerknüllt* (*zen*) and *decapentaplegic* (*dpp*) (Kirov et al., 1993). While the direct activation and repression of Dorsal has been reported, other downstream targets of Dorsal also act to activate or repress gene expression, so it is not always clear what is the direct or indirect role of Dorsal. In the absence of Dorsal, a twisted cuticle is formed, where the only cuticle present is that derived from the dorsal region in a wildtype embryo (Roth et al., 1989). Dorsal is also necessary for gastrulation, through its activation of *twi* and *sna*. When both *twi* and *sna* are lost, the presumptive mesoderm does not invaginate (Leptin and Grunewald, 1990). In addition, the neurogenic ectoderm is also lost in the absence of Dorsal (Roth et al., 1989).

It is clear the levels of Dorsal are especially important in correctly patterning the DV axis, however, much of this work has been done in fixed tissues. While the dynamics of Dorsal have been explored, it remains unclear exactly how these dynamics affect downstream targets. In addition to the known role of Toll signaling degrading Cactus, it is possible that there are other contributing factors that lead to the correct nuclear Dorsal levels. These include post-translational modifications, which could act to affect import or export rates (Norris and Manley, 1992; Whalen and Steward, 1993; Gillespie and Wasserman, 1994;

Drier et al., 1999); shuttling, which is thought to move Dorsal protein ventrally so it can become more concentrated (Carrell et al., 2017); DNA binding, which is thought to affect the concentration of nuclear proteins (Al Asafen et al., 2018; Athilingam et al., 2022); and nuclear spacing, which is thought to affect the nuclear concentration by moving nuclei dorsally (Xue et al., 2023). These mechanisms for controlling Dorsal nuclear levels are not mutually exclusive, and could all be occurring to regulate Dorsal levels.

In addition to these mechanisms there are potentially other mechanisms that may regulate Dorsal that have been reviewed before, mainly focused on the role of Toll signaling and Cactus inhibition (Stein and Stevens, 2014; Schloop et al., 2020). Other potential protein interactions that may play an important role in determining the nuclear concentration of Dorsal include Tamo, a nuclear import regulator shown to interact with Dorsal (Minakhina et al., 2003); CRM1, a nuclear export factor shown to be important for export of Dorsal when it is blocked by drug treatment (DeLotto et al., 2007); and WntD, a possible inhibitor of Dorsal that has been shown to affect *twi* and *sna* expression (Ganguly et al., 2005). Also, Dorsal is thought to act synergistically with *Twi* to activate target gene expression in the presumptive mesoderm (Ip et al., 1992b; Shirokawa and Courey, 1997). Below, we focus our review on how post-translational modifications, shuttling, DNA binding, and nuclear spacing lead to correct nuclear Dorsal levels.

## **1. POST-TRANSLATIONAL MODIFICATION OF DORSAL**

One potential mechanism that could be utilized to refine Dorsal nuclear concentration levels is through post-translational modifications, such as phosphorylation. Dorsal is known to be

phosphorylated, and different residues have been identified as being phosphorylated (Norris and Manley, 1992; Whalen and Steward, 1993; Gillespie and Wasserman, 1994; Drier et al., 1999). In addition, NF $\kappa$ B, the mammalian homolog of Dorsal, is known to be phosphorylated (Viatour et al., 2005). Drier et al mutated six Serine residues, S70, S79, S103, S213, S312, and S317. When all six Serine residues were mutated to Alanine residues, Dorsal nuclear import was blocked (Drier et al., 1999). Drier et al. argued that only S317 affects the distribution of phosphorylated forms. However, these sites have not been confirmed to be phosphorylated by mass spectrometry, and were not detected in a system-wide assay of phosphorylation, which detected two phosphorylation sites, S389 and S665 (Hilger et al., 2009).

The strength of the nuclear localization signal (NLS) and nuclear export signal (NES) are key in regulation of nuclear proteins. Dorsal's NLS and NES have been identified (Xylourgidis et al., 2006; DeLotto et al., 2007), and S665, a serine residue that has been observed to be phosphorylated (Hilger et al., 2009) is part of a NES (Xylourgidis et al., 2006; DeLotto et al., 2007). A simple model is that Toll signaling phosphorylates one of Dorsal's NLS or NES sequences, either activating a NLS or blocking a NES. An increase in the import rate and a decrease in the export rate would serve to increase Dorsal nuclear concentration. This is supported by evidence that removing Cactus is not sufficient to get uniform Dorsal nuclear levels around the embryo (Roth et al., 1991; Bergmann et al., 1996). In this model, Toll acts to both phosphorylate Cactus and Dorsal, resulting in the degradation of Cactus so Dorsal is free to enter the nucleus, and phosphorylation of a NES decreases the export rate allowing accumulation of nuclear Dorsal.

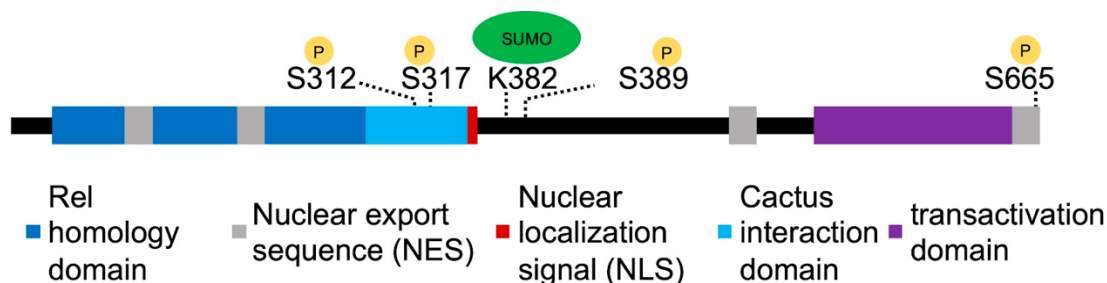


**Figure 1. Organization of Dorsal protein domains.**

The different domains of Dorsal, with known sites of phosphorylation or SUMOylation indicated with yellow or green circles, respectively.

Dorsal does not have to be exclusively phosphorylated by Toll signaling, and could be phosphorylated by other factors, either in addition to or instead of Toll signaling. For example, Dorsal has been reported to be phosphorylated at serine residue 312 near the NLS by the c-AMP dependent protein kinase (PKA) (Briggs et al., 1998), although others were unable to detect this phosphorylation (Drier et al., 1999). S312 was found to be important for regulating import and interaction with importin in cell culture (Briggs et al., 1998). However Drier et al. did not detect that it was phosphorylated, but rather hypothesized that it may control protein stability in vivo (Drier et al., 1999). Regardless of the source of the phosphorylation, such modifications could lead to increased or decreased nuclear Dorsal levels by affecting its import or export rates. Furthermore, these modifications could be constitutive, or could be modulated by downstream events of Dorsal activation to either increase or decrease nuclear Dorsal levels.

While it is known that Cactus acts to inhibit Dorsal by localizing it in the cytoplasm (Roth et al., 1991), that could be accomplished by different mechanisms. One possible

mechanism to localize Dorsal to the cytoplasm when bound to Cactus is by blocking access to Dorsal's NLS, which would prevent import into the nucleus. Another possible mechanism to localize Dorsal to the cytoplasm when bound by Cactus is that if Cactus has a very potent NES, it could be strong enough to bias the complex to the cytoplasm. Both of these mechanisms would prevent nuclear Dorsal enrichment, albeit in functionally different ways. By blocking a NLS, Cactus would be preventing Dorsal from entering the nucleus. By having a potent NES, Cactus would be quickly moving Dorsal out of the nucleus. There is evidence to support that Dorsal-Cactus complexes enter the nucleus as Dorsal has been observed to rapidly shuttle in and out of nuclei in the dorsal domain (DeLotto et al., 2007). There could be additional mechanisms, but once Cactus is degraded, it could reveal the NLS on Dorsal and increase import rate, or remove a potent NES and decrease export rate, allowing Dorsal to accumulate in the nucleus.

Post-translational modification, in this case by phosphorylation, would allow changes in nuclear Dorsal levels to occur very quickly. In addition to Pelle kinase, another kinase recently shown to affect Dorsal nuclear localization is Raf kinase, a MAP3K (Lusk et al., 2022). Lusk et al. found a strong dorsalizing phenotype when they screened a new library of mutations, which mapped to Raf kinase. They then observed that Dorsal is cytoplasmic in this mutant and Dorsal targets like Twist are expressed at low levels (Lusk et al., 2022). This raises the possibility that Raf could participate directly in phosphorylating Dorsal or Cactus, but it cannot be ruled out that Raf is involved elsewhere in the pathway.

In addition to the action of kinases, the inverse can also be used to modulate import and export. Specifically, if a protein is phosphorylated, a phosphatase could be employed to dephosphorylate a protein and affect import or export rates. Cactus has been found to be phosphorylated and degraded in response to calcium (Liu et al., 1997), and it is believed that calcium also leads to the dephosphorylation of Dorsal (Kubota and Gay, 1995). Thus by adding or removing phosphates through the action of kinases and phosphatases, the rate of import/export can be carefully and quickly modulated. Dorsal has also been shown to be SUMOylated and when a mutant was generated that prevents SUMOylation, Dorsal was found to more strongly activate, suggesting that SUMOylation may serve as part of a negative feedback loop to modulate transcription levels of dorsal targets (Hegde et al., 2022). It is also possible that SUMOylation of Dorsal triggers its nuclear export as has been demonstrated for the *Drosophila* transcription factor Medea (Miles et al., 2008).

## **2. SHUTTLING**

Another potential mechanism affecting the nuclear levels of Dorsal is shuttling. Specifically, shuttling would occur due to facilitated diffusion, where Dorsal, bound to Cactus, moves from the dorsal side of the embryo to the ventral side (Carrell et al., 2017). This would occur because a gradient of Dorsal-Cactus is formed where Dorsal-Cactus complexes are highest on the dorsal side and lowest on the ventral side as Cactus is degraded as a result of Toll signaling. In this model, the nuclei act as sinks, removing Dorsal from the cytoplasm so that Dorsal becomes more concentrated ventrally.

To test this model, Carrell et al. used a photoactivatable green fluorescent protein (paGFP), which allows activation of paGFP in a small window and then the distribution of signal can be tracked over time. They found that on the ventral side, signal was only detected in ~6-7 nuclei surrounding the area of activation, whereas on the dorsal side, signal was detected in the entire field of view after 90 min (Carrell et al., 2017). This supports the model that Dorsal can shuttle towards the ventral side from the dorsal side. To further test how diffusion rates may play a role, they also decreased the mobility of Dorsal by attaching monomeric GFP (mGFP) and dimeric GFP (dGFP). They found that decreasing the mobility increased the width of the Dorsal gradient (Carrell et al., 2017). This increase in width was also associated with a decrease in peak levels. This suggests that shuttling could be an important factor in defining the gradient and also in controlling the nuclear concentration of Dorsal.

A necessary component of the shuttling system is that free Dorsal does not diffuse as fast as Dorsal-Cactus complex, and Carrell et al. suggest this occurs by nuclear uptake of Dorsal acting as a sink (Carrell et al., 2017). Thus this mechanism requires strong nuclear import of Dorsal such that it accumulates in nuclei. Shuttling would then enhance this effect by increasing the concentration of Dorsal so more could be imported. Thus post-translational modification and shuttling are not mutually exclusive and could both occur simultaneously. In addition, shuttling could be enhanced by affecting Dorsal's import and export rate. This model would suggest that Cactus's role is actually twofold. Not only does it prevent Dorsal from accumulating in dorsal nuclei, it also would facilitate accumulation of Dorsal in the ventral nuclei via shuttling.

### 3. DNA BINDING

An additional mechanism that could affect Dorsal nuclear concentration is the rate of DNA binding. It has been recently posited that nuclear levels of Dorsal and Bicoid are decreased when DNA binding is blocked (Al Asafen et al., 2018; Athilingam et al., 2022). Al Asafen et al. used Raster Image Correlation Spectroscopy to quantify the mobility of Dorsal. They found that cytoplasmic Dorsal had similar diffusion coefficients and that the main difference was the diffusion coefficient of nuclear Dorsal. They also performed Fluorescence Recovery After Photobleaching (FRAP) and measured the import and export rate of Dorsal, finding that the export rate was lower on the ventral side, which they then correlated to increased localization with histones (Al Asafen et al., 2018). Thus they concluded that DNA binding was leading to increased levels of nuclear Dorsal and a decreased export rate.

Similarly, Athilingam et. al found that Bcd binding to DNA resulted in slower mobility (Athilingam et al., 2022). They used fluorescence correlation spectroscopy (FCS) to measure mobility but, in contrast to Al Asafen et al., they found that the diffusion coefficient was different in the posterior than in the anterior regardless of whether they measured it in the nucleus or cytoplasm. They also used various mutant forms of Bicoid to determine that DNA binding was important for determining the rate of Bicoid diffusion (Athilingam et al., 2022). Although they did not look directly at import/export rates and nuclear concentration, their work supports that DNA binding could play a role in determining nuclear concentration.

While both these papers suggest that DNA binding is what leads to increased nuclear concentration, neither one directly tested this by removing DNA binding domains and measuring nuclear concentration. Thus, there remains an open question of causality: does increased DNA binding lead to increased nuclear concentration, or does increased nuclear concentration lead to increased DNA binding? It is possible that the decreased nuclear export rates measured on the ventral side for Dorsal, actually lead to the increased DNA binding hypothesized by Al Asafen et al. as opposed to the increased DNA binding leading to an increase in nuclear concentration.

If this model is true, it could suggest an additional mechanism for how Cactus works. While Cactus could block nuclear import or contain a potent NES to increase nuclear export as discussed previously, Cactus could also work simply by blocking Dorsal binding to DNA. By blocking DNA binding under the assumptions of the model, Cactus would work in concert with the NLS and NES sequence on Dorsal to bias Dorsal-Cactus complexes for export. This model requires DNA binding to be strong enough to block or prevent export by the NES. Once again, these mechanisms for how Cactus prevents nuclear Dorsal accumulation need not be mutually exclusive. Cactus could contain a potent NES and also prevent DNA binding. Thereby effectively sequestering Dorsal in the cytoplasm.

Similarly, DNA binding can work in concert with controlling nuclear import/export rates by post-translational modification and shuttling. Specifically, DNA binding could alter the pool of Dorsal that is available to the export machinery, which would affect the

export rate. The import/export rate could then be further modulated by phosphorylation. Finally, shuttling could then serve to bring more Dorsal to the ventral side. One can imagine that a low Dorsal nuclear export rate, strong binding to DNA, and shuttling could all occur simultaneously to determine the final nuclear concentration levels.

#### **4. NUCLEAR SPACING**

An additional consideration for determining the nuclear concentration of Dorsal is the density of nuclei. One can imagine that if the concentration of cytoplasmic Dorsal is uniform around the embryo, but nuclei are less dense on the ventral side, that this would increase Dorsal nuclear levels ventrally. It has been shown that nuclei are denser on the dorsal side of the embryo than the ventral side of the embryo (Xue et al., 2023). Xue et al. determined that Dorsal and Decapentaplegic (Dpp), the *Drosophila* homolog of BMP, are important regulators of this change in nuclei density. Dorsal is known to spatially regulate *dpp* expression to the dorsal side of the embryo, where Dpp acts as a ligand to activate BMP signaling and produce pMad (Ferguson and Anderson, 1992a, 1992b; Kirov et al., 1993). Xue et al. determined that Dpp/BMP signaling was primarily responsible for the movement of nuclei to the dorsal side of the embryo. They also identified the downstream effectors of this process, *frazzled* and *GUK-holder*, and noted a change in expression of DV genes when these genes are mutated (Xue et al., 2023). They determined that these changes occurred as a result of changes to the Dorsal gradient, specifically the peak levels of Dorsal were reduced at the ventral midline, and

the gradient was wider. They suggest that these changes in the Dorsal gradient are a direct result from the loss of cell movements mediated by frazzled and GUK-holder. They propose a model where Dorsal and Dpp cause nuclei density to change and this change in turn feeds back into proper gradient formation and target gene expression (Xue et al., 2023). While they cannot rule out additional direct or indirect roles for these factors downstream of Dorsal or Dpp, the changes to the Dorsal and Dpp gradient correspond well to the changes observed in gene expression. This suggests that nuclear spacing does indeed play an important role in correct nuclear concentration levels of Dorsal.

Nuclear spacing and shuttling would likely enhance the effect of each other if they occur together, but could occur independently. Without shuttling, short range diffusion could occur as nuclei move away so that the ventral nuclei that are left have a larger pool of Dorsal available to them. However, shuttling could further enhance this effect by moving more Dorsal to these ventral nuclei. Nuclear spacing and shuttling would increase Dorsal levels over time until the nuclei reach saturation or steady state levels.

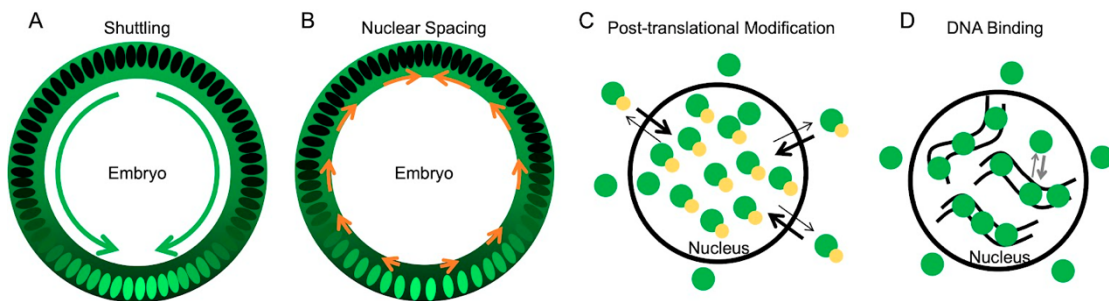


**Figure 2. Mechanisms potentially contributing to Dorsal nuclear levels.**

(A) A model of shuttling, where Dorsal-Cactus diffuses towards the ventral midline as Toll signaling degrades Cactus and Dorsal enters ventral and lateral

nuclei. Dorsal concentration both in the nucleus and cytoplasm is shown in green. Green arrows represent the flow of Dorsal-Cactus. (B) A model of how changes in nuclear spacing, where nuclei move more dorsally, could leave fewer nuclei on the ventral side which uptake the cytoplasmic Dorsal. Orange arrows represent the movement of nuclei towards the dorsal side. (C) A model of how phosphorylation could bias import/export rates such that phosphorylated Dorsal is nuclear. Dorsal is in green, phosphorylation in yellow. (D) A model of how DNA binding may reduce the pool of Dorsal available for export, thus allowing Dorsal to accumulate in nuclei. Curved black lines represent DNA, and Dorsal is in green.

### **SUMMARY AND UNANSWERED QUESTIONS REGARDING THE CONTROL OF NUCLEAR DORSAL LEVELS**

While each of these proposed mechanisms could individually determine the final Dorsal nuclear levels, they are not mutually exclusive and could work together. For example, the nuclear import/export rate could be fixed or it could be modulated dynamically to increase or decrease Dorsal levels. In addition, DNA binding could play a role in additionally affecting the nuclear export rate. As Dorsal binds to DNA, it could be exported more slowly. Shuttling could move more Dorsal ventrally, increasing the available Dorsal to be imported into nuclei. Finally, nuclear spacing could work to achieve a similar outcome to shuttling where the cytoplasmic Dorsal levels increase with fewer nuclei to uptake Dorsal, which results in an increased concentration of Dorsal in

ventral nuclei. Regardless, the import/export rate is fundamentally important for all of these mechanisms, as Dorsal must be able to enter and exit the nucleus.

It has been shown that timing of nuclear import may be an important mechanism for controlling the time of gene activation in *Xenopus laevis* (Nguyen et al., 2022). Nguyen et al. used proteomics and mass spectrometry to determine the levels of cytoplasmic and nuclear protein, and compare these values over different timepoints. They found that the times that proteins enter the nucleus varied widely. They also found that the timing of transcription factor import and the onset of gene transcription were strongly correlated. In addition, the importin affinities of various proteins also correlated with the timing of their nuclear import. They then validated these observations using microscopy of nuclei in cell free droplets of egg lysate to measure the time of nuclear import for a subset of proteins and found that the order of nuclear import determined by microscopy agreed with the proteomics data (Nguyen et al., 2022). Taken together, their data suggests a model where importin affinity controls the timing of nuclear import and subsequent gene transcription in early embryo development.

Perturbations to these mechanisms affecting Dorsal nuclear levels are likely to have direct effects on target gene expression. Although previous studies on post-translational modifications such as phosphorylation did not test target gene expression directly, they did measure Dorsal levels and find them to be much lower than in wildtype, which would result in a decrease in high threshold targets and potentially intermediate threshold targets and low threshold targets depending on the strength of the mutant (Briggs et al., 1998;

Drier et al., 1999). Shuttling has been shown to play a role in reducing the width of *sna* (Carrell et al., 2017), and is likely to decrease the domain of other high threshold targets. While the effects of preventing DNA binding were not measured (Al Asafen et al., 2018), a significant decrease in nuclear Dorsal would result in a loss of high threshold targets, and potentially intermediate threshold targets. Finally, when mutating *fra*, an effector involved in nuclear spacing, there were changes in six DV target genes regulated by Dorsal or Dpp. The *race* expression domain was reduced, the rhomboid (*rho*) domain was expanded, the muscle segment homeobox (*msh*) domain was expanded, the *ind* domain was reduced, the *vnd* domain was reduced, and the *sna* domain was expanded (Xue et al., 2023). Thus, the fine tuning of nuclear Dorsal levels through post-transcriptional modification, shuttling, DNA binding, and nuclear spacing play an important role in correctly positioning boundaries of expression domains.

We set out to develop a method for controlling nuclear Dorsal levels and used this method to determine how the dynamics and levels of nuclear Dorsal affect target gene expression. To do this, we used two optogenetic tags, a Blue-Light Inducible Degradation (BLID) tag (Bonger et al., 2014) and a Light inducible Export System (LEXY) tag (Niopek et al., 2016) to control Dorsal levels with blue light. Using BLID and LEXY, we tested how removal of Dorsal affects target gene expression, including whether Dorsal was continuously needed. We discovered a molecular ratchet that works downstream of Dorsal that is able to support high threshold Dorsal targets in the absence of Dorsal. We also tested the timing of Dorsal action to determine when Dorsal was important for target gene expression and compared the effects of removal of Dorsal using BLID and LEXY.

We found that the low levels of Dorsal generated by LEXY maintain proper expression of low threshold targets, while low threshold target boundaries change in BLID. We also found that the transient levels of Dorsal in LEXY disrupted the downstream ratchet.

## REFERENCES

- Al Asafen, H., Clark, N. M., Jacobsen, T., Sozzani, R., and Reeves, G. T. (2018). Dorsal/NF- $\kappa$ B exhibits a dorsal-to-ventral mobility gradient in the *Drosophila* embryo. *bioRxiv*. doi: 10.1101/320754.
- Anderson, K. V., Bokla, L., and Nüsslein-Volhard, C. (1985). Establishment of dorsal-ventral polarity in the *Drosophila* embryo: the induction of polarity by the Toll gene product. *Cell* 42, 791–798.
- Anderson, K. V., and Nüsslein-Volhard, C. (1984). Information for the dorsal--ventral pattern of the *Drosophila* embryo is stored as maternal mRNA. *Nature* 311, 223–227.
- Athilingam, T., Nelanuthala, A. V. S., Breen, C., Wohland, T., and Saunders, T. E. (2022). Long-ranged formation of the Bicoid gradient requires multiple dynamic modes that spatially vary across the embryo. *bioRxiv*. doi: 10.1101/2022.09.28.509874.
- Belvin, M. P., Jin, Y., and Anderson, K. V. (1995). Cactus protein degradation mediates *Drosophila* dorsal-ventral signaling. *Genes Dev.* 9, 783–793.
- Bergmann, A., Stein, D., Geisler, R., Hagenmaier, S., Schmid, B., Fernandez, N., et al. (1996). A gradient of cytoplasmic Cactus degradation establishes the nuclear localization gradient of the dorsal morphogen in *Drosophila*. *Mech. Dev.* 60, 109–123.
- Bonger, K. M., Rakhit, R., Payumo, A. Y., Chen, J. K., and Wandless, T. J. (2014). General method for regulating protein stability with light. *ACS Chem. Biol.* 9, 111–115.
- Briggs, L. J., Stein, D., Goltz, J., Corrigan, V. C., Efthymiadis, A., Hübner, S., et al. (1998). The cAMP-dependent protein kinase site (Ser312) enhances dorsal nuclear import through facilitating nuclear localization sequence/importin interaction. *J. Biol. Chem.* 273, 22745–22752.

- Carrell, S. N., O'Connell, M. D., Jacobsen, T., Pomeroy, A. E., Hayes, S. M., and Reeves, G. T. (2017). A facilitated diffusion mechanism establishes the Dorsal gradient. *Development* 144, 4450–4461.
- Charatsi, I., Luschnig, S., Bartoszewski, S., Nüsslein-Volhard, C., and Moussian, B. (2003). Krapfen/dMyd88 is required for the establishment of dorsoventral pattern in the *Drosophila* embryo. *Mech. Dev.* 120, 219–226.
- Chen, L.-Y., Wang, J.-C., Hyvert, Y., Lin, H.-P., Perrimon, N., Imler, J.-L., et al. (2006). Weckle is a zinc finger adaptor of the toll pathway in dorsoventral patterning of the *Drosophila* embryo. *Curr. Biol.* 16, 1183–1193.
- Daigneault, J., Klemetsaune, L., and Wasserman, S. A. (2013). The IRAK homolog Pelle is the functional counterpart of I $\kappa$ B kinase in the *Drosophila* Toll pathway. *PLoS One* 8, e75150.
- DeLotto, R., DeLotto, Y., Steward, R., and Lippincott-Schwartz, J. (2007). Nucleocytoplasmic shuttling mediates the dynamic maintenance of nuclear Dorsal levels during *Drosophila* embryogenesis. *Development* 134, 4233–4241.
- Dissing, M., Giordano, H., and DeLotto, R. (2001). Autoproteolysis and feedback in a protease cascade directing *Drosophila* dorsal-ventral cell fate. *EMBO J.* 20, 2387–2393.
- Drier, E. A., Huang, L. H., and Steward, R. (1999). Nuclear import of the *Drosophila* Rel protein Dorsal is regulated by phosphorylation. *Genes Dev.* 13, 556–568.
- Driever, W., and Nüsslein-Volhard, C. (1988a). A gradient of bicoid protein in *Drosophila* embryos. *Cell* 54, 83–93.
- Driever, W., and Nüsslein-Volhard, C. (1988b). The bicoid protein determines position in the *Drosophila* embryo in a concentration-dependent manner. *Cell* 54, 95–104.
- Edwards, D. N., Towb, P., and Wasserman, S. A. (1997). An activity-dependent network of interactions links the Rel protein Dorsal with its cytoplasmic regulators. *Development* 124, 3855–3864.
- Ferguson, E. L., and Anderson, K. V. (1992a). Decapentaplegic acts as a morphogen to organize dorsal-ventral pattern in the *Drosophila* embryo. *Cell* 71, 451–461.
- Ferguson, E. L., and Anderson, K. V. (1992b). Localized enhancement and repression of the activity of the TGF-beta family member, decapentaplegic, is necessary for dorsal-ventral pattern formation in the *Drosophila* embryo. *Development* 114, 583–597.

- Ganguly, A., Jiang, J., and Ip, Y. T. (2005). *Drosophila* WntD is a target and an inhibitor of the Dorsal/Twist/Snail network in the gastrulating embryo. *Development* 132, 3419–3429.
- Gillespie, S. K., and Wasserman, S. A. (1994). Dorsal, a *Drosophila* Rel-like protein, is phosphorylated upon activation of the transmembrane protein Toll. *Mol. Cell. Biol.* 14, 3559–3568.
- Grosshans, J., Bergmann, A., Haffter, P., and Nüsslein-Volhard, C. (1994). Activation of the kinase Pelle by Tube in the dorsoventral signal transduction pathway of *Drosophila* embryo. *Nature* 372, 563–566.
- Hashimoto, C., Gerttula, S., and Anderson, K. V. (1991). Plasma membrane localization of the Toll protein in the syncytial *Drosophila* embryo: importance of transmembrane signaling for dorsal-ventral pattern formation. *Development* 111, 1021–1028.
- Hashimoto, C., Hudson, K. L., and Anderson, K. V. (1988). The Toll gene of *Drosophila*, required for dorsal-ventral embryonic polarity, appears to encode a transmembrane protein. *Cell* 52, 269–279.
- Hegde, S., Sreejan, A., Gadgil, C. J., and Ratnaparkhi, G. S. (2022). SUMOylation of Dorsal attenuates Toll/NF- $\kappa$ B signaling. *Genetics* 221. doi: 10.1093/genetics/iyac081.
- Hilger, M., Bonaldi, T., Gnad, F., and Mann, M. (2009). Systems-wide analysis of a phosphatase knock-down by quantitative proteomics and phosphoproteomics. *Mol. Cell. Proteomics* 8, 1908–1920.
- Ip, Y. T., Park, R. E., Kosman, D., Bier, E., and Levine, M. (1992a). The dorsal gradient morphogen regulates stripes of rhomboid expression in the presumptive neuroectoderm of the *Drosophila* embryo. *Genes Dev.* 6, 1728–1739.
- Ip, Y. T., Park, R. E., Kosman, D., Yazdanbakhsh, K., and Levine, M. (1992b). dorsal-twist interactions establish snail expression in the presumptive mesoderm of the *Drosophila* embryo. *Genes Dev.* 6, 1518–1530.
- Kirov, N., Zhelnin, L., Shah, J., and Rushlow, C. (1993). Conversion of a silencer into an enhancer: evidence for a co-repressor in dorsal-mediated repression in *Drosophila*. *EMBO J.* 12, 3193–3199.
- Kubota, K., and Gay, N. J. (1995). Calcium destabilises *Drosophila* cactus protein and dephosphorylates the dorsal transcription factor. *Biochem. Biophys. Res. Commun.* 214, 1191–1196.

- LeMosy, E. K., Tan, Y. Q., and Hashimoto, C. (2001). Activation of a protease cascade involved in patterning the *Drosophila* embryo. *Proc. Natl. Acad. Sci. U. S. A.* 98, 5055–5060.
- Leptin, M., and Grunewald, B. (1990). Cell shape changes during gastrulation in *Drosophila*. *Development* 110, 73–84.
- Liu, Z. P., Galindo, R. L., and Wasserman, S. A. (1997). A role for CKII phosphorylation of the cactus PEST domain in dorsoventral patterning of the *Drosophila* embryo. *Genes Dev.* 11, 3413–3422.
- Lusk, J. B., Chua, E. H. Z., Kaur, P., Sung, I. C. H., Lim, W. K., Lam, V. Y. M., et al. (2022). A non-canonical Raf function is required for dorsal-ventral patterning during *Drosophila* embryogenesis. *Sci. Rep.* 12, 7684.
- Miles, W. O., Jaffray, E., Campbell, S. G., Takeda, S., Bayston, L. J., Basu, S. P., et al. (2008). Medea SUMOylation restricts the signaling range of the Dpp morphogen in the *Drosophila* embryo. *Genes Dev.* 22, 2578.
- Minakhina, S., Yang, J., and Steward, R. (2003). Tamo selectively modulates nuclear import in *Drosophila*. *Genes Cells* 8, 299–310.
- Moncrieffe, M. C., Grossmann, J. G., and Gay, N. J. (2008). Assembly of oligomeric death domain complexes during Toll receptor signaling. *J. Biol. Chem.* 283, 33447–33454.
- Morisato, D. (2001). Spätzle regulates the shape of the Dorsal gradient in the *Drosophila* embryo. *Development* 128, 2309–2319.
- Neuman-Silberberg, F. S., and Schüpbach, T. (1993). The *Drosophila* dorsoventral patterning gene *gurken* produces a dorsally localized RNA and encodes a TGF alpha-like protein. *Cell* 75, 165–174.
- Neuman-Silberberg, F. S., and Schüpbach, T. (1996). The *Drosophila* TGF-alpha-like protein *Gurken*: expression and cellular localization during *Drosophila* oogenesis. *Mech. Dev.* 59, 105–113.
- Nguyen, T., Costa, E. J., Deibert, T., Reyes, J., Keber, F. C., Tomschik, M., et al. (2022). Differential nuclear import sets the timing of protein access to the embryonic genome. *Nat. Commun.* 13, 5887.
- Niopek, D., Wehler, P., Roensch, J., Eils, R., and Di Ventura, B. (2016). Optogenetic control of nuclear protein export. *Nat. Commun.* 7, 10624.

- Norris, J. L., and Manley, J. L. (1992). Selective nuclear transport of the *Drosophila* morphogen dorsal can be established by a signaling pathway involving the transmembrane protein Toll and protein kinase A. *Genes Dev.* 6, 1654–1667.
- Nüsslein-Volhard, C., Lohs-Schardin, M., Sander, K., and Cremer, C. (1980). A dorso-ventral shift of embryonic primordia in a new maternal-effect mutant of *Drosophila*. *Nature* 283, 474–476.
- Price, J. V., Clifford, R. J., and Schüpbach, T. (1989). The maternal ventralizing locus torpedo is allelic to faint little ball, an embryonic lethal, and encodes the *Drosophila* EGF receptor homolog. *Cell* 56, 1085–1092.
- Reach, M., Galindo, R. L., Towb, P., Allen, J. L., Karin, M., and Wasserman, S. A. (1996). A gradient of cactus protein degradation establishes dorsoventral polarity in the *Drosophila* embryo. *Dev. Biol.* 180, 353–364.
- Reeves, G. T., Trisnadi, N., Truong, T. V., Nahmad, M., Katz, S., and Stathopoulos, A. (2012). Dorsal-ventral gene expression in the *Drosophila* embryo reflects the dynamics and precision of the dorsal nuclear gradient. *Dev. Cell* 22, 544–557.
- Roth, S., Hiromi, Y., Godt, D., and Nüsslein-Volhard, C. (1991). cactus, a maternal gene required for proper formation of the dorsoventral morphogen gradient in *Drosophila* embryos. *Development* 112, 371–388.
- Roth, S., Stein, D., and Nüsslein-Volhard, C. (1989). A gradient of nuclear localization of the dorsal protein determines dorsoventral pattern in the *Drosophila* embryo. *Cell* 59, 1189–1202.
- Schejter, E. D., and Shilo, B. Z. (1989). The *Drosophila* EGF receptor homolog (DER) gene is allelic to faint little ball, a locus essential for embryonic development. *Cell* 56, 1093–1104.
- Schloop, A. E., Bandodkar, P. U., and Reeves, G. T. (2020). Formation, interpretation, and regulation of the *Drosophila* Dorsal/NF- $\kappa$ B gradient. *Curr. Top. Dev. Biol.* 137, 143–191.
- Sen, J., Goltz, J. S., Stevens, L., and Stein, D. (1998). Spatially restricted expression of pipe in the *Drosophila* egg chamber defines embryonic dorsal-ventral polarity. *Cell* 95, 471–481.
- Shen, B., and Manley, J. L. (1998). Phosphorylation modulates direct interactions between the Toll receptor, Pelle kinase and Tube. *Development* 125, 4719–4728.

- Shen, B., and Manley, J. L. (2002). Pelle kinase is activated by autophosphorylation during Toll signaling in *Drosophila*. *Development* 129, 1925–1933.
- Shirokawa, J. M., and Courey, A. J. (1997). A direct contact between the dorsal rel homology domain and Twist may mediate transcriptional synergy. *Mol. Cell. Biol.* 17, 3345–3355.
- Stathopoulos, A., Van Drenth, M., Erives, A., Markstein, M., and Levine, M. (2002). Whole-genome analysis of dorsal-ventral patterning in the *Drosophila* embryo. *Cell* 111, 687–701.
- Stein, D. S., and Stevens, L. M. (2014). Maternal control of the *Drosophila* dorsal-ventral body axis. *Wiley Interdiscip. Rev. Dev. Biol.* 3, 301–330.
- Steward, R. (1989). Relocalization of the dorsal protein from the cytoplasm to the nucleus correlates with its function. *Cell* 59, 1179–1188.
- Steward, R., Zusman, S. B., Huang, L. H., and Schedl, P. (1988). The dorsal protein is distributed in a gradient in early *Drosophila* embryos. *Cell* 55, 487–495.
- Towb, P., Bergmann, A., and Wasserman, S. A. (2001). The protein kinase Pelle mediates feedback regulation in the *Drosophila* Toll signaling pathway. *Development* 128, 4729–4736.
- Viatour, P., Merville, M.-P., Bours, V., and Chariot, A. (2005). Phosphorylation of NF-kappaB and IkappaB proteins: implications in cancer and inflammation. *Trends Biochem. Sci.* 30, 43–52.
- Whalen, A. M., and Steward, R. (1993). Dissociation of the dorsal-cactus complex and phosphorylation of the dorsal protein correlate with the nuclear localization of dorsal. *J. Cell Biol.* 123, 523–534.
- Xue, Y., Krishnan, A., Chahda, J. S., Schweickart, R. A., Sousa-Neves, R., and Mizutani, C. M. (2023). The epithelial polarity genes frazzled and GUK-holder adjust morphogen gradients to coordinate changes in cell position with cell fate specification. *PLoS Biol.* 21, e3002021.
- Xylourgidis, N., Roth, P., Sabri, N., Tsarouhas, V., and Samakovlis, C. (2006). The nucleoporin Nup214 sequesters CRM1 at the nuclear rim and modulates NFkappaB activation in *Drosophila*. *J. Cell Sci.* 119, 4409–4419.
- Yang, J., and Steward, R. (1997). A multimeric complex and the nuclear targeting of the *Drosophila* Rel protein Dorsal. *Proc. Natl. Acad. Sci. U. S. A.* 94, 14524–14529.

- Zhang, Z., Stevens, L. M., and Stein, D. (2009a). Sulfation of eggshell components by Pipe defines dorsal-ventral polarity in the *Drosophila* embryo. *Curr. Biol.* 19, 1200–1205.
- Zhang, Z., Zhu, X., Stevens, L. M., and Stein, D. (2009b). Distinct functional specificities are associated with protein isoforms encoded by the *Drosophila* dorsal-ventral patterning gene pipe. *Development* 136, 2779–2789.

*Chapter 2***LIGHT-DEPENDENT N-END RULE-MEDIATED DISRUPTION OF PROTEIN FUNCTION IN SACCHAROMYCES CEREVISIAE AND DROSOPHILA MELANOGASTER**

This chapter was written with Leslie M. Stevens, Goheun Kim, Theodora Koromila, John W. Steele, Angelike Stathopoulos, and David S. Stein, and published in PLoS Genet. 2021 May 17;17(5):e1009544. This project was initiated in the Stein lab and most experiments were performed in the Stein lab. Live imaging in *Drosophila* was performed in the Stathopoulos lab.

**ABSTRACT**

Here we describe the development and characterization of the photo-N-degron, a peptide tag that can be used in optogenetic studies of protein function in vivo. The photo-N-degron can be expressed as a genetic fusion to the amino termini of other proteins, where it undergoes a blue light-dependent conformational change that exposes a signal for the class of ubiquitin ligases, the N-recognins, which mediate the N-end rule mechanism of proteasomal degradation. We demonstrate that the photo-N-degron can be used to direct light-mediated degradation of proteins in *Saccharomyces cerevisiae* and *Drosophila melanogaster* with fine temporal control. In addition, we compare the effectiveness of the photo-N-degron with that of two other light-dependent degrons that have been developed in their abilities to mediate the loss of function of Cactus, a component of the dorsal-ventral patterning system in the *Drosophila* embryo. We find that like the photo-N-degron, the blue light-inducible degradation (B-LID) domain, a light-activated degron that must be placed

at the carboxy terminus of targeted proteins, is also effective in eliciting light-dependent loss of Cactus function, as determined by embryonic dorsal-ventral patterning phenotypes. In contrast, another previously described photosensitive degron (psd), which also must be located at the carboxy terminus of associated proteins, has little effect on Cactus-dependent phenotypes in response to illumination of developing embryos. These and other observations indicate that care must be taken in the selection and application of light-dependent and other inducible degrons for use in studies of protein function *in vivo*, but importantly demonstrate that N- and C-terminal fusions to the photo-N-degron and the B-LID domain, respectively, support light-dependent degradation *in vivo*.

#### **AUTHOR SUMMARY**

Much of what we know about biological processes has come from the analysis of mutants whose loss-of-function phenotypes provide insight into their normal functions. However, for genes that are required for viability and which have multiple functions in the life of a cell or organism one can only observe mutant phenotypes produced up to the time of death. Normal functions performed in wild-type individuals later than the time of death of mutants cannot be observed. In one approach to overcoming this limitation, a class of peptide degradation signals (degrons) have been developed, which when fused to proteins-of-interest can target those proteins for degradation in response to various stimuli (temperature, chemical agents, co-expressed proteins, or light). Here we describe a new inducible degron (the photo-N-degron or PND), which when fused to the N-terminus of a protein can induce N-end rule-mediated degradation in response to blue-light illumination and have validated its use in both yeast and *Drosophila* embryos. Moreover, using the

*Drosophila* embryonic patterning protein Cactus, we show that like the PND, the previously-described B-LID domain, but not the previously-described photosensitive degron (psd), can produce detectable light-inducible phenotypes in *Drosophila* embryos that are consistent with the role of Cactus in dorsal-ventral patterning.

## **INTRODUCTION**

More than a century of genetic analysis underlies much of our understanding of biology. Unbiased genetic screens utilizing chemical mutagens, ionizing radiation or insertional mutagenesis with transposons or retroviruses and, more recently, reverse genetic strategies capable of generating precisely targeted mutations have been critical in uncovering the genes, proteins and mechanisms underlying normal physiology as well as the processes that go awry in various disease states. However, for genes with products that are required early in the life of an organism, it can be challenging to generate loss-of-function mutant individuals in which later phenotypes associated with protein loss can be examined. While the use of site-specific recombination systems to generate clones of cells lacking expression of a protein in the background of an otherwise viable individual [1–4] can, in some cases, overcome this barrier, proteins already present may perdure for some time and even multiple cell generations after mutant clone induction, which can complicate the analysis of the loss-of-function phenotypes. This is especially problematic in situations in which it is desirable to achieve rapid protein inactivation, such as investigations of protein function at specific stages of the cell cycle, during cell migration and morphogenesis, or during neuronal signaling. Moreover, for genes encoding proteins that are necessary for cell viability, cell death following the generation of mutant clones can obscure the detection

and analysis of more subtle phenotypes resulting from protein loss-of-function.

Similarly, RNA interference via the expression of dsRNA or siRNAs, which has been used to interrogate the function of vital genes in a cellular or tissue-specific manner [5,6] often achieves only partial elimination of the protein-of-interest and is also susceptible to the problem of protein perdurance noted above.

Another approach to the study of proteins with functions essential for organismal or cell viability is the use of temperature-sensitive (TS) mutations. However, although methods for the rational design of TS alleles encoding proteins-of-interest exist [7–10], these approaches are associated with drawbacks that can limit their general applicability. Dohmen et al. [11] devised a general approach for expressing TS proteins, relying upon the N-end rule pathway for ubiquitin/proteasome-mediated degradation [12–14], which degrades proteins bearing N-terminal amino acid residues other than methionine under the control of ubiquitin ligases known as UBRs or N-recognins [15,16]. Dohmen et al. [11] showed that a peptide comprising a TS version of the mouse dihydrofolate reductase protein carrying an N-terminal arginine (the temperature dependent or “td” degron) could, when fused to the amino terminus of a several yeast proteins, render the resulting fusion proteins inactive and lead to their degradation at 37° C but not at 23° C. This TS phenotype was dependent upon UBR1, the yeast N-recognin [12,15,17]. The td degron has been used to investigate protein function in a number of systems including budding yeast, fission yeast and vertebrate tissue culture cells [18–23]. Many organisms cannot survive at 37° C, the temperature at which the td degron mediates protein degradation. Accordingly, the low temperature-controlled (lt) degron [24], which operates over a lower temperature range

(16°C to 29°C), was generated by modifying the td degron, which expands the organisms in which this method can be applied. However, TS mutants, including the td and It degrons cannot be used to study protein function in homeothermic organisms such as mammals, which maintain a constant internal temperature.

A number of other degrons have been developed, which induce the proteins to which they have been attached to undergo degradation in response to addition of small molecules such as the rapamycin analogue Shield-1 [25,26] or auxin [27–29]. These approaches are highly dependent upon the extent and rapidity with which the small molecule can be administered to or depleted from the target cell/tissue/organism. Furthermore, the auxin system as well as several other inducible degron systems require the co-expression of a heterologous specificity-conferring factor together with the degron-tagged target protein [30–33]. While these approaches can provide tissue specificity, based on the expression pattern of the specificity conferring factors, they are obviously influenced and potentially limited in utility by the time required for induction and expression or loss of these factors.

In recent years, a number of novel strategies have been developed in which light is employed to modulate protein behavior in powerful new approaches to examining biological processes. These new technologies, which comprise the rapidly expanding area of optogenetics [34,35], have revolutionized several realms of biomedical research, leading to the expression of light-sensitive membrane channels [36–38] and the generation of proteins that undergo light-dependent conformational changes that affect their activity [39–41], cellular localization [42–44], and protein-protein interactions [45,46].

We began our studies intending to combine recent advances in the understanding of light-modulated proteins and of ubiquitin/proteasome-mediated protein degradation to develop techniques that permit light-activated degradation of target proteins. In addition to overcoming the limitations associated with the conditional approaches described above, such a system could potentially enable a level of temporal and spatial precision not possible using currently available systems for perturbing gene expression. Many of the gene products required for correct embryonic development in *Drosophila* are expressed maternally and deposited as mRNAs or proteins into the developing egg during oogenesis, for later function in the embryo. For those gene products required for viability of the female fly, or during oogenesis to produce an egg, it is difficult to examine the phenotypic consequences of loss of function of proteins produced maternally that are required to support progeny embryogenesis. Thus, the ability to rapidly eliminate otherwise stable proteins with the application of light could provide a valuable tool for the examination of loss-of-function phenotypes whose visualization would be precluded by the perturbation of earlier loss-of-function phenotypes.

Proteins containing LOV domains respond to environmental stimuli such as Light, Oxygen and Voltage by undergoing conformational changes [47,48]. Light-dependent members of this class of proteins utilize flavin cofactors as chromophores to function as blue-light sensitive photoreceptors in bacteria [49], fungi [50,51] and plants [52]. Structural studies of one of the two LOV domains present in phototropin 1 of *Avena sativa* (common oat)

(phLOV2) showed that under blue light illumination, the flavin-binding region dissociates from and unwinds an adjacent alpha helical region termed J $\alpha$  [53–55]. Other studies have recently established that proteins bearing modified LOV domains can be induced to degrade in response to light [56,57].

Here we report on the development of an additional light-dependent degron that makes use of the phLOV2 domain from *Avena sativa* (oat), which we term the photo-N-degron (PND). When attached to the N-terminus of several proteins which are then expressed in yeast, the PND induces light-dependent N-end rule-mediated loss of function, owing to protein degradation. We also show that in *Drosophila* embryos, the PND can induce a rapid light-dependent loss of Cactus, the cognate inhibitor of Dorsal, the fly orthologue of the mammalian transcription factor NF $\kappa$ B [58]. Cactus and Dorsal are components of the signal transduction pathway that defines *Drosophila* embryonic dorsal-ventral (DV) polarity [59] and light-induced degradation of PND-tagged Cactus leads to alterations in DV patterning. Finally, we compare the abilities of the psd [56], the B-LID domain [57], and the PND, finding that, like the PND, the B-LID domain directs robust elimination of Cactus function, while the psd degron leads to only a subtle phenotypic difference upon illumination. Our results demonstrate that the PND can be a powerful tool for conditional elimination of proteins-of-interest for phenotypic studies in vivo and stress the need for care in the selection of engineered degrons for use in studies of protein function.

## RESULTS

The LOV2 domain from plant phototropin 1 bearing an N-end rule targeted arginine domain directs light dependent loss-of-function phenotypes in yeast

### **a. Ura3p.**

As noted above, proteins carrying LOV-sensitive domains respond to various environmental stimuli by undergoing conformational changes [47,48]. We reasoned that if properly positioned at the amino terminus of a protein-of-interest, light-dependent unwinding of the  $\alpha$  helix within the LOV domain could act analogously to the temperature-dependent unfolding of DHFRts to facilitate degradation of the fusion protein by the N-end rule degradation pathway. Proteins with atypical N-terminal amino acid can be generated experimentally by expressing the protein-of-interest as in-frame fusions to the C-terminus of ubiquitin. Because the ubiquitin monomer is cleaved co-translationally through the action of a deubiquitinating enzyme [11,12,60], it does not mark the protein for proteasomal degradation and the amino acid immediately following the ubiquitin becomes the N-terminal residue of the fully translated protein.

Accordingly, we engineered constructs that would generate a protein bearing an N-terminal ubiquitin moiety followed by an arginine residue (R), which would correspond to the amino terminus after co-translational removal of ubiquitin. The arginine was followed by the 144 amino acid LOV2 domain of phototropin 1 from *Avena sativa* (phLOV2), a single in-frame copy of the HA epitope [61] and finally the coding sequence of the yeast orotidine-5'-phosphate decarboxylase protein, Ura3p, which is encoded by the URA3 gene. The basic structure of this Ubi-R-phLOV2-HA-Ura3p fusion protein and how it is presumed to direct

light-inducible degradation of Ura3p is depicted in Fig 1A and 1L, respectively. Because it was not known whether the addition of the R-phLOV2 element would render the fusion proteins too labile or too stable to detect phenotypic differences under dark versus illuminated conditions, we constructed additional plasmids to express versions of the protein in which putative stabilizing or destabilizing stretches of amino acids, from DHFR and DHFRts, respectively [11], were inserted between the R-phLOV2 domain and Ura3p. All of the constructs were generated using the plasmid backbone of pPW17R [11], a yeast centromere plasmid that expresses introduced genes under the control of the CUP1 copper-inducible promoter. However, because all three of these constructs behaved identically in the tests outlined below, only the results obtained in studies of the construct expressing U-R-phLOV2-HA-Ura3p, without additional DHFR or DHFRts sequences, are described below and shown in Fig 1.

The plasmid encoding Ubi-R-phLOV2-HA-Ura3p was introduced into YPH500, a UBR1 *ura3* mutant strain [62], and into its (Ubr1/N-recogin-lacking) mutant derivative, JD15 [11]. YPH500 and JD15 are the Ubr1-expressing and Ubr1-lacking strains used in all of the yeast studies in this work. In addition to the *ura3* mutation, this strain carries additional nutritional mutations enabling selection for the presence of plasmids introduced into these two yeast strains. The full genotypes of the two yeast strains are shown in the Materials and Methods section. The abilities of the introduced Ubi-R-phLOV2-HA-Ura3p plasmid to restore a Ura<sup>+</sup> phenotype to cells grown in the dark or under blue light illumination were examined. The plasmid conferred a Ura<sup>+</sup> phenotype on UBR1 *ura3* cells plated in the dark (Fig 1C, top row, first yeast patch), but failed to rescue the *ura3* mutant phenotype when

the cells were grown under blue light (Fig 1C, middle row, first yeast patch), provided that the yeast had initially been seeded on the plate in a single layer. When viewed microscopically, a Ura<sup>+</sup> phenotype (growth) was observed in the dark (Fig 1D), but, in contrast, blue light illumination led to arrest of growth, in many cases as single cells (Fig 1E). When introduced into the *ubr1Δ ura3* yeast strain, the plasmid conferred a Ura<sup>+</sup> phenotype in both dark and blue (and red) light conditions (Fig 1C, all rows, second yeast patch), indicating that the Ubr1 ubiquitin ligase protein is required for blue light-dependent loss of Ura3p activity. To show that the light-dependence was dependent on the presence of the LOV domain, we also tested a plasmid encoding Ubi-R-DHFR-HA-Ura3p [11], which conferred a Ura<sup>+</sup> phenotype that was not light dependent, in both *UBR1 ura3* and *ubr1Δ ura3* yeast strains (Fig 1C, all rows, yeast patches 3 and 4). The flavin-containing chromophore that elicits the light-dependent conformational change in the phLOV2 domain absorbs blue light specifically. To confirm that the light-dependent Ura<sup>-</sup> phenotype was specific to blue light, we grew *UBR1 ura3* cells bearing the Ubi-R-phLOV2-HA-Ura3p construct under red light and showed that they exhibited a Ura<sup>+</sup> phenotype (Fig 1C, bottom row, first yeast patch).

As an additional test of the role of the *A. sativa* LOV2 domain (i.e. phLOV2) in the light-dependence of Ura<sup>+/-</sup> phenotypes observed above, we also generated a plasmid encoding Ura3p with an N-terminal arginine residue and HA tag, but lacking the phLOV2 domain (Fig 1B). When introduced into *UBR1 ura3* host cells and placed under selection for synthesis of uracil, a Ura<sup>-</sup> phenotype (no growth) was observed in both dark conditions and under blue light illumination (Fig 1H and 1I). Conversely, when introduced into *ura3 ubr1Δ*

cells, the cells grew robustly in the absence of added uracil in both the dark and under blue-light illumination (Fig 1J and 1K). These observations strongly suggest that in the absence of the phLOV2 domain, the presence of a simple N-end rule-targeted amino terminus renders the Ura3p protein too unstable to support the synthesis of uracil. In the dark, the presence of the phLOV2 domain immediately C-terminal to an amino terminal arginine residue stabilizes Ura3p against constitutive degradation by the N-end rule pathway. Upon blue light illumination, the phLOV2 domain presumably unfolds and this stabilizing effect is lost.

We also generated constructs analogous to the ones described above in which the LOV-domain-containing *Neurospora crassa* circadian clock regulator Vivid [50,51] or its LOV domain alone (vvdLOV), both bearing N-terminal arginine residues, substituted for the phLOV2 domain from *A. sativa* carrying an amino terminal arginine. However, as the ability of these constructs to supply Ura3p activity did not differ under blue light versus darkness, they were not pursued further in these studies.

The results outlined above, as well as data to be described below, demonstrate that the Ubi-R-phLOV2 cassette represents a transferrable element that, when attached to heterologous proteins at their N-terminus, can confer rapid, blue light- and Ubr1/N-recognin-dependent N-end rule mediated degradation. This degradation is sufficient to produce a loss-of-function phenotype. This forms the basis for naming the element the photo-N-degron (PND). Fig 1L shows a schematic representation of the envisioned process through which

the PND bearing an N-terminal arginine residue is generated and leads to degradation of protein to which it has been fused.

#### **b. yEmRFP.**

In order to explore the ability of the PND cassette to direct the loss of other proteins, we added it in-frame to the amino terminus of yEmRFP [63] (Fig 2A), a version of the mCherry mRFP variant that is optimized for yeast codons. As described above for Ura3p, this construct was carried on the plasmid backbone obtained from the pPW17R yeast centromere plasmid and expressed in the YPH500 (UBR1) and JD15 (*ubr1*Δ) strains under blue light illumination and in darkness. As a control, a construct expressing N-end rule-targeted Arg-yEmRFP lacking the phLOV2 domain was expressed under the same conditions (Fig 2B). As the yEmRFP protein confers no selective advantage or disadvantage upon yeast cells, patches of UBR1 and *ubr1*Δ cells expressing either PND-yEmRFP or Arg-yEmRFP grew up robustly under either blue light illumination or in darkness.

UBR1 cells expressing PND-yEmRFP exhibited easily detectable levels of red fluorescence when grown in the dark (Fig 2C). In contrast, under blue light illumination the fluorescence was almost undetectable (Fig 2D). In the *ubr1*Δ mutant strain, there was no significant difference in the fluorescence levels between dark and blue light conditions (Fig 2E and 2F). Thus, PND-yEmRFP exhibited blue light and UBR1-dependent loss of fluorescence. No difference in fluorescence was observed between dark and blue light conditions in yeast expressing R-yEmRFP (Fig 2G and 2H), indicating that the presence

of the PND cassette was responsible for the light-dependent effect seen in Fig 2C and 2D. Similarly, when grown in the *ubr1* $\Delta$  strain there was no light-dependent change in fluorescence associated with R-yEmRFP (Fig 2I and 2J). It is notable, however, that in the UBR1 background, cells expressing R-yEmRFP exhibited stronger fluorescence than did cells expressing PND-yEmRFP (note the differences in exposure time between Fig 2C and 2G). This suggests that unlike the situation observed for Ura3p, in which the simple amino terminal R-tagged protein version was apparently less stable than the PND-tagged version of Ura3p, the amino terminal R-tagged version of yEmRFP appeared to be more stable than the PND-tagged form.

### **c. Cdc28p.**

To investigate whether the blue light-induced loss of PND-containing proteins could rapidly produce a mutant phenotype such as cell cycle arrest, we generated UBR1 and *ubr1* $\Delta$  strains bearing PND-tagged versions of the Cdc28p cell cycle regulatory protein. CDC28 encodes a cyclin-dependent kinase that has multiple roles in the *S. cerevisiae* cell cycle [64]. Temperature-sensitive mutants of *cdc28* grown at non-permissive temperature [64,65], or cells in which the expression of a dominant negative version of Cdc28p have been expressed [66], arrest in the G1 phase of the cell cycle in an unbudded state. Cell growth continues, however, resulting in enlarged cells, including ones with long outgrowths, similar to the phenotype of cells exposed to mating pheromone [67]. For these experiments, we introduced the gene construct on the plasmid backbone derived from the yeast integrating plasmid, pPW66R [11]. After a homologous recombination event, the endogenous CDC28 gene was interrupted by an insertion of the plasmid that also

introduced a PND-HA-tagged version of CDC28 under the transcriptional control of the CUP1 copper-inducible promoter (Fig 3A).

UBR1 cells expressing PND-Cdc28p that were plated in a single layer and incubated under illumination failed to generate colonies and were often arrested as individual cells (Fig 3C). Many of these cells exhibited the phenotype described above for TS mutants of *cdc28* grown at non-permissive temperatures [11,65] and for cells expressing the dominant-negative CDC28p [11,65,66]: enlarged cells, many with long outgrowths (Fig 3C). In contrast, when these cells were plated and incubated in the dark, they exhibited robust growth (Fig 3B), as did *ubr1* $\Delta$  cells expressing PND-HA-Cdc28p grown under both dark (Fig 3D) and light (Fig 3E) conditions. These cells exhibited normal size and morphology and many exhibited buds, consistent with normal growth and cell division. These results demonstrate that the PND tag directed blue-light dependent loss of Cdc28p activity that was rapid and sufficient to produce a cell cycle arrest phenotype.

### **THE PND DIRECTS LIGHT-DEPENDENT PROTEIN DEGRADATION**

The results reported above strongly suggest that upon exposure to blue light, the PND facilitates Ubr1p-dependent ubiquitination of the fusion protein and its subsequent proteasomal degradation. To test directly whether the PND-dependent loss-of-function phenotypes were associated with protein loss, we carried out Western blot analysis of PND-HA-Cdc28p expressed under light or dark conditions. Starting with a fresh overnight culture grown in the dark, a small volume was inoculated into liquid selective medium and grown in darkness to early log phase (an optical density [OD] of approximately 0.2). At

this point ( $T = 0$ ), the culture was divided in half, with one culture continuing to grow in darkness while the other was grown under blue light illumination. Samples were taken at  $T = 0$  and 5 subsequent hourly time points and processed for Western blotting.

As can be seen in Fig 4B, following exposure to light, the amount of PND-HA-Cdc28p in UBR1 cells decreased markedly in the first hour after exposure and remained at a low level for at least 5 hours. In contrast, when those cells were grown in darkness, the level of PND-HA-Cdc28p levels remained stable throughout the course of the experiment (Fig 4A). As expected, *ubr1* $\Delta$  cells expressed a steady level of PND-HA-Cdc28p when grown in the dark or under illumination (Fig 4C and 4D). Thus, the Ubr1p- and light-dependent loss of Cdc28p activity observed in UBR1 *ura3* cells was associated with a significant loss of PND-HA-Cdc28p, consistent with its light-dependent ubiquitination and degradation.

It has been shown for some proteins that the N-end rule degradation occurs post-translationally. For others, however, the presence of a destabilizing N-end, together with other protein-specific properties, leads to considerable degradation of nascent peptides in the process of translation (i.e. co-translational degradation) [68]. We realized that if the PND element were primarily facilitating the degradation of nascent proteins during translation, its utility as a method for producing loss-of-function phenotypes would be considerably constrained. To investigate this possibility, we examined light-mediated loss of PND-HA-Cdc28p in UBR1 *ura3* cells grown in the presence and absence of the translational inhibitor cycloheximide. These experiments were carried out on a much shorter timescale than those described above, with cycloheximide added at  $T = 0$  and

samples taken every 15 minutes following the onset of illumination. Loss of PND-HA-Cdc28p from UBR1 ura3 cells grown under illumination was rapid (Fig 5B), with most of the protein lost within 15 minutes after the onset of illumination. If the degradation of PND-HA-Cdc28p were occurring solely or primarily during translation, in cells in which translation was inhibited by cycloheximide there should be no marked difference in degradation rates seen in dark versus blue light conditions. In the presence of cycloheximide, there was still a rapid light-induced loss of PND-HA-Cdc28p (Fig 5D) that was not seen in dark conditions (Fig 5C), indicating that the degradation was not dependent upon concomitant translation. While this analysis does not rule out the possibility that some nascent PND-HA-Cdc28p undergoes Ubr1-mediated degradation during translation, it conclusively demonstrates that mature, full-length PND-HA-Cdc28p protein undergoes rapid degradation upon exposure to light, which allows the loss-of-function phenotype of *cdc28* to appear soon after the onset of illumination. The rapidity with which a PND-directed loss-of-function phenotype can be detected for a given protein, or indeed the rapidity with which the loss-of-function phenotype directed by any conditional degron can be detected, depends upon the rate of depletion of mature protein from the cells. Insofar as different proteins exhibit different intrinsic stabilities, this must be detected empirically for any protein-of-interest. Those proteins which exhibit both rapid degron-dependent co-translational degradation and rapid degradation of mature, synthesized protein are likely to be the best subjects for analysis using the PND as well as other conditional degrons.

Taken together, our analysis of the light-dependent loss of PND-HA-Cdc28p conclusively demonstrates that the PND represents a transferrable element that can confer rapid, blue

light-dependent degradation of heterologous proteins via the N-end rule pathway, at least for some proteins. The rapid nature of PND-mediated degradation and the lack of significant levels of target protein perdurance are demonstrated by Western blot analysis and by our observations that UBR1 cells expressing either PND-HA-Ura3p or PND-HA-Cdc28p under selective conditions often arrested as single cells under blue light illumination (Figs 1E and 3C), indicating that levels of protein required for function were depleted within one cell division cycle.

### **THE PND AND THE B-LID DOMAIN DIRECT BLUE LIGHT-DEPENDENT PROTEIN LOSS-OF-FUNCTION AND DEGRADATION IN DROSOPHILA EMBRYOS**

Having demonstrated the effectiveness of the PND in eliciting light-dependent degradation in yeast, we were then interested to test the extent to which it could be used to generate light-dependent phenotypes in a multicellular organism. Accordingly, we examined the effects of the PND upon a modified version of the *Drosophila* dorsal-ventral (DV) patterning protein Cactus [69–71]. In early embryos produced by wild-type females, Cactus is distributed throughout the cytoplasm, where it binds to the Dorsal protein [69,71–73] and prevents it from entering the nucleus. Cactus undergoes graded ubiquitin/proteasome-dependent degradation along the DV axis in response to Toll receptor signaling on the ventral side of the embryo [74–76], thus releasing Dorsal to enter nuclei in a graded manner [77–79] with highest nuclear Dorsal levels on the ventral side of the embryo. Toll signaling and Cactus degradation occur over a brief time window during the syncytial blastoderm stage of embryogenesis, which makes Cactus an ideal candidate for testing the ability of

the PND to elicit protein degradation and consequent loss-of-function phenotypes. We generated a transgene in which the PND-HA region was fused to the amino terminus of a modified version of Cactus [Cactus(3ala)] [80], in which serines 74, 78, and 116 have been converted to alanine residues (Fig 6A). Cactus(3ala) is insensitive to Toll receptor-dependent phosphorylation, ubiquitination, and degradation. As a result, it binds constitutively to Dorsal protein, inhibits its nuclear uptake and is therefore dominantly dorsalizing. Accordingly, from this point we refer to Cactus(3ala) as CactDN (for Cactus Dominant Negative, owing to its dominant negative effect upon Dorsal function and DV patterning) and the PND-HA-tagged version as PND-HA-CactDN.

Several transgenic lines carrying PND-HA-CactDN (Fig 6A) were generated and the transgenes expressed under the control of the female germline-expressed Gal4 driver, nanos-Gal4:VP16 [81]. The hatch rates of embryos associated with four independent insertions of the PND-HA-CactDN-bearing transgene were pooled. Because CactDN is dominantly dorsalizing, we expected that dark-reared embryos derived from mothers carrying PND-HA-CactDN would have a very low hatch rate. Consistent with this prediction, all embryos failed to hatch. In contrast, 90.4% of the embryos that were exposed to blue light starting within 1 hour of egg deposition and reared at 25°C hatched (Table 1). As noted above, the embryos cultured in darkness failed to hatch and these embryos were dorsalized (see below).

During the course of these studies, reports appeared which described the analysis of two other light-dependent degrons that rely upon the plant phototropin 1 LOV2 domain.

Renicke et al. [56], engineered a photosensitive degron (psd), comprised of the phLOV2 from *Arabidopsis thaliana* combined with a synthetic peptide similar to the ubiquitin-independent degradation signal from murine Ornithine Decarboxylase (ODC) [82–84]. Proteins carrying the psd at their carboxy termini exhibited blue-light dependent degradation in yeast. Bongers et al. [26] showed that a four amino acid long peptide, arg-arg-arg-gly, when fused to the carboxy terminus of a protein-of-interest, led to rapid proteasome-mediated degradation in mammalian cells. This degron was combined with a modified version of the *Avena sativa* phLOV2 domain and showed that this blue light-inducible degradation (B-LID) domain could confer light-dependent degradation upon proteins in both cultured mammalian cells and zebrafish embryos [26,57]. To examine the effectiveness of these two degrons in *Drosophila*, we generated constructs and transgenic lines in which the psd and the B-LID domain were fused in-frame to the carboxy terminus of CactDN, referred to as CactDN-psd and CactDN-B-LID respectively (Fig 6B and 6C).

As was observed for PND-HA-CactDN, all of the CactDN-B-LID embryos that were cultured in the dark failed to hatch, while 84.8% of the embryos that were reared under blue light starting within 1 hour of egg deposition did hatch (Table 1).

When reared in darkness, none of the CactDN-psd embryos hatched. Similarly, when reared under the same blue light illumination conditions that had resulted in hatching PND-HA-CactDN and CactDN-B-LID embryos, no CactDN-psd hatchlings were observed (Table 1).

Dorsalized embryos can be classed as falling into the following classes, based on the severity of the phenotype, which is determined based on the cuticular pattern elements present or absent as follows (Classifications are from Roth et al. [69], with modifications. See Fig 7 for representative phenotypes): completely dorsalized, lacking any dorsal/ventral polarity, D0; strongly dorsalized, D1; moderately dorsalized, D2; and weakly dorsalized, D3. The designation UH, seen in Fig 7 and Table 2, denote unhatched but otherwise, apparently normal embryos.

Both PND-HA-CactDN-expressing and CactDN-B-LID-expressing embryos exhibited dorsalized phenotypes when cultured in the dark. As noted above, when grown under illumination, most PND-HA-CactDN embryos hatched. In contrast, when they were grown in darkness the majority of these embryos exhibited either a moderate (D2) or weakly (D3) dorsalized cuticular phenotypes (Table 2). Despite some line-to-line variability, presumably owing to different levels of expression, for 8 of the 9 transgenic lines for which unhatched, dark-incubated embryos were counted and categorized, the largest cohort of embryos exhibited a D3 phenotype, followed by the cohort of embryos exhibiting a D2 phenotype. The small number of light-exposed embryos that remained unhatched also included moderately and weakly dorsalized embryos (data not shown). Similarly, while most CactDN-B-LID embryos grown under illumination hatched, the embryos grown in darkness exhibited phenotypes ranging from completely dorsalized (D0) to weakly dorsalized (D3), with the largest number of embryos exhibiting a strongly dorsalized (D1) phenotype. This was the case both collectively and for the majority (6) of individual lines tested (9). In 2 of the 9 lines, D2 embryos were the largest cohort, while in one line, D0

embryos made up the largest cohort. Thus, despite the range in phenotypes among dark-grown embryos, CactDN-B-LID appears to be a more effective inhibitor of Dorsal protein function than PND-HA-CactDN; consequently, a lower proportion of illuminated CactDN-B-LID embryos hatch.

Because no CactDN-psd embryos exposed to light hatched, in order to determine whether light had any influence over the CactDN-psd protein, we compared the phenotypes of unhatched embryos grown under illumination with that of dark grown embryos (Table 2). In both cases, the majority of embryos exhibited a completely dorsalized D0 phenotype (in 18/18 transgenic lines tested). A small decrease in the proportion of D0 embryos and a small increase in the proportions of D1 and D2 embryos were observed in the embryos that were exposed to light (in 10/18 lines tested). However, if the trend observed for the effect of the three degrons upon CactDN were extended to other proteins-of-interest in *Drosophila*, the level of phenotypic changes elicited by the psd would be unlikely to be useful in phenotypic studies. However, as noted above in our studies of Ura3p and yEmRFP, bearing either an amino terminal PND or an amino terminal arginine residue, different degrons can elicit different levels of stability, in a protein dependent manner. Therefore, we cannot rule out the possibility for other proteins expressed in *Drosophila* embryos or other tissues, the psd may provide useful light-dependent changes in activity.

We also carried out Western blot analysis to assess the effect of blue light exposure upon protein levels of the PND-HA-CactDN and CactDN-B-LID transgenes and to examine how the embryonic phenotypes correlated with protein levels. Western blot analysis of extracts

of embryos produced by PND-HA-CactDN- and CactDN-B-LID-expressing females was consistent with efficient light-dependent degradation of these two proteins (Fig 8). For each of these two constructs, extracts were generated from 2–4 hour-old embryos that had either been subjected to blue light illumination or allowed to develop in darkness. In order to avoid detection of the endogenous Cactus protein, Western blots of PND-HA-CactDN-expressing extracts were probed with an anti-HA antibody. Owing to the absence of the HA tag in CactDN-B-LID, an antibody directed against Cactus was used to probe blots bearing that fusion protein. Although the expected molecular weight of wild-type Cactus protein is 53.8 kD, it has been demonstrated that Cactus protein migrates on SDS-PAGE gels with an apparent molecular weight of 69–72 kD [72]; Developmental Studies Hybridoma Bank, University of Iowa). That, together with the addition of the PND or the B-LID domain, was therefore expected to generate mature proteins of approximately 88–91 kD. Extracts from 2- to 4-hour old PND-HA-CactDN embryos that had been laid and incubated in the dark exhibited the presence of a band of approximately 90 kD, corresponding to PND-HA-CactDN, which disappeared in embryos incubated under illumination (Fig 8A). Similarly, extracts from 2- to 4-hour old CactDN-B-LID-expressing embryos from two independent transgenic lines exhibited a loss of the protein band corresponding to CactDN-B-LID in response to illumination (Fig 8B). Although the extent of protein loss differed between the two transgenic lines, presumably due to differences in expression between the two lines tested, in both cases a marked decrease in levels of CactDN-B-LID protein was detected in the extracts of light-exposed embryos, in comparison to their dark-incubated counterparts.

In order to more directly assess the phenotypic consequences of degron-mediated loss of CactDN activity, live imaging of embryos was carried out to visualize the behavior of fluorescent GFP-tagged Dorsal protein [85] expressed under the control of the endogenous dorsal gene transcriptional regulatory elements, together with each of the three degron-tagged versions of CactDN (Figs 9 and 10). Illumination of embryos with a blue laser (488nm) was performed to manipulate the degron-tagged proteins, enabling comparison of the dynamics of Dorsal nuclear accumulation controlled by PND-HA-CactDN, CactDN-B-LID, and CactDN-psd. In these experiments, the protein levels and activities were expected to vary depending on the length of exposure, the intensity of light, and the intrinsic stability of the degron fusion proteins, thus requiring optimization of the conditions of illumination. In this way, it was determined that embryos exposed to more than 20 min of high power 488nm wavelength light displayed developmental defects likely due to phototoxicity unrelated to effects upon DV patterning. Accordingly, in these experiments, embryos were first allowed to develop under low power (3.1%) 488nm laser illumination until early nuclear cycle (nc) 12. Embryos were then illuminated with blue light (488nm) for 20 minutes at 10% laser power (high power), a condition that permitted perturbation of CactusDN activity without eliciting phototoxicity. After 20 minutes of illumination, the embryos were returned to low power 488nm laser illumination in order to limit further degradation of the degron-tagged CactDN proteins. In addition to activating the LOV domain chromophore associated with the light-dependent degrons, 488 nm light is also absorbed by and leads to emission by GFP. Nevertheless, 20 minutes of high power 488 nm laser light exposure did not result in Dorsal-GFP photobleaching that precluded its subsequent visualization.

Control embryos expressing Dorsal-GFP exhibited the formation of a normal Dorsal-to-Ventral nuclear gradient of the fusion protein (Fig 9B–9B''' and S1 Movie), even under blue-light illumination (Fig 9B' and 9B''). Prior to illumination at nc12, a point at which Dorsal-GFP had begun to enter the nuclei of the otherwise wild-type embryo (Fig 9B), embryos expressing each of the degron-tagged versions of CactusDN exhibited a perturbation of Dorsal-GFP nuclear uptake (Figs 9C, 9D, 9E, 9F, 10A, and 10B). In PND-HA-CactusDN- and CactusDN-B-LID-expressing embryos that were exposed to low power 488nm laser light, Dorsal-GFP remained predominantly cytoplasmic through nuclear cycles 12–14 (Fig 9D–9D''' and S3 Movie, and Fig 9F–9F''' and S5 Movie), a phenotype which is explained by the continuing presence of degron-tagged CactusDN protein; however, transient and sporadic low levels of nuclear Dorsal-GFP were observed at nc13 and nc14, likely owing to a slow rate of degradation of degron-tagged CactusDN occurring in the presence of low intensity blue light. These low levels of nuclear Dorsal-GFP are consistent with the dorsalized cuticular phenotypes observed for most dark-cultured PND-HA-CactusDN and CactusDN-B-LID embryos (Table 2). In contrast to their low power-illuminated counterparts, PND-HA-CactusDN- and CactusDN-B-LID-expressing embryos that were exposed to high power blue laser light exhibited nuclear accumulation of Dorsal-GFP during nc13 (Fig 9C' and S2 Movie, and Fig 9E' and S4 Movie, respectively) and by nc14, these embryos exhibited conspicuous ventral-to-dorsal nuclear gradients of Dorsal-GFP (Fig 9C'' and S2 Movie and Fig 9E'' and S4 Movie). By stage 6 of embryogenesis, ventral cells within these embryos began to display normally polarized cell movements (Fig 9C''' and 9E'''), consistent with the onset of ventral furrow formation. The normal polarization of nuclear Dorsal-GFP accumulation and cell movements is presumably due to the loss of

degron-tagged CactDN protein, enabling endogenous wild-type Cactus protein to engage with and control Toll receptor signal-mediated nuclear uptake of the Dorsal-GFP fusion protein. Together, the comparable nature of phenotypes observed via confocal microscopy coupled with laser illumination, and by cuticle preparations following overhead blue-light illumination with a grid of LED bulbs strongly supports the use of the PND and the B-LID domain as effective tools for controlled elimination of targeted proteins-of-interest in *Drosophila* embryos. Moreover, the observation of substantial nuclear accumulation of Dorsal-GFP as early as 1 minute after high power blue light illumination (see Fig 9E' and S4 Movie, which was obtained 1 minute after the onset of high-power blue laser light illumination) demonstrates the utility of these elements for the analyses of loss-of-function phenotypes requiring fine time resolution and/or rapid onset.

As noted above, in CactDN-psd-expressing embryos that were not exposed to high power blue light, Dorsal-GFP protein was never detected predominantly in nuclei (Fig 10B–10B''' and S7 Movie), consistent with the completely dorsalized cuticular phenotypes exhibited by CactusDN-psd cultured in darkness (Fig 7A). Dorsal-GFP was also present predominantly in the cytoplasm of illuminated CactDN-psd embryos (Fig 10A, 10A', and 10A'''' and S6 Movie, and Fig 10C and 10C'' and S8 Movie) consistent with the cuticular phenotypes and with a greater stability, lower sensitivity to blue light, and/or slower rate of degradation than either PND-HA-CactDN, or CactDN-B-LID. However, these embryos did exhibit a brief cell cycle-dependent period of Dorsal-GFP nuclear localization of about 1–2 minutes immediately prior to the mitoses of nuclear cycles 13 and 14 (Fig 10A'', 10C', and 10C''', and S6 and S8 Movies). These results may indicate that in the embryo, where

the relatively stable CactDN-psd is continuously being translated from maternally provisioned mRNA, the high intensity blue light provided by a laser is sufficient to eliminate enough CactDN-psd by the end of a nuclear cycle to allow Dorsal-nuclear uptake on the ventral side of the embryo, with continued synthesis of CactDN-psd following mitosis again being sufficient to sequester Dorsal-GFP in the cytoplasm. Alternatively, these particular conditions may reveal a previously unappreciated cell cycle-dependent enhancement of either Dorsal nuclear uptake, or of psd-mediated proteasomal degradation immediately prior to mitosis in early *Drosophila* embryos. A conclusive explanation of these events requires the development of a fluorescently-tagged version of CactDN-psd that would permit direct live imaging of the behavior of this protein in response to blue laser light.

Based on the observations reported above, both the PND and the B-LID domain confer easily distinguished light-dependent phenotypes when fused to CactDN and therefore exhibit promise for use in the analysis of phenotypes associated with loss-of-function for other proteins, at least in the context of the early embryo. In view of the current discrepancy in phenotypes elicited in CactDN-psd in response to incident versus laser illumination, we cannot currently conclude that the psd element is a generally useful tool for studies aiming at perturbing the action of tagged proteins-of-interest in *Drosophila* embryos. However, when fused to other proteins, expressed in other tissues, or under different treatment regimens, the psd might direct useful, light-dependent changes in protein levels and function.

## **DISCUSSION**

Our studies clearly demonstrate that the Photo-N-degron can be a valuable tool for the generation of conditional loss-of-function phenotypes in yeast. Previous reports describing the psd [56] and the B-LID domain [56,57] provided us with the opportunity to compare the effectiveness of the obligately N-terminal PND with that of the obligately C-terminal psd and the B-LID domain, in mediating light-dependent degradation of our model protein Cactus in *Drosophila* embryos. Insofar as the addition of an N- or C-terminal extension can disrupt the function of some proteins, the availability of light-dependent degrons that can function at either the N- or C-termini of proteins increases the versatility and likelihood of success for investigations involving light-mediated protein degradation. Our analyses indicate that the PND that we developed, as well as the B-LID domain, but not the psd, are capable of simply and effectively mediating temporally-specific elimination of CactDN within the single cell syncytial blastoderm embryo.

One advantage of light-induced degrons is that they can act rapidly and allow much greater temporal control than degrons regulated by the application or depletion of small molecules or by the induced expression of protein activators. Moreover, exposure to blue light is unlikely to produce the changes in enzyme or cellular behavior that changes in temperature are likely to engender. However, our attempts to determine the extent to which the light-dependent degrons can mediate precise spatially-restricted protein degradation using CactDN as a target have been inconclusive. Further studies, likely involving other protein

targets, are necessary to resolve this issue. However, subcellular resolution employing lasers to provide illumination [39,40] has been demonstrated with a variety of other optogenetic techniques, so there is reason for optimism that light-dependent degrons may also be able to provide fine spatial resolution of protein degradation.

A potential drawback to the light-inducible degron approach is that the target cells/tissues must be accessible to light. In our experiments using PND-tagged Ura3p and Cdc28p in yeast cells grown on agar plates for example, strong loss-of-function phenotypes were only detected when cells were distributed in a single layer and illuminated. Light-dependent degrons have been shown to be effective for phenotypic analysis in single cells [56,57] and in transparent organisms such as the nematode *Caenorhabditis elegans* [86] and the zebrafish [57]. In addition to yeast cells, our studies indicate that *Drosophila* eggs/embryos are sufficiently transparent to enable phenotypic studies of the effects of protein loss using light-dependent degrons. The use of light-dependent degrons in organisms that are not transparent is likely to be more technically challenging. However, optogenetic studies involving light-activated ion channels have been carried out in mice using fiberoptic delivery of blue light or small wirelessly powered light-emitting implants [87–90], suggesting this approach might be applied to the use of light-activated degrons.

In our studies of degron-tagged CactDN, the fusion proteins were not supplying normal Cactus function but rather were exerting dominant negative inhibition on Dorsal nuclear localization leading to embryo dorsalization. For most applications, we envision a more conventional use of these degrons that would involve the introduction of a functional

degron-tagged version of protein-of-interest substituting for the corresponding endogenous gene, similar to our analysis of degron-tagged versions of Ura3p and Cc28p in yeast. In this context, blue light-mediated degradation of the degron-tagged protein would reveal the loss-of-function phenotype of the protein-of-interest. This would require that the degron-tagged version of the protein retain sufficient functional activity to be able to rescue the mutant phenotype to viability in the dark and to exhibit sufficient sensitivity to light for function to be eliminated or strongly diminished under illumination.

A variety of factors should be considered when utilizing light-dependent or other classes of conditional degrons in an experimental context. As noted above, the first consideration is the position at which the degron will be placed in the protein-of-interest. Currently, possible locations are limited to the N- or C-termini of proteins-of-interest. However, degrons that can be introduced at internal sites within proteins may be developed in the future. Secondly, individual proteins can exhibit widely different intrinsic stabilities, with mammalian proteins exhibiting half-lives ranging from 10 minutes to over a century [91,92], and they can behave differently when tagged with particular degrons. Our studies of CactDN in *Drosophila* embryos show that different degrons can influence the stability of the same protein to different extents, even in the uninduced state. While CactDN-psd led to complete dorsalization of expressing embryos under dark conditions, indicating that the degron-tagged protein is very stable, PND-HA-CactDN did not. Under dark conditions, most embryos expressing this construct exhibited only weak or moderate dorsalization. It is likely that the presence of an N-end arginine residue destabilizes CactDN to some extent, even under dark conditions. Similarly, only 13.7% of embryos expressing CactDN-B-LID

under dark conditions produced completely dorsalized DO embryos, indicating some B-LID domain-dependent degradation of the fusion protein even in the dark. In addition to the choice of degron used in a particular study, these observations also have important implications for how degron-tagged proteins should be expressed in experimental investigations. The advent of CRISPR/Cas9-directed approaches for gene replacement [93,94] provides the opportunity to simultaneously eliminate endogenous gene (and protein) expression while placing the degron-tagged version of the gene under correct spatial and temporal control of transcription. Moreover, the availability of these CRISPR/Cas9-dependent gene replacement approaches make possible similar conditional phenotypic studies using degron-tagged proteins in non-traditional model organisms [95–98]. However, as the addition of a degron to the protein-of-interest is likely to reduce the stability of that protein in comparison to its wild-type counterpart even in the absence of illumination, the expression levels of the degron-tagged protein by the CRISPR/Cas9-introduced gene may be insufficient to provide wild-type levels of rescuing protein. In such cases, an alternate approach for expression may be necessary, in which the rescuing degron-tagged protein is transcribed at higher than endogenous levels, in a genetic background homozygous for loss-of-function alleles of the corresponding endogenous gene. In support of this possibility, our recent study found that while Dorsal-B-LID fusions exhibited effective photosensitive degradation [99], the expression levels of the CRISPR-introduced construct were lower than that of the endogenous protein with embryonic phenotypes suggesting that some degradation of the protein was occurring in the absence of illumination.

It is not yet clear whether the behavior of CactDN, under the influence of the three light-dependent degrons reflect differences in the intrinsic stabilities of the fusion proteins, or differences in the rates and/or effectiveness of the ubiquitin/proteasomal pathways targeting their degradation, or both. The three degrons present in these constructs are targeted by different pathways leading to proteasomal degradation. PND-directed protein degradation operates via the Ubr/N-recogin class of ubiquitin E3 ligases [15–17]. The structure of the B-LID domain suggests that its degradation is mediated by the DesCEND (Destruction via C-end degrons) mechanism, via Cul2, a RING domain-containing ubiquitin ligase, together with an Elongin B/C protein [26,100,101]. The psd is similar to the destabilizing element present in mouse ODC [82–84], a very labile protein that undergoes proteasome-mediated degradation that is independent of ubiquitin. This lability likely results from its lack of a stable structure, together with the presence of a cysteine-alanine rich domain that is involved in recognition by the proteasome [102–104]. More recently, however, it has been shown that the light-activated degradation of some psd-tagged ER transmembrane proteins as well as some psd-tagged soluble cytoplasmic proteins is dependent upon the ERAD-C and its associated ubiquitination machinery [105,106]. Accordingly, experimental utilization of any individual degron will require the presence of the relevant degradation machinery in the cells in which the protein-of-interest is to be targeted for elimination.

Based on our studies, experiments designed to eliminate proteins-of-interest in early *Drosophila* embryos would be more likely to be informative if either the B-LID domain or the PND were utilized, at least under the overhead LED illumination conditions used for embryos on plates. Though not effective in eliciting light-dependent degradation of CactDN in embryos, the extent to which the psd can elicit light-dependent degradation of other proteins, or in other tissues in *Drosophila*, remains to be determined. Effective degradation of some proteins under the control of the psd might require more intense blue light illumination provided by a laser. Alternatively, for proteins that are extremely labile, the psd might be optimal for the detection of robust differences in phenotype that are dependent upon blue light. It is worth pointing out that although the psd was not effective in eliciting the degradation of CactDN in *Drosophila* embryos illuminated on plates, in *C. elegans*, light-induced degradation of psd-tagged Synaptotagmin resulted in a robust reduction of locomotion within 15 minutes of illumination [86]; within one hour, worm behavior and patch-clamp recordings of miniature postsynaptic currents were affected almost to the same degree as observed in worm mutants for *snt-1*, a loss-of-function mutation in the gene encoding Synaptotagmin. As should be clear from the discussion above, a significant challenge to the application of inducible degron technology to the analysis of protein function is identifying an appropriate degron system that is "tuned" to the particular protein under study. Thus, the most effective degrons for different proteins and different tissues will vary and some initial empirical analysis will likely be required in identifying the right degron for the job.

## MATERIALS AND METHODS

### Yeast and *Drosophila* strains and maintenance

Yeast strains YPH500 (MAT $\alpha$  ade2-101 his3- $\Delta$ 200 leu2- $\Delta$ 1 lys2-801 trp1- $\Delta$ 62 ura3-52) and JD15 (MAT $\alpha$  ade2-101 his3- $\Delta$ 200 leu2- $\Delta$ 1 lys2-801 trp1- $\Delta$ 62 ubr1 $\Delta$ ::LEU2 ura3-52) were kind gifts of Dr. Jürgen Dohmen. Yeast were grown in liquid culture in either YPD or Synthetic Complete drop-out (SD) media with added supplements, but lacking those amino acids necessary for selection of introduced plasmid elements, or for selection for URA3 activity. Growth on plates was on YPD or SD media supplemented with 2% Bacto-agar. For the induction of genes under the control of the CUP1 promoter, Cupric sulfate was added to medium at a concentration of 0.1 mM using a 1000x stock solution (0.1M Cupric sulfate in water). Plasmids were introduced into yeast using the LiAc/SS carrier DNA/PEG method [107].

The wild-type *Drosophila melanogaster* strain used to generate transformant lines in this study was a w1118/w1118 mutant derivative of OregonR. Fly stocks were maintained and embryos collected employing standard conditions and procedures. The nanos-Gal4:VP16 transcriptional driver element is described in Van Doren et al. [81]. The mat- $\alpha$ 4-tub-Gal4:VP16 transcriptional driver element is described in Häcker and Perrimon [108]. The 25 kb transgene encoding dorsal-GFP under the control of the endogenous dorsal gene transcriptional elements is described in Reeves et al. [85].

## Plasmid constructs

### *Yeast.*

Plasmids pPW43 and pPW17R (both kind gifts of Dr. Jürgen Dohmen) are yeast centromere plasmids derived from plasmid pNKY48 [109], which bear sequences encoding the UBI-R-DHFRts N-degron, and its wild-type counterpart (UBI-R-DHFR), fused in frame to one copy of the HA epitope [61], followed by the Ura3p open reading frame. Transcription of the gene expressing the Ura3p fusion protein is driven by the copper-inducible CUP1 promoter. These plasmids served as the starting point for the engineering of constructs bearing the light-sensitive degron described in this work. Initially, both plasmids were restriction digested with NotI, and the cut ends filled in, followed by recircularization, resulting in the elimination of the unique NotI site in both plasmids, thus yielding pPW43-NotI- and pPW17R-NotI-.

Both of these plasmids were then subjected to mutagenesis by inverse PCR, followed by recircularization by ligation, using the following two oligonucleotides: /5'Phos/TCCGTGGCGGCCGCCTCTTAGCCTTAGCACAAGATGTAAG and /5'Phos/TCCGGCGGGCGCGCCATGGTTCGACCATTGAACTGCATCG, yielding the two plasmids pPW-UBI-R-NotI/AscI-DHFRts-HA-URA3 and pPW-UBI-R-NotI/AscI-DHFR-HA-URA3. This step placed the last two glycine codons of yeast ubiquitin and the subsequent arginine codon in the context of a NotI site and placed an additional AscI site between the NotI site and the sequences encoding DHFRts and DHFR, respectively. pPW17R-NotI- was also subjected to mutagenesis by inverse PCR, followed by recircularization by ligation, using the following two oligonucleotides:

/5'Phos/TCCGTGGCGGCCGCCTCTTAGCCTTAGCACAAGATGTAAG and  
 /5'Phos/TCCGGCGGGCGCGCCGGTACCTACCCA, yielding the plasmid pPW-UBI-R-  
 NotI/AscI-HA-URA3, from which the DHFR sequences had been excised.

The two oligonucleotides:  
 5'GGCTAAGAGGCGGCCGCTTGGCTACTACACTTGAACGTATTGAG and  
 5'CGAACCATGGCGCGCCCAAGTTCTTTTGCCGCCTCATCAATATTTTC were  
 used for high fidelity PCR amplification of a DNA fragment encoding 143 amino acid long  
 segment of the *A. sativa* phototropin 1 protein, encompassing the LOV2 domain, using a  
 DNA clone encoding the phot1 gene (a kind gift of Drs. Tong-Seung Tseng and Winslow  
 Briggs) as a template.

Similarly, the two oligonucleotides: 5'  
 GGCTAAGAGGCGGCCGCGAGCCATACCGTGAACCTCGAGCACCATG and  
 5'CGAACCATGGCGCGCCCTTCCGTTTCGCACTGGAAACCCATGCTG were used  
 for high fidelity PCR amplification of a DNA fragment encoding the 185 amino acid long  
*Neurospora crassa* Vivid protein [50] minus its initiation codon, but including its associated  
 LOV domain (vvdFL), using a vivid cDNA (a kind gift of Drs. Arko DasGupta, Jay Dunlap  
 and Jennifer Loros) as a template.

Similarly, the two oligonucleotides:  
 5'GGCTAAGAGGCGGCCGCCATACGCTCTACGCTCCCGGCGGTTATGAC and  
 5'CGAACCATGGCGCGCCCTTCCGTTTCGCACTGGAAACCCATGCTG were used  
 for high fidelity PCR amplification of a DNA fragment encoding a 150 amino acid long

stretch of *Neurospora crassa* Vivid protein lacking the first 36 codons, which corresponds to the region encoding the LOV domain (vvdLOV), using a vivid cDNA (a kind gift of Drs. Arko DasGupta, Jay Dunlap and Jennifer Loros) as a template.

The resulting amplification products were digested with NotI and AscI and ligated to similarly digested pPW-UBI-R-NotI/AscI-DHFRts-HA-URA3, pPW-UBI-R-NotI/AscI-DHFR-HA-URA3, and pPW-UBI-R-NotI/AscI-HA-URA3, yielding the following plasmids:

pPW-UBI-R-phLOV2-DHFRts-HA-URA3

pPW-UBI-R-vvdFL(for full-length)-DHFRts-HA-URA3

pPW-UBI-R-vvdLOV-DHFRts-HA-URA3

pPW-UBI-R-phLOV2- DHFR-HA-URA3

pPW-UBI-R-vvdF1-DHFR-HA-URA3

pPW-UBI-R-vvdLOV-DHFR-HA-URA3

pPW-UBI-R-phLOV2-HA-URA3 (= pPW-PND-HA-Ura3p)

pPW-UBI-R-vvdFL-HA-URA3

pPW-UBI-R-vvdFLOV-HA-URA3

yEmRFP is a yeast codon optimized version of the mCherry mRFP variant [63]. To generate a construct that expresses a PND-tagged version of yEmRFP the two oligonucleotides:

5'GTCACTGAGGCGCGCCATGGTTTCAAAAGGTGAAGAAGATAATATGGC and  
5' GGGTTATTTATATAATTCATCCATACCACCAG were used for high fidelity PCR amplification, using a cDNA encoding yEmRFP (a kind gift of D. Neta Dean) as a template. The resulting amplification product was digested with AscI and ligated to AscI/SmaI-digested pPW-UBI-R-phLOV2-HA-URA3. This resulted in the replacement of sequences encoding the HA tag and URA3 by the yEmRFP open reading frame, fused in frame to the PND, in plasmid pPW-PND-yEmRFP. The same AscI/SmaI digested PCR fragment was also ligated to AscI/SmaI-digested pPW-UBI-R-NotI/AscI-HA-URA3, again replacing the HA-tag and URA3 by the yEmRFP open reading frame, in this case generating an yEmRFP construct bearing an N-end rule targeted amino terminal arginine residue, but which does not contain the phLOV2 element (pPW-R-yEmRFP).

Plasmid pPW66R is a yeast integrating vector in which the sequences encoding the DHFRts N-degron have been placed upstream and in-frame with the sequences encoding the HA epitope tag and the first 95 codons of the CDC28 gene [11]. Recombination between the CDC28 sequences present on the plasmid and the endogenous chromosomal CDC28 gene results in the interruption of the endogenous CDC28 gene and its replacement by an DHFRts N-degron- and HA epitope-tagged version of the full-length 299 codon CDC28 gene, under the control of the CUP1 promoter. This recombination event also

results in the insertion of a wild-type version of the URA3 gene, permitting selection for chromosomal insertions on medium lacking uracil. pPW-UBI-R-phLOV2-HA-URA3(pPW-PND-HA-Ura3p) contains an AgeI/KpnI restriction fragment that includes the sequences encoding most of the ubiquitin protein and the entire LOV domain of the PND. Substitution of this AgeI/KpnI fragment for a corresponding fragment in pPW66R results in a precise replacement of the DHFRts N-degron by the PND. However, prior to carrying out this subcloning step, it was first necessary to eliminate a second KpnI site present in pPW66R. Accordingly, we carried out partial digestion of pPW66R with KpnI in the presence of ethidium bromide. Linear DNA obtained following this digestion was treated with Klenow enzyme in the presence of dNTPs to generate blunt ends, then recircularized by ligation, followed by screening for clones in which the correct KpnI site had been destroyed (pPW66R-1Kpn). The AgeI/KpnI DNA restriction fragment encoding the PND was isolated from pPW-PND-HA-Ura3p and ligated to AgeI/KpnI-digested pPW66R-1Kpn from which the DHFRts N-degron sequences had been excised, resulting in plasmid pPW66R-PND-HA-cdc28. This plasmid was linearized with MscI, which digests a site within the CDC28 gene, then transformed into both the YPH500 (UBR1 ura3) and JD15 (ubr1 $\Delta$  ura3) strains of yeast, and clones in which the plasmid had integrated into the endogenous CDC28 gene were identified for further analysis.

### *Drosophila.*

CactDN is a mutant version of the Cactus protein in which serines 74, 78, and 116 have been converted to alanine residues [80], rendering the protein insensitive to Toll receptor dependent phosphorylation, and subsequent ubiquitination and degradation. This protein

binds constitutively to the Dorsal protein, resulting in its sequestration in the cytoplasm.

Females expressing CactDN in their germlines produce embryos with a dominant-negative dorsalized phenotype. We reasoned that the expression of a PND-tagged version of CactDN in otherwise wild-type females would result in larvae that were dorsalized when early embryogenesis progressed in darkness, and normalized when embryos developed under illumination, owing to the degradation of CactDN, which would enable Dorsal to come under the regulation of endogenous wild-type Cactus protein. We generated a PND-tagged version of Cactus as follows:

First, the two oligonucleotides: /5'Phos/TGGCCGCTTGGCTACTACACTTGAACG and /5'Phos/CCTCTTAGCCTTAGCACAAGATGTAAGG were used for high fidelity inverse PCR-mediated in vitro mutagenesis of the plasmid pPW-UBI-R-phLOV2-HA-URA3, in order to eliminate the NotI site at the junction between the ubiquitin open reading frame and the arginine codon preceding the LOV2 domain. This yielded plasmid pPW-UBI-NotIminus-R-phLOV2-HA-URA3.

Next, the two oligonucleotides: 5'GATCGAGCGGCCGCAAAATGCAGATTTTCGTCAAGACTTTGACCGG and 5'GATCGAGGATCCCCTCCTAAAAATGCAGCGTAATCTGGAACATCG were used for high fidelity PCR, using pPW-UBI-R-phLOV2-HA-URA3 as a template, in order to generate an amplification product comprising the ubiquitin open reading frame, arginine codon, LOV domain, and HA tag. This amplification product was restriction-digested with NotI and BamHI and the DNA fragment encoding the PND was purified.

The two oligonucleotides:  
 5'ACGTACGGATCCGAGCCCAACAAAAGCAGCGGAGGC and  
 5'ACGTACGCTAGCTCAGGCAACTGTCATGGGATTGCCACCG were used for high  
 fidelity PCR, using a plasmid carrying the open reading frame corresponding to CactDN  
 [80] as a template. The amplification product was then restriction digested with BamHI  
 and NheI and the DNA fragment encoding CactDN purified.

Finally, the *Drosophila* germline expression vector pUASp [110], was digested with NotI  
 and XbaI and the larger fragment purified. This fragment was combined with the  
 NotI/BamHI PND fragment and the BamHI/NheI CactDN fragment, generating pUASp-  
 PND-HA-CactDN, in which the UBI gene, and the R-phLOV2, HA tag, and CactDN  
 coding sequences were present in-frame and under the transcriptional control of the Gal4  
 upstream activating sequences enhancer element. This plasmid was introduced into the  
*Drosophila* genome by conventional P-element-mediated transposition following  
 microinject of embryos at Rainbow Transgenics, Inc.

The psd (for photosensitive degron) [56] is comprised of the LOV2 domain from  
*Arabidopsis thaliana* phototropin 1 protein combined with a 23 amino acid in length  
 unstructured peptide from a synthetic degron [83] that was derived from a natural degron  
 present in murine ornithine decarboxylase [84]. In order to generate a version of CactDN  
 whose degradation was under the control of the psd, the two oligonucleotides:  
 5'ACTGACGGATCCGAGAGGTGAACAAAAGTTGATTTCTGAAGAAGATTTGAA

CGGTG and 5'CATGACACTAGTTATTGGAAGTACAAGTTTTTCAGAACCAGCC.

were used for high fidelity PCR, using a plasmid carrying sequences encoding a copy of the myc epitope tag in frame with the psd [56] (a kind gift of Christof Taxis). The amplification product was restriction digested with BamHI and SpeI and ligated to plasmid pUASp that had been restriction digested with BamHI and XbaI, resulting in plasmid pUASp-myc-psd. Next, the two oligonucleotides: 5'ACGTGATCGCGGCCGCAAATGCCGAGCCCAACAAAAGCAGCGGAGGC and 5'GATCGAGGATCCGCAACTGTCATGGGATTGCCACCGTTG were used for high fidelity PCR, using a plasmid carrying the open reading frame corresponding to CactDN as a template. The amplification product was then restriction digested with NotI and BamHI and ligated to similarly digested pUASp-myc-psd, yielding plasmid pUASp-CactDN-psd, in which the CactDN coding sequences, the myc epitope and the psd were present in-frame and under the transcriptional control of the Gal4 upstream activating sequences enhancer element. This plasmid was introduced into the Drosophila genome by conventional P-element-mediated transposition following microinject of embryos at Rainbow Transgenics, Inc.

The four amino acid sequence arg-arg-arg-gly (RRRG), fused to the C-terminus of a protein results in rapid proteasomal degradation of the protein in mammalian cells [26]. The combination of a mutated variant of the Avena sativa LOV2 core domain with the RRRG peptide resulted in the formation of a light-dependent degron, referred to as the B-LID domain [57].

In order to generate a version of CactDN whose degradation was under the control of the B-LID domain, the two oligonucleotides: 5'GACGAGCTGGATCCGACGCGTTTCTTGGCTACTACACTTGAACG and 5' GCGGATCGTCTAGACTAACCTCGCCGCCTTGCCGCCTCATC. were used for high fidelity PCR, using a plasmid carrying sequences encoding the B-LID domain, pBMN HAYFP-LOV24 (Addgene #49570) [57]. The amplification product was purified and restriction digested with BamHI and XbaI and ligated to similarly digested pUASp, yielding plasmid pUASp-B-LID. Subsequently, the NotI/BamHI digested DNA fragment encoding CactDN that is described above was ligated to similarly digested pUASp-B-LID, yielding pUASp-CactDN-B-LID, in which the CactDN and the B-LID domain sequences have been fused in-frame and have been placed under the transcriptional of the Gal4 upstream activator sequences enhancer element. This plasmid was introduced into the *Drosophila* genome by conventional P-element-mediated transposition following microinject of embryos at Rainbow Transgenics, Inc.

### **Examination of yeast phenotypes resulting from light exposure**

For yeast grown on solid medium, individual colonies carrying the constructs being tested were suspended in 100  $\mu$ l of sterile water and serial 10-fold dilutions were generated. 5  $\mu$ l droplets of each of the serial dilutions were applied to a petri dish containing appropriate selective media. The dilution that had resulted in the deposition of a single layer of separated cells, as observed under a dissecting microscope at 80X, was used to determine

the phenotypic consequences of light exposure. Over the course of these studies, it became apparent that in order to achieve reliable determinations of the light-dependent phenotypes of yeast carrying the PND-tagged Ura3p and Cdc28p constructs on plates, it was necessary to plate those yeast strains in a single layer on the agar surface. These observations indicated that when cells were plated at higher density, in more than a single layer, the cells at the surface shielded underlying cells from light exposure. Plates were incubated at 30°C (cover side up) at a distance of 6 cm from a Blue 225 LED 13.8 Watt/110 Volt Square Grow Light Panel (LEDwholesalers 2501BU) and examined after 24 and 48 hours of incubation. Control replica plates were incubated in a light/tight container in the same incubator. To test the effects of red light on yeast cell phenotypes, similar plates were grown under a Red 225 LED 13.8 Watt/110 Volt Square Grow Light Panel (LEDwholesalers 2501RD) and examined after 24 and 48 hours, again in tandem with duplicate plates that were grown in a light/tight container.

### **Western blot analysis of PND-Cdc28p expressed in yeast**

For yeast grown in liquid culture, overnight cultures of cells were grown up in 6 mls of SD medium with appropriate selection. The next morning, a small volume of the culture was diluted into 200 mls of selective SD medium to achieve an OD between .06 and .08. The 200 mls were divided into four 50-ml cultures in 250 ml baffled Erlenmeyer flasks and grown with shaking (200 rpm) at 30° C in the dark for 4–6 hours. The cultures were combined and the OD measured. The experiment was started when the OD was between 0.1 and 0.2. At time 0 an initial sample was taken that corresponded to ~5 ODs, and the remaining culture was divided evenly between the four flasks. For the time course

experiments, the two flasks containing the cultures to be grown in the dark were covered in foil. To provide illumination for the cultures to be grown in the light, a White and Blue High-Power LED Aquarium light, (2518W+B, LEDwholesalers) was suspended 18 cm above the platform on which the culture flasks were shaken. Only the blue LED bulbs were used during culture growth. At each time point, the cultures in the two flasks receiving the same treatment were combined and the OD determined. A volume corresponding to 2.5 ODs was removed and the remaining culture evenly distributed between the two flasks and returned to shaking. For the cycloheximide experiments, after time 0 all the flasks were either kept in the dark or they were all illuminated, with two of the flasks receiving cycloheximide to a concentration of 100 mM. For these experiments, the OD was determined only at time 0 and at the end point (60 minutes). Collected samples were centrifuged at 1700 RPM (4° C) in a 50 ml conical tube for 3 minutes. The supernatant was discarded, and the cell pellets were resuspended in 1 ml of water and centrifuged for 3 minutes at 1600 rpm in an Eppendorf tube. The supernatant was removed and the pelleted cells were frozen in liquid nitrogen.

Protein was extracted from the samples following the alkaline lysis method of Kushnirov [111]. For each 2.5 ODs of material, the pellet was solubilized in 100 µl H<sub>2</sub>O. 100 µl of 0.2M NaOH was added and the contents gently mixed. The tubes were incubated for 5 minutes at room temperature, then centrifuged for 10 seconds at 13,200 rpm in an Eppendorf centrifuge. The supernatant was discarded and the pellet was resuspended in 75 µl of 1X Laemmli gel sample buffer. The sample was then boiled for 3 minutes and spun at 13,200 rpm for 5 minutes. The supernatant was removed to a new tube and frozen in

liquid nitrogen. Protein concentration were determined using the Bio-Rad Protein Assay reagent (Cat# 500–0006, Bio-Rad Laboratories, Hercules, CA). For Western blots, 75 or 100 µg of protein were loaded per lane.

After blotting, the top and bottom half of the gels were separated just below the 49 kD molecular weight marker. The top half was incubated in rabbit anti-HA epitope tag (Rockland antibodies & assays, Cat. #600-401-384S) at a dilution of 1:5,000, while the bottom half was incubated in mouse anti-Glyceraldehyde-3-phosphate dehydrogenase (GAPDH/GA1R) from ThermoFisher Scientific (Cat. # MA5-15738) at a dilution of 1:10,000. Respective secondary antibodies were HRP-conjugated goat anti-rabbit IgG and goat anti-mouse IgG polyclonal antibodies from Jackson Laboratories (Cat. #s 111-035-003 and 115-035-003) both used at a dilution of 1:10,000. All antibody incubations were carried out overnight at 4°C.

### **Examination of *Drosophila* cuticular phenotypes and hatch rates resulting from light exposure**

For studies of the effects of illumination on cuticular phenotypes and on hatch rates associated with photo-N-degron-mediated protein degradation in embryos, females expressing the degron-tagged CactDN pUASp [110] constructs under the control of the nanos-Gal4:VP16 [81] transcriptional driver element were collected and introduced with males into egg collection cages on yeasted apple juice agar plates. For light-exposed embryos, females were allowed to lay eggs for 1 hour in the dark at 25°C, at which time the plates were removed and transferred cover side up to a shelf in another 25°C incubator

at a distance of 6 cm from a Blue 225 LED 13.8 Watt/110 Volt Square Grow Light Panel (LEDwholesalers 2501BU). Embryos were allowed to develop for at least 48 hours and cuticles prepared from unhatched eggs present on the plates. Females of the same genotype were also allowed to lay eggs in the dark and embryos allowed to develop for at least 48 hours, in order to assess the phenotypes of embryos in which the degron-tagged CactDN proteins had not been exposed to light, also by preparing and examining cuticle preparations from unhatched eggs.

Larval cuticles were prepared according to Van der Meer [112]. Dorsal/Ventral phenotypes of embryos were classified as described in Roth et al. [69], with modifications as follows. DO embryos are completely dorsalized, exhibiting only dorsally-derived cuticle with fine hairs all around their DV circumference. D1 embryos are strongly dorsalized, exhibiting only dorsal and dorsolateral (Filzkörper material) structures. D2 embryos are moderately dorsalized, exhibiting dorsal, dorsolateral, and ventrolateral structures. These embryos displayed Filzkörper or Filzkörper material as well as narrower than normal bands of ventral denticles. D3 embryos are weakly dorsalized and display Filzkörper and ventral denticles of normal width. These embryos exhibited a twisted, or tail-up/U-shaped phenotype, consistent with a disruption of mesoderm tissue, the ventral-most pattern element in the embryo and often exhibited disruptions of the head skeleton. UH (for unhatched) refers to embryos exhibiting apparently normal cuticular pattern elements, but which failed to hatch from the egg.

### **Live imaging of embryos**

Embryos were collected one and a half hours after egg deposition, dechorionated by hand, and staged in halocarbon 27 oil. Embryos expressed Dorsal-GFP under the control of the endogenous dorsal gene transcriptional regulatory elements [85] together with the degra-tagged CactDN construct expressed under the control of the mat- $\alpha$ 4-tub-Gal4:VP16 transcriptional driver element [108]. All the embryos were prepared under red filtered light (red film—Neewer, 10087407) to avoid possible degradation of degra-tagged CactDN by light emitted by microscopes. Embryos at nuclear cycle (nc) 11 were mounted in Halocarbon 27 oil (Sigma-Aldrich) between a glass slide and a coverslip using glue dissolved in heptane with folded double-sided tape placed between the slide and the coverslip. Embryos were imaged on a Zeiss LSM 800 confocal microscope using a 25x oil immersion objective. To increase time-resolution, we used a 0.8 digital magnification. Images were captured at 512 x 512 pixel resolution with the pinhole set to a diameter of 50  $\mu$ m. At each time point, a stack of 30 z-plane images separated by 0.3  $\mu$ m were captured, spanning the nuclear layer.

To test efficiency of loss of activity of the degra-tagged CactDN constructs upon blue laser illumination, 488nm light (“blue laser”) at either low (2–3.1%) or high (8.6–10%) laser power was applied to the experimental embryos able to stimulate GFP fluorescence emission (i.e. 3.1%) as well as to induce both GFP fluorescence as well as degra-tagged Cactus degradation (i.e. 10%). While for control embryos, 488 nm laser light also was applied but only at low power, a setting that is able to stimulate GFP fluorescence emission but is not expected to contribute substantially to the loss of degra-tagged Cactus (or

directs very slow degradation relative to high power illumination). Unless otherwise noted, embryos exposed to blue laser (488 nm) illumination were imaged under three conditions as outlined in Fig 9A: (i) imaging was initiated at nc12 using the 488nm laser at 3.1% power (or 2% for CactDN-B-LID); (ii) 10min later (nc13) power was increased to 10% (or 8.6% for CactDN-B-LID) and applied for a period of 20min; and after a resting period of 35min, imaging was reinitiated at low power (2–3.1%) until late nc14/gastrulation. S1, S2, S4, and S6 Movies are a compilation of these three imaging sessions. For the low-blue light condition (S3, S5, and S7 Movies), the embryos were imaged with low power 488nm laser light sufficient to illuminate the Dorsal-GFP but expected to have little impact on photosensitive-degrons, from the onset of nc12 to nc14 and after 35min rest, approximately at late nc14/gastrulation an image was captured again. S8 Movie, a compilation of two imaging sessions, was initiated (i) earlier at nc12, starting with blue laser (488 nm) illumination for 20 min at 10% laser power and then followed by imaging (ii) at 488 nm at 3.1% laser power until nc14. Emission signal for low laser power was collected from 495–541 nm and for high laser illumination from 400-541nm. Movies displaying Z-stack projections (scanned area: S1–S5 movies 0.8x and S6-S8 1.2x) of the Dorsal-GFP gradient were obtained using Fiji/ImageJ software. Images in Figs 9 and 10 were generated as selected stacks of 15–20 z-plane images (planes with high background were avoided) from timed frames of each equivalent movie. The laser power can fluctuate with any set-up over time and thus must be empirically defined for each set of experiments (e.g. The first experiments that were carried out with CactDN-B-LID/Dorsal-GFP required less laser power for both visualization of Dorsal-GFP and elimination of CactDN-B-LID).

### **Western blot analysis of Cactus constructs expressed in *Drosophila* embryos**

For Western blot analysis of Cactus proteins, eggs laid by transgenic females expressing the CactDN-B-LID or PND-HA-CactDN construct under the transcriptional control of the nanos-Gal4:VP16 [81] transcriptional driver element were collected at 2–4 hours after egg deposition on yeasted apple juice/agar plates. Eggs were laid and incubated in either dark condition or blue light condition at 25°C until collection, in ambient light. Following collection, eggs were dechorionated in 50% Chlorox bleach, transferred to 1.7 ml microcentrifuge tubes, and homogenized with a microcentrifuge tube-compatible pestle in roughly equal volume of lysis buffer (25 mM Tris, pH 7.5 /0.15 M NaCl /0.3% NP-40 /1mM EDTA/ 1mM EGTA /0.2mM N-ethylmaleimide, containing protease inhibitors [Pierce Protease Inhibitor Tablets, EDTA-free, Pierce Biotechnology, Rockford, IL]). Protein concentrations in the homogenates were determined using the Bio-Rad Protein Assay reagent. For each embryo extract, a volume corresponding to total protein of 200 µg for the CactDN-B-LID sample and 50 µg for the PND-CactDN was subjected to SDS polyacrylamide gel electrophoresis. Following electroblotting to nitrocellulose membranes, the CactDN-B-LID blot was incubated with monoclonal primary antibodies against either Cactus (1/500) (Mouse Monoclonal 3H12, DSHB, Hybridoma deposited by Steward, R.) or Tubulin (1:1,000) (Mouse Monoclonal clone DM1A, Product# T6199, Sigma-Aldrich, St. Louis, MO). The PND-HA-CactDN blot was incubated with anti-HA (1:1000)(Mouse Monoclonal 16B12, Prod# MMS-101P, Covance Inc., Emeryville, CA). Blots were washed and incubated with Peroxidase-conjugated Goat Anti-Mouse IgG

(1:10,000 for CactDN-B-LID and 1:5,000 for PND-HA-CactDN) (Code# 115-035-003, Jackson ImmunoResearch Laboratories, West Grove, PA). Signal was detected using the SuperSignal West Pico Chemiluminescent Substrate (Prod# 34080, Pierce Biotechnology, Rockford, IL). The PND-HA-CactDN blot was imaged using a C-DiGit blot scanner and Image Studios Software (LI-COR Biosciences).

## REFERENCES

1. Dang DT, Perrimon N. Use of a yeast site-specific recombinase to generate embryonic mosaics in *Drosophila*. *Dev Genet*. 1992;13: 367–375.
2. Chou TB, Perrimon N. Use of a yeast site-specific recombinase to produce female germline chimeras in *Drosophila*. *Genetics*. 1992;131: 643–653.
3. Gu H, Marth J, Orban P, Mossmann H, Rajewsky K. Deletion of a DNA polymerase beta gene segment in T cells using cell type-specific gene targeting. *Science*. 1994. pp. 103–106. doi:10.1126/science.8016642
4. Xu T, Rubin GM. Analysis of genetic mosaics in developing and adult *Drosophila* tissues. *Development*. 1993;117: 1223–1237.
5. Dietzl G, Chen D, Schnorrer F, Su K-C, Barinova Y, Fellner M, et al. A genome-wide transgenic RNAi library for conditional gene inactivation in *Drosophila*. *Nature*. 2007;448: 151–156.
6. Elbashir SM, Harborth J, Lendeckel W, Yalcin A, Weber K, Tuschl T. Duplexes of 21-nucleotide RNAs mediate RNA interference in cultured mammalian cells. *Nature*. 2001;411: 494–498.
7. Chakshusmathi G, Mondal K, Lakshmi GS, Singh G, Roy A, Ch RB, et al. Design of temperature-sensitive mutants solely from amino acid sequence. *Proc Natl Acad Sci U S A*. 2004;101: 7925–7930.
8. Zeidler MP, Tan C, Bellaiche Y, Cherry S, Häder S, Gayko U, et al. Temperature-sensitive control of protein activity by conditionally splicing inteins. *Nat Biotechnol*. 2004;22: 871–876.
9. Tan G, Chen M, Foote C, Tan C. Temperature-sensitive mutations made easy: generating conditional mutations by using temperature-sensitive inteins that function within different temperature ranges. *Genetics*. 2009;183: 13–22.

10. Poultney CS, Butterfoss GL, Gutwein MR, Drew K, Gresham D, Gunsalus KC, et al. Rational Design of Temperature-Sensitive Alleles Using Computational Structure Prediction. *PLoS ONE*. 2011. p. e23947. doi:10.1371/journal.pone.0023947
11. Dohmen RJ, Wu P, Varshavsky A. Heat-inducible degron: a method for constructing temperature-sensitive mutants. *Science*. 1994;263: 1273–1276.
12. Bachmair A, Finley D, Varshavsky A. In vivo half-life of a protein is a function of its amino-terminal residue. *Science*. 1986. pp. 179–186. doi:10.1126/science.3018930
13. Varshavsky A. The N-end rule pathway and regulation by proteolysis. *Protein Sci*. 2011;20: 1298–1345.
14. Sriram SM, Kim BY, Kwon YT. The N-end rule pathway: emerging functions and molecular principles of substrate recognition. *Nat Rev Mol Cell Biol*. 2011;12: 735–747.
15. Bartel B, Wüning I, Varshavsky A. The recognition component of the N-end rule pathway. *EMBO J*. 1990;9: 3179–3189.
16. Tasaki T, Mulder LCF, Iwamatsu A, Lee MJ, Davydov IV, Varshavsky A, et al. A Family of Mammalian E3 Ubiquitin Ligases That Contain the UBR Box Motif and Recognize N-Degrans. *Molecular and Cellular Biology*. 2005. pp. 7120–7136. doi:10.1128/mcb.25.16.7120-7136.2005
17. Madura K, Dohmen RJ, Varshavsky A. N-recognin/Ubc2 interactions in the N-end rule pathway. *J Biol Chem*. 1993;268: 12046–12054.
18. Labib K, Tercero JA, Diffley JF. Uninterrupted MCM2-7 function required for DNA replication fork progression. *Science*. 2000;288: 1643–1647.
19. Lindner K, Gregán J, Montgomery S, Kearsey SE. Essential role of MCM proteins in premeiotic DNA replication. *Mol Biol Cell*. 2002;13: 435–444.
20. Kanemaki M, Sanchez-Diaz A, Gambus A, Labib K. Functional proteomic identification of DNA replication proteins by induced proteolysis in vivo. *Nature*. 2003;423: 720–724.
21. Gregan J, Lindner K, Brimage L, Franklin R, Namdar M, Hart EA, et al. Fission yeast Cdc23/Mcm10 functions after pre-replicative complex formation to promote Cdc45 chromatin binding. *Mol Biol Cell*. 2003;14: 3876–3887.
22. Kearsey SE, Gregan J. Using the DHFR Heat-Inducible Degron for Protein Inactivation in *Schizosaccharomyces pombe*. *Methods in Molecular Biology*. 2009. pp. 483–492. doi:10.1007/978-1-60327-815-7\_27

23. Bernal JA, Venkitaraman AR. A vertebrate N-end rule degron reveals that Orc6 is required in mitosis for daughter cell abscission. *J Cell Biol.* 2011;192: 969–978.
24. Faden F, Ramezani T, Mielke S, Almudi I, Nairz K, Froehlich MS, et al. Phenotypes on demand via switchable target protein degradation in multicellular organisms. *Nat Commun.* 2016;7: 12202.
25. Banaszynski LA, Chen L-C, Maynard-Smith LA, Ooi AGL, Wandless TJ. A rapid, reversible, and tunable method to regulate protein function in living cells using synthetic small molecules. *Cell.* 2006;126: 995–1004.
26. Bonger KM, Chen L-C, Liu CW, Wandless TJ. Small-molecule displacement of a cryptic degron causes conditional protein degradation. *Nat Chem Biol.* 2011;7: 531–537.
27. Tan X, Calderon-Villalobos LIA, Sharon M, Zheng C, Robinson CV, Estelle M, et al. Mechanism of auxin perception by the TIR1 ubiquitin ligase. *Nature.* 2007;446: 640–645.
28. Nishimura K, Fukagawa T, Takisawa H, Kakimoto T, Kanemaki M. An auxin-based degron system for the rapid depletion of proteins in nonplant cells. *Nat Methods.* 2009;6: 917–922.
29. Natsume T, Kanemaki MT. Conditional Degrons for Controlling Protein Expression at the Protein Level. *Annual Review of Genetics.* 2017. pp. 83–102. doi:10.1146/annurev-genet-120116-024656
30. Taxis C, Stier G, Spadaccini R, Knop M. Efficient protein depletion by genetically controlled deprotection of a dormant N-degron. *Molecular Systems Biology.* 2009. p. 267. doi:10.1038/msb.2009.25
31. Taxis C, Knop M. TIPI: TEV Protease-Mediated Induction of Protein Instability. *Methods in Molecular Biology.* 2012. pp. 611–626. doi:10.1007/978-1-61779-474-2\_43
32. Armenti ST, Lohmer LL, Sherwood DR, Nance J. Repurposing an endogenous degradation system for rapid and targeted depletion of *C. elegans* proteins. *Development.* 2014;141: 4640–4647.
33. Yamaguchi N, Colak-Champollion T, Knaut H. zGrad is a nanobody-based degron system that inactivates proteins in zebrafish. *Elife.* 2019;8. doi:10.7554/eLife.43125
34. Deisseroth K, Feng G, Majewska AK, Miesenbock G, Ting A, Schnitzer MJ. Next-Generation Optical Technologies for Illuminating Genetically Targeted Brain Circuits. *Journal of Neuroscience.* 2006. pp. 10380–10386. doi:10.1523/jneurosci.3863-06.2006

35. Johnson HE, Toettcher JE. Illuminating developmental biology with cellular optogenetics. *Current Opinion in Biotechnology*. 2018. pp. 42–48. doi:10.1016/j.copbio.2018.02.003
36. Nagel G, Szellas T, Huhn W, Kateriya S, Adeishvili N, Berthold P, et al. Channelrhodopsin-2, a directly light-gated cation-selective membrane channel. *Proceedings of the National Academy of Sciences*. 2003. pp. 13940–13945. doi:10.1073/pnas.1936192100
37. Zhang Y-P, Oertner TG. Optical induction of synaptic plasticity using a light-sensitive channel. *Nat Methods*. 2007;4: 139–141.
38. Zhang F, Wang L-P, Brauner M, Liewald JF, Kay K, Watzke N, et al. Multimodal fast optical interrogation of neural circuitry. *Nature*. 2007. pp. 633–639. doi:10.1038/nature05744
39. Wu YI, Frey D, Lungu OI, Jaehrig A, Schlichting I, Kuhlman B, et al. A genetically encoded photoactivatable Rac controls the motility of living cells. *Nature*. 2009;461: 104–108.
40. Levskaya A, Weiner OD, Lim WA, Voigt CA. Spatiotemporal control of cell signalling using a light-switchable protein interaction. *Nature*. 2009;461: 997–1001.
41. Huang A, Amourda C, Zhang S, Tolwinski NS, Saunders TE. Decoding temporal interpretation of the morphogen Bicoid in the early *Drosophila* embryo. *eLife*. 2017. doi:10.7554/elife.26258
42. Strickland D, Lin Y, Wagner E, Matthew Hope C, Zayner J, Antoniou C, et al. TULIPs: tunable, light-controlled interacting protein tags for cell biology. *Nature Methods*. 2012. pp. 379–384. doi:10.1038/nmeth.1904
43. Johnson HE, Goyal Y, Pannucci NL, Schüpbach T, Shvartsman SY, Toettcher JE. The Spatiotemporal Limits of Developmental Erk Signaling. *Developmental Cell*. 2017. pp. 185–192. doi:10.1016/j.devcel.2016.12.002
44. Keenan SE, Blythe SA, Marmion RA, -V. Djabrayan NJ, Wieschaus EF, Shvartsman SY. Rapid Dynamics of Signal-Dependent Transcriptional Repression by Capicua. *Developmental Cell*. 2020. pp. 794–801.e4. doi:10.1016/j.devcel.2020.02.004
45. Shimizu-Sato S, Huq E, Tepperman JM, Quail PH. A light-switchable gene promoter system. *Nat Biotechnol*. 2002;20: 1041–1044.

46. Kennedy MJ, Hughes RM, Peteya LA, Schwartz JW, Ehlers MD, Tucker CL. Rapid blue-light-mediated induction of protein interactions in living cells. *Nature Methods*. 2010. pp. 973–975. doi:10.1038/nmeth.1524
47. Crosson S, Rajagopal S, Moffat K. The LOV Domain Family: Photoresponsive Signaling Modules Coupled to Diverse Output Domains†. *Biochemistry*. 2003. pp. 2–10. doi:10.1021/bi0269781
48. Briggs WR. The LOV domain: a chromophore module servicing multiple photoreceptors. *Journal of Biomedical Science*. 2007. pp. 499–504. doi:10.1007/s11373-007-9162-6
49. Losi A, Polverini E, Quest B, Gärtner W. First evidence for phototropin-related blue-light receptors in prokaryotes. *Biophys J*. 2002;82: 2627–2634.
50. Heintzen C, Loros JJ, Dunlap JC. The PAS Protein VIVID Defines a Clock-Associated Feedback Loop that Represses Light Input, Modulates Gating, and Regulates Clock Resetting. *Cell*. 2001. pp. 453–464. doi:10.1016/s0092-8674(01)00232-x
51. Schwerdtfeger C. VIVID is a flavoprotein and serves as a fungal blue light photoreceptor for photoadaptation. *The EMBO Journal*. 2003. pp. 4846–4855. doi:10.1093/emboj/cdg451
52. Briggs WR, Christie JM. Phototropins 1 and 2: versatile plant blue-light receptors. *Trends Plant Sci*. 2002;7: 204–210.
53. Harper SM. Structural Basis of a Phototropin Light Switch. *Science*. 2003. pp. 1541–1544. doi:10.1126/science.1086810
54. Harper SM, Christie JM, Gardner KH. Disruption of the LOV–J $\alpha$  Helix Interaction Activates Phototropin Kinase Activity†. *Biochemistry*. 2004. pp. 16184–16192. doi:10.1021/bi048092i
55. Yao X, Rosen MK, Gardner KH. Estimation of the available free energy in a LOV2–J $\alpha$  photoswitch. *Nature Chemical Biology*. 2008. pp. 491–497. doi:10.1038/nchembio.99
56. Renicke C, Schuster D, Usherenko S, Essen L-O, Taxis C. A LOV2 domain-based optogenetic tool to control protein degradation and cellular function. *Chem Biol*. 2013;20: 619–626.
57. Bongor KM, Rakhit R, Payumo AY, Chen JK, Wandless TJ. General Method for Regulating Protein Stability with Light. *ACS Chemical Biology*. 2014. pp. 111–115. doi:10.1021/cb400755b

58. Steward R. Dorsal, an embryonic polarity gene in *Drosophila*, is homologous to the vertebrate proto-oncogene, *c-rel*. *Science*. 1987. pp. 692–694. doi:10.1126/science.3118464
59. Stein DS, Stevens LM. Maternal control of the *Drosophila* dorsal-ventral body axis. *Wiley Interdisciplinary Reviews: Developmental Biology*. 2014. pp. 301–330. doi:10.1002/wdev.138
60. Varshavsky A. Ubiquitin Fusion Technique and Related Methods. *Methods in Enzymology*. 2005. pp. 777–799. doi:10.1016/s0076-6879(05)99051-4
61. Wilson IA, Niman HL, Houghten RA, Cherenon AR, Connolly ML, Lerner RA. The structure of an antigenic determinant in a protein. *Cell*. 1984. pp. 767–778. doi:10.1016/0092-8674(84)90412-4
62. Sikorski RS, Hieter P. A system of shuttle vectors and yeast host strains designed for efficient manipulation of DNA in *Saccharomyces cerevisiae*. *Genetics*. 1989;122: 19–27.
63. Keppler-Ross S, Noffz C, Dean N. A New Purple Fluorescent Color Marker for Genetic Studies in *Saccharomyces cerevisiae* and *Candida albicans*. *Genetics*. 2008. pp. 705–710. doi:10.1534/genetics.108.087080
64. Reed SI. The Role of p34 Kinases in the G1 to S-Phase Transition. *Annual Review of Cell Biology*. 1992. pp. 529–561. doi:10.1146/annurev.cb.08.110192.002525
65. Hartwell LH, Mortimer RK, Culotti J, Culotti M. Genetic Control of the Cell Division Cycle in Yeast: V. Genetic Analysis of *cdc* Mutants. *Genetics*. 1973;74: 267–286.
66. Mendenhall MD, Richardson HE, Reed SI. Dominant negative protein kinase mutations that confer a G1 arrest phenotype. *Proceedings of the National Academy of Sciences*. 1988. pp. 4426–4430. doi:10.1073/pnas.85.12.4426
67. Bücking-Throm E, Duntze W, Hartwell LH, Manney TR. Reversible arrest of haploid yeast cells at the initiation of DNA synthesis by a diffusible sex factor. *Experimental Cell Research*. 1973. pp. 99–110. doi:10.1016/0014-4827(73)90424-2
68. Turner GC, Varshavsky A. Detecting and measuring cotranslational protein degradation in vivo. *Science*. 2000;289: 2117–2120.
69. Roth S, Hiromi Y, Godt D, Nüsslein-Volhard C. *cactus*, a maternal gene required for proper formation of the dorsoventral morphogen gradient in *Drosophila* embryos. *Development*. 1991;112: 371–388.

70. Geisler R, Bergmann A, Hiromi Y, Nüsslein-Volhard C. *cactus*, a gene involved in dorsoventral pattern formation of *Drosophila*, is related to the I $\kappa$ B gene family of vertebrates. *Cell*. 1992. pp. 613–621. doi:10.1016/0092-8674(92)90595-4
71. Kidd S. Characterization of the *Drosophila cactus* locus and analysis of interactions between *cactus* and dorsal proteins. *Cell*. 1992;71: 623–635.
72. Whalen AM, Steward R. Dissociation of the dorsal-*cactus* complex and phosphorylation of the dorsal protein correlate with the nuclear localization of dorsal. *J Cell Biol*. 1993;123: 523–534.
73. Isoda K, Nusslein-Volhard C. Disulfide cross-linking in crude embryonic lysates reveals three complexes of the *Drosophila* morphogen dorsal and its inhibitor *cactus*. *Proceedings of the National Academy of Sciences*. 1994. pp. 5350–5354. doi:10.1073/pnas.91.12.5350
74. Belvin MP, Jin Y, Anderson KV. *Cactus* protein degradation mediates *Drosophila* dorsal-ventral signaling. *Genes Dev*. 1995;9: 783–793.
75. Bergmann A, Stein D, Geisler R, Hagenmaier S, Schmid B, Fernandez N, et al. A gradient of cytoplasmic *Cactus* degradation establishes the nuclear localization gradient of the dorsal morphogen in *Drosophila*. *Mech Dev*. 1996;60: 109–123.
76. Reach M, Galindo RL, Towb P, Allen JL, Karin M, Wasserman SA. A Gradient of *Cactus* Protein Degradation Establishes Dorsoventral Polarity in the *Drosophila* Embryo. *Developmental Biology*. 1996. pp. 353–364. doi:10.1006/dbio.1996.0308
77. Rushlow CA, Han K, Manley JL, Levine M. The graded distribution of the dorsal morphogen is initiated by selective nuclear transport in *Drosophila*. *Cell*. 1989;59: 1165–1177.
78. Steward R. Relocalization of the dorsal protein from the cytoplasm to the nucleus correlates with its function. *Cell*. 1989;59: 1179–1188.
79. Roth S, Stein D, Nüsslein-Volhard C. A gradient of nuclear localization of the dorsal protein determines dorsoventral pattern in the *Drosophila* embryo. *Cell*. 1989;59: 1189–1202.
80. Fernandez NQ, Grosshans J, Goltz JS, Stein D. Separable and redundant regulatory determinants in *Cactus* mediate its dorsal group dependent degradation. *Development*. 2001;128: 2963–2974.
81. Van Doren M, Williamson AL, Lehmann R. Regulation of zygotic gene expression in *Drosophila* primordial germ cells. *Curr Biol*. 1998;8: 243–246.

82. Ghoda L, van Daalen Wetters T, Macrae M, Ascherman D, Coffino P. Prevention of rapid intracellular degradation of ODC by a carboxyl-terminal truncation. *Science*. 1989. pp. 1493–1495. doi:10.1126/science.2928784
83. Jungbluth M, Renicke C, Taxis C. Targeted protein depletion in *Saccharomyces cerevisiae* by activation of a bidirectional degron. *BMC Syst Biol*. 2010;4: 176.
84. Takeuchi J, Chen H, Hoyt MA, Coffino P. Structural elements of the ubiquitin-independent proteasome degron of ornithine decarboxylase. *Biochem J*. 2008;410: 401–407.
85. Reeves GT, Trisnadi N, Truong TV, Nahmad M, Katz S, Stathopoulos A. Dorsal-ventral gene expression in the *Drosophila* embryo reflects the dynamics and precision of the dorsal nuclear gradient. *Dev Cell*. 2012;22: 544–557.
86. Hermann A, Liewald JF, Gottschalk A. A photosensitive degron enables acute light-induced protein degradation in the nervous system. *Curr Biol*. 2015;25: R749–50.
87. Adamantidis AR, Zhang F, Aravanis AM, Deisseroth K, de Lecea L. Neural substrates of awakening probed with optogenetic control of hypocretin neurons. *Nature*. 2007;450: 420–424.
88. Sparta DR, Stamatakis AM, Phillips JL, Hovelsø N, van Zessen R, Stuber GD. Construction of implantable optical fibers for long-term optogenetic manipulation of neural circuits. *Nature Protocols*. 2012. pp. 12–23. doi:10.1038/nprot.2011.413
89. Ho JS, Tanabe Y, Iyer SM, Christensen AJ, Grosenick L, Deisseroth K, et al. Self-Tracking Energy Transfer for Neural Stimulation in Untethered Mice. *Physical Review Applied*. 2015. doi:10.1103/physrevapplied.4.024001
90. Montgomery KL, Yeh AJ, Ho JS, Tsao V, Iyer SM, Grosenick L, et al. Wirelessly powered, fully internal optogenetics for brain, spinal and peripheral circuits in mice. *Nature Methods*. 2015. pp. 969–974. doi:10.1038/nmeth.3536
91. Verzijl N, DeGroot J, Thorpe SR, Bank RA, Shaw JN, Lyons TJ, et al. Effect of collagen turnover on the accumulation of advanced glycation end products. *J Biol Chem*. 2000;275: 39027–39031.
92. Song X, Zhou T, Jia H, Guo X, Zhang X, Han P, et al. SProtP: a web server to recognize those short-lived proteins based on sequence-derived features in human cells. *PLoS One*. 2011;6: e27836.

93. Yang H, Wang H, Shivalila CS, Cheng AW, Shi L, Jaenisch R. One-step generation of mice carrying reporter and conditional alleles by CRISPR/Cas-mediated genome engineering. *Cell*. 2013;154: 1370–1379.
94. Gratz SJ, Ukken FP, Dustin Rubinstein C, Thiede G, Donohue LK, Cummings AM, et al. Highly Specific and Efficient CRISPR/Cas9-Catalyzed Homology-Directed Repair in *Drosophila*. *Genetics*. 2014. pp. 961–971. doi:10.1534/genetics.113.160713
95. Ikmi A, McKinney SA, Delventhal KM, Gibson MC. TALEN and CRISPR/Cas9-mediated genome editing in the early-branching metazoan *Nematostella vectensis*. *Nat Commun*. 2014;5: 5486.
96. Perry KJ, Henry JQ. CRISPR/Cas9-mediated genome modification in the mollusc, *Crepidula fornicata*. *genesis*. 2015. pp. 237–244. doi:10.1002/dvg.22843
97. Kistler KE, Vosshall LB, Matthews BJ. Genome Engineering with CRISPR-Cas9 in the Mosquito *Aedes aegypti*. *Cell Reports*. 2015. pp. 51–60. doi:10.1016/j.celrep.2015.03.009
98. Ceasar SA, Antony Ceasar S, Rajan V, Prykhozhiy SV, Berman JN, Ignacimuthu S. Insert, remove or replace: A highly advanced genome editing system using CRISPR/Cas9. *Biochimica et Biophysica Acta (BBA) - Molecular Cell Research*. 2016. pp. 2333–2344. doi:10.1016/j.bbamcr.2016.06.009
99. Irizarry J, McGehee J, Kim G, Stein D, Stathopoulos A. Twist-dependent ratchet functioning downstream from Dorsal revealed using a light-inducible degron. *Genes Dev*. 2020;34: 965–972.
100. Lin H-C, Yeh C-W, Chen Y-F, Lee T-T, Hsieh P-Y, Rusnac DV, et al. C-Terminal End-Directed Protein Elimination by CRL2 Ubiquitin Ligases. *Molecular Cell*. 2018. pp. 602–613.e3. doi:10.1016/j.molcel.2018.04.006
101. Koren I, Timms RT, Kula T, Xu Q, Li MZ, Elledge SJ. The Eukaryotic Proteome Is Shaped by E3 Ubiquitin Ligases Targeting C-Terminal Degrons. *Cell*. 2018;173: 1622–1635.e14.
102. Rosenberg-Hasson Y, Bercovich Z, Ciechanover A, Kahana C. Degradation of ornithine decarboxylase in mammalian cells is ATP dependent but ubiquitin independent. *European Journal of Biochemistry*. 1989. pp. 469–474. doi:10.1111/j.1432-1033.1989.tb15138.x
103. Murakami Y, Matsufuji S, Kameji T, Hayashi S-I, Igarashi K, Tamura T, et al. Ornithine decarboxylase is degraded by the 26S proteasome without ubiquitination. *Nature*. 1992. pp. 597–599. doi:10.1038/360597a0

104. Jariel-Encontre I, Bossis G, Piechaczyk M. Ubiquitin-independent degradation of proteins by the proteasome. *Biochimica et Biophysica Acta (BBA) - Reviews on Cancer*. 2008. pp. 153–177. doi:10.1016/j.bbcan.2008.05.004
105. Berner N, Reutter K-R, Wolf DH. Protein Quality Control of the Endoplasmic Reticulum and Ubiquitin–Proteasome-Triggered Degradation of Aberrant Proteins: Yeast Pioneers the Path. *Annual Review of Biochemistry*. 2018. pp. 751–782. doi:10.1146/annurev-biochem-062917-012749
106. Scheffer J, Hasenjäger S, Taxis C. Degradation of integral membrane proteins modified with the photosensitive degron module requires the cytosolic endoplasmic reticulum–associated degradation pathway. *Molecular Biology of the Cell*. 2019. pp. 2558–2570. doi:10.1091/mbc.e18-12-0754
107. Gietz RD, Daniel Gietz R, Schiestl RH. High-efficiency yeast transformation using the LiAc/SS carrier DNA/PEG method. *Nature Protocols*. 2007. pp. 31–34. doi:10.1038/nprot.2007.13
108. Häcker U, Perrimon N. DRhoGEF2 encodes a member of the Dbl family of oncogenes and controls cell shape changes during gastrulation in *Drosophila*. *Genes Dev*. 1998;12: 274–284.
109. Alani E, Kleckner N. A new type of fusion analysis applicable to many organisms: protein fusions to the URA3 gene of yeast. *Genetics*. 1987;117: 5–12.
110. Rørth P. Gal4 in the *Drosophila* female germline. *Mech Dev*. 1998;78: 113–118.
111. Kushnirov VV. Rapid and reliable protein extraction from yeast. *Yeast*. 2000;16: 857–860.
112. Van der Meer JM. Optical clean and permanent whole mount preparation for phase-contrast microscopy of cuticular structures of insect larvae. *Drosoph Inf Serv*. 1977;52: 160.
113. Evan GI, Lewis GK, Ramsay G, Bishop JM. Isolation of monoclonal antibodies specific for human c-myc proto-oncogene product. *Mol Cell Biol*. 1985;5: 3610–3616.

## Figures and Legends

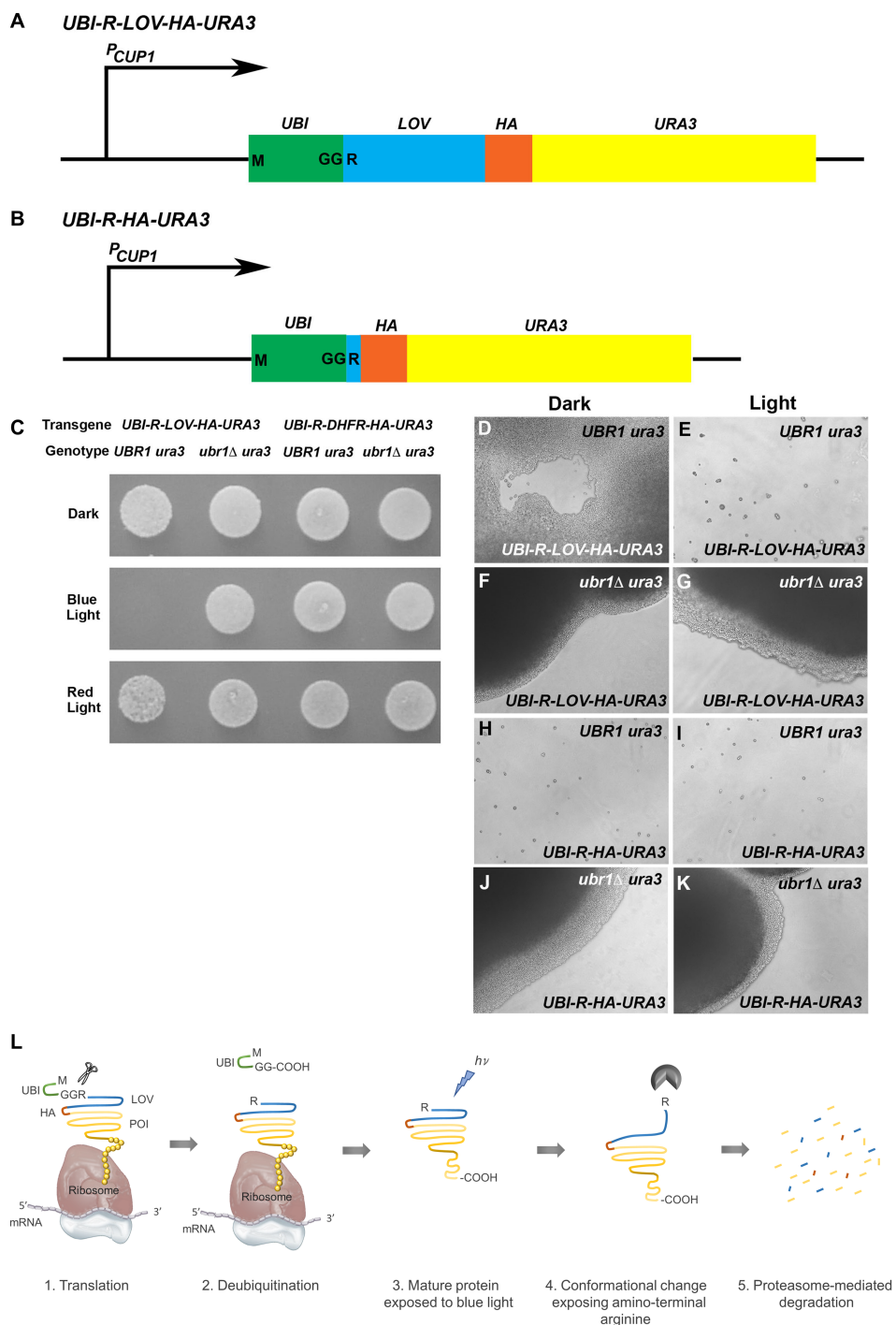


**Fig 1. An amino terminal domain encoding ubiquitin, fused to the LOV2 domain from oat phototropin I mediates blue light/N-end rule-mediated loss of Ura3p function in yeast.**

(A) A schematic diagram showing the organization of the construct encoding blue/light, N-end rule targeted Ura3p, under the transcriptional control of the copper-inducible CUP1 promoter (PCUP1). From 5' to 3', the transgene encodes a single copy of the ubiquitin open reading frame (UBI), the LOV2 domain from plant phototropin I (LOV), a single copy of the influenza hemagglutinin epitope (HA), and the open reading frame encoding the yeast Ura3p protein (URA3). Protein synthesis initiates at the ubiquitin initiation codon (M) and the pair of glycine residues at the C-terminus of the ubiquitin open reading frame (GG) are followed immediately by an arginine codon (R). The ubiquitin domain is removed co-translationally, leaving the arginine residue immediately preceding the LOV domain as the N-terminal residue of the mature protein. In the corresponding UBI-R-DHFR-HA-URA3 construct, the sequence encoding the LOV2 domain have been replaced by DHFR coding sequences bearing an N-terminal arginine residue. (B) A schematic diagram of UBI-R-HA-URA3, which lacks the sequences encoding the light-sensitive LOV domain. (C) The UBI-R-LOV-HA-URA3 and UBI-R-DHFR-HA-URA3 transgenes were introduced into UBR1 ura3 and ubr1 $\Delta$  ura3 mutant cells (introduced transgenes and yeast genotypes shown at top of panel), which were seeded onto selective plates lacking uracil and incubated in either darkness, under blue-light, or under red-light illumination. Under blue light, the UBI-R-LOV-HA-URA3 construct failed to restore growth in the absence of uracil, indicating the sensitivity of the expressed R-phLOV2-HA-Ura3p protein to blue

light. When incubated under blue light in the absence of the Ubr1p activity (*ubr1Δ ura3*), growth in the absence of uracil was restored. In contrast to R-phLOV2-HA-Ura3p, the R-DHFR-HA-Ura3p protein did not confer light sensitivity upon growth in the absence of uracil. (D-K) Yeast cells expressing either UBI-R-phLOV2-HA-URA3 (D-G) or UBI-R-HA-URA3 (H-K) (transgenes shown at bottom of panels) were expressed in either Ubr1p-expressing (*UBR1 ura3*) (D, E, H, I) or Ubr1p-lacking (*ubr1Δ ura3*) (F, G, J, K) genetic backgrounds and incubated on selective plates lacking uracil either in darkness (D, F, H, J) or under blue light illumination (E, G, I, K). In the presence of Ubr1p and incubated under blue light illumination (E), UBI-R-phLOV2-HA-Ura3p-expressing cells arrested mainly as single cells, arguing that the light/Ubr1p-mediated loss of Ura3p protein function was rapid. In contrast, when grown in the dark (D) or in a *ubr1Δ* mutant background (G), these cells proliferated normally. In contrast, cells bearing a wild-type *UBR1* gene and expressing UBI-R-HA-URA3, arrested as single cells both in darkness and under illumination (H, I), indicating that the presence of an N-end rule targeted arginine, in the absence of the phLOV2 domain, rendered the encoded protein functionally inactive regardless of light conditions (G, H), while the absence of the Ubr1p ubiquitin ligase protein left the R-HA-Ura3p protein functional in darkness and under blue light illumination (J, K). (L) shows a schematic representation of the mechanism through which R-phLOV-HA-tagged protein is presumed to be synthesized and degraded in response to blue-light illumination.

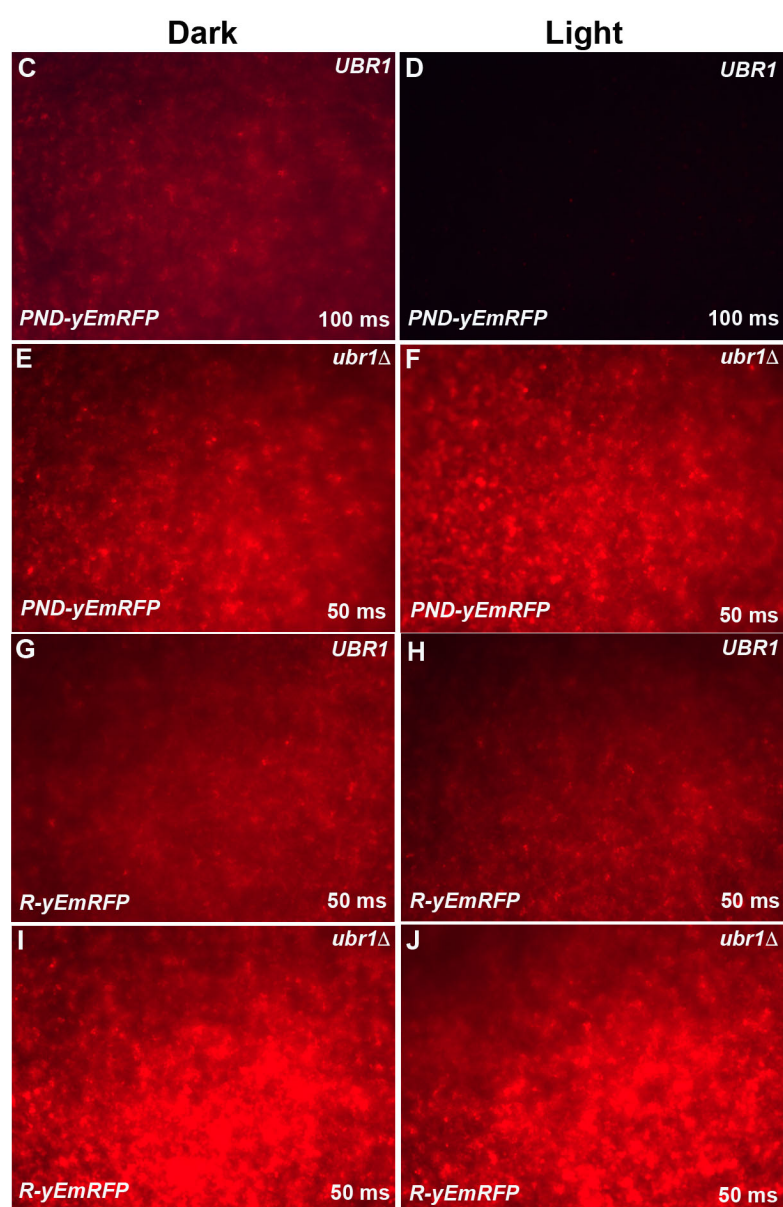
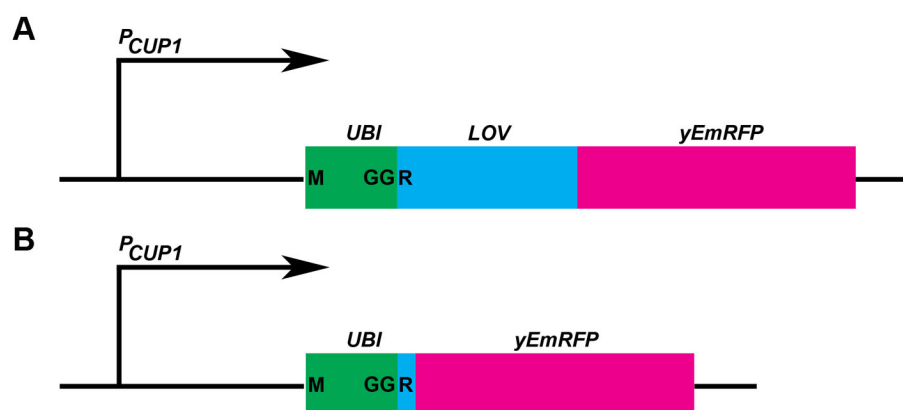


**Fig 2. The PND mediates blue light/Ubr1-dependent loss of yEmRFP-associated fluorescence in yeast.**

Two constructs encoding yEmRFP bearing either the PND (PND-yEmRFP) (A, C, D, E, F) or a single arginine (R) residue (R-yEmRFP) (B, G, H, I, J) at the amino terminus were introduced into UBR1 (C, D, G, H) and *ubr1*Δ (E, F, I, J) strains of yeast (labelled at top right of each panel) and seeded onto selective plates. Following 48 hours growth to confluence in darkness (C, E, G, I) or under blue light illumination (D, F, H, J) the surfaces of the patches were imaged for red fluorescence. Photographic imaging was carried out on the same day and under the same conditions, with the time of exposure (50 or 100 milliseconds [ms], noted at bottom right of each panel) the same for each of the light/dark pairings. This permitted a determination of relative levels of expression between light/dark pairings and between the strains and the constructs that they carried. Yeast expressing PND-yEmRFP in the presence of Ubr1p, exhibited a dramatic decrease in response to illumination (C, D). In the absence of Ubr1p, yeast bearing this construct expressed higher levels of fluorescence that were not affected by illumination (E, F). Yeast expressing R-yEmRFP in the presence of Ubr1p expressed levels of fluorescence that did not depend upon illumination and were greater than that expressed by PND-yEmRFP (compare G, H to C and note the difference in exposure times), while fluorescence levels were highest when this construct was expressed in yeast lacking Ubr1p, regardless of illumination (I, J). These results indicate that the PND leads to blue light/Ubr1p dependent loss of yEmRFP activity. Moreover, in the context of yEmRFP, the presence of the phLOV2 domain in the

PND results in a less stable protein than yEmRFP bearing a simple N-end rule-targeted arginine.

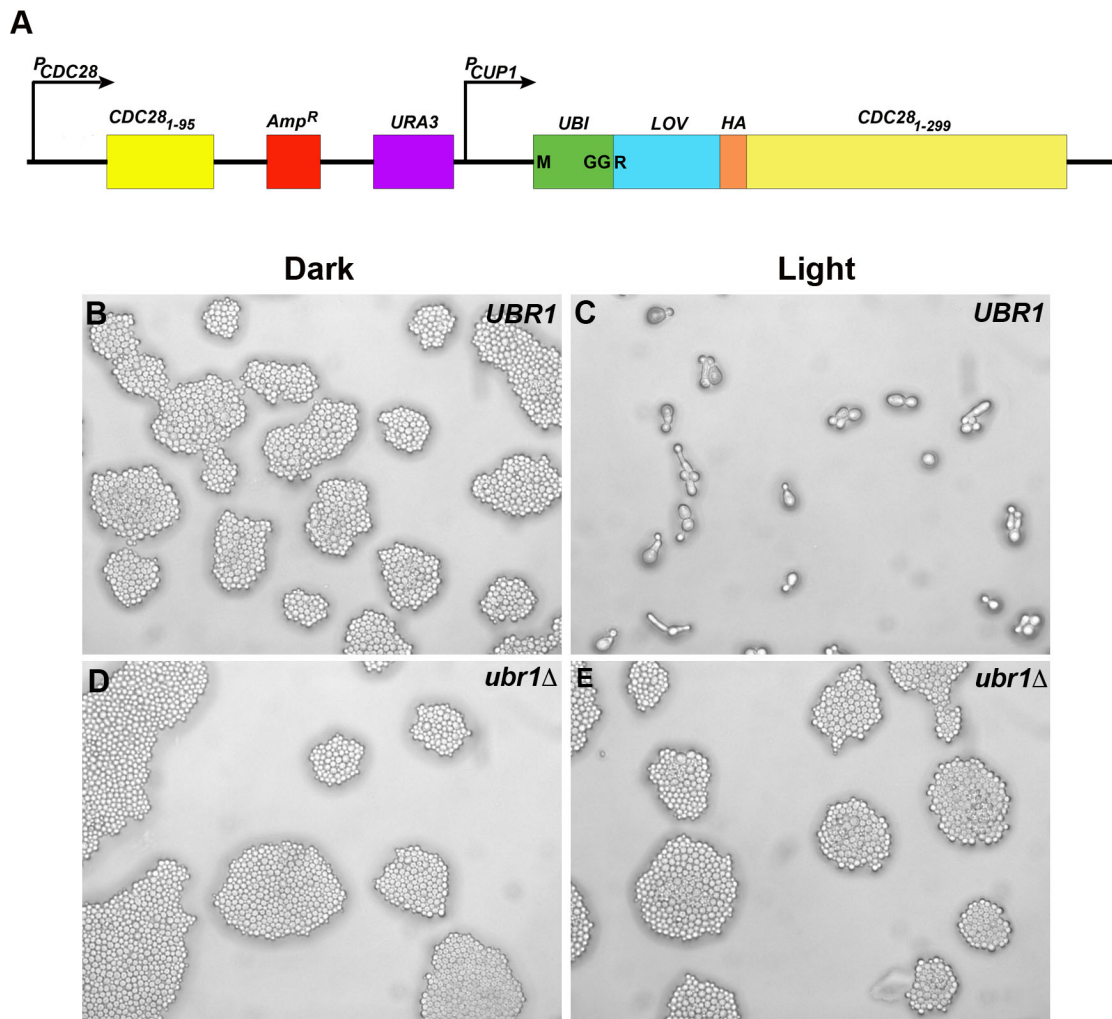


**Fig 3. Yeast cells in which the endogenous CDC28 gene has been replaced by PND-HA-CDC28 exhibit blue light/Ubr1-dependent cell cycle defects.**

A schematic diagram of the site of chromosomal insertion of the PND-HA-CDC28 transgene-bearing plasmid is shown in (A). Homologous recombination results in the insertion of the entire plasmid at the genomic site of the restriction site (Msc I) that was used to linearize the plasmid. This results in the interruption of the endogenous CDC28

gene and its replacement by the PND-tagged form, under the transcriptional control of the copper-inducible CUP1 promoter. Cells were plated on selective medium and grown in the dark (B, D) and under blue-light illumination (C, E) in both UBR1 (B, C) and *ubr1* $\Delta$  (D, E) genetic backgrounds. Note that UBR1 cells expressing PND-HA-Cdc28p under illumination (C) arrest as large single cells exhibiting long outgrowths, similar to what has been described for TS mutants of *cdc28* grown at non-permissive temperatures [65], and for cells expressing the dominant-negative Cdc28p [66].

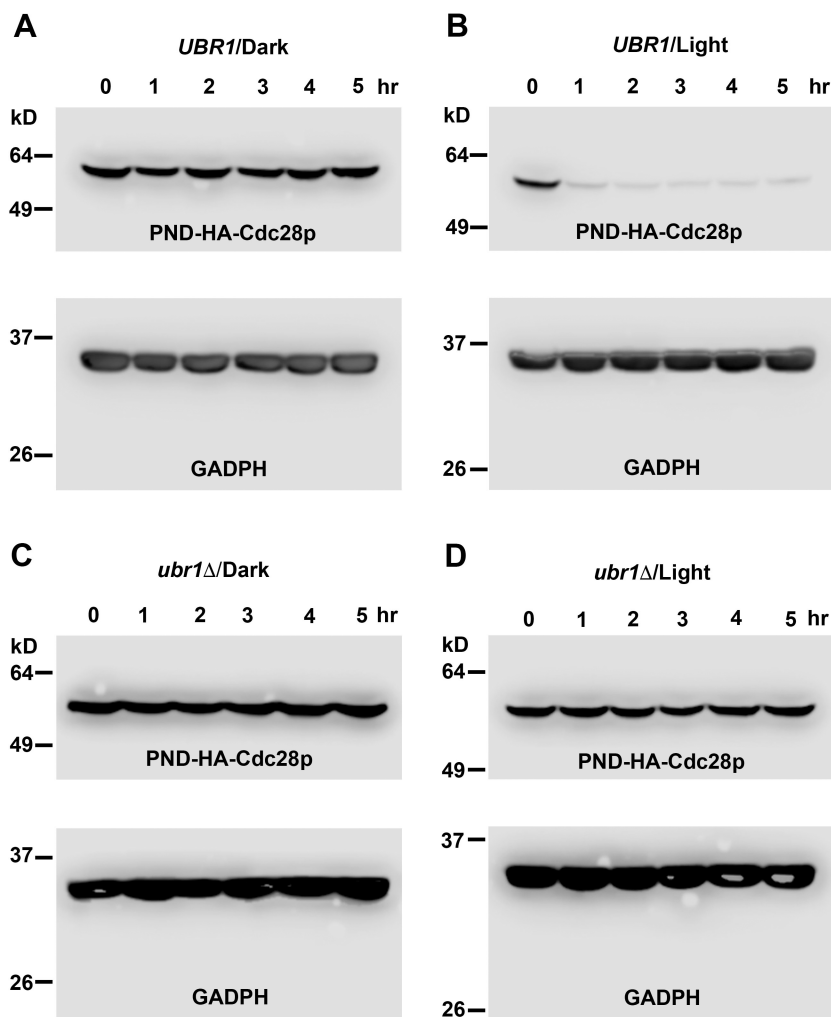


**Fig 4. PND-HA-Cdc28p undergoes blue light/Ubr1-dependent degradation.**

Cells expressing a chromosomal insertion of PND-HA-Cdc28p in either a *UBR1* (A, B) or *ubr1Δ* (C, D) genetic background were grown in liquid culture in darkness to log phase, then divided and allowed to continue growth in darkness (A, C) or under blue-light illumination (B, D). Samples of culture medium were taken at 1-hour intervals and cells were processed for Western blot analysis. Western blots were divided into upper and lower

sections with the upper sections probed using an antibody directed against the HA epitope in PND-HA-Cdc28p and the lower segments probed with an antibody directed against the endogenous protein Glyceraldehyde-3-phosphate dehydrogenase (GAPDH), which served as a loading control. Note that PND-HA-Cdc28p levels exhibited a dramatic decrease when grown in UBR1 cells under illumination (B). Growth in darkness (A) or under illumination in the absence of Ubr1p (D) resulted in constant levels of PND-HA-Cdc28p.

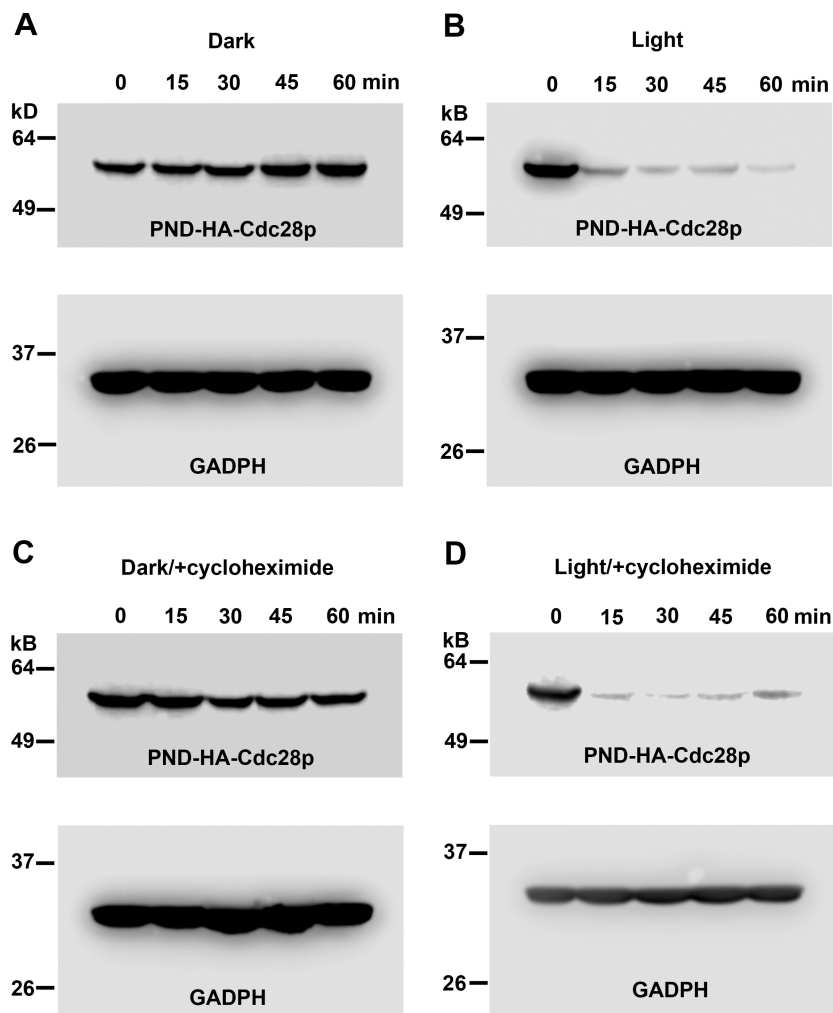
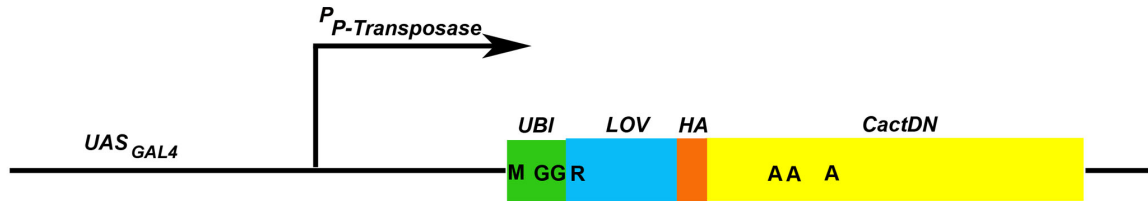


**Fig 5. Mature PND-HA-Cdc28P undergoes rapid light dependent degradation.**

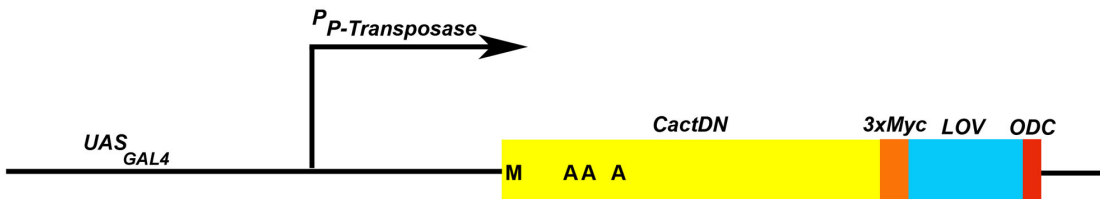
Cells expressing PND-HA-Cdc28p in a UBR1 genetic background were grown in liquid culture in darkness to log phase, then divided and allowed to continue growth in darkness (A, C) or under blue-light illumination (B, D) in either the absence (A, B) or presence (C, D) of the translational inhibitor cycloheximide. Samples of culture medium were taken at 15-minute intervals and cells were processed for Western blot analysis, with an upper

portion of each blot probed with an antibody against the HA epitope in PND-HA-Cdc28p and a lower portion probed with an antibody directed against endogenous GADPH, which served as a protein loading control. In the presence of Ubr1p, light-dependent loss of PND-HA-Cdc28p was very rapid, likely occurring within a single cell cycle, regardless of the absence (B) or presence (D) of cycloheximide.

**A PND-HA-CactDN**



**B CactDN-psd**



**C CactDN-B-LID**

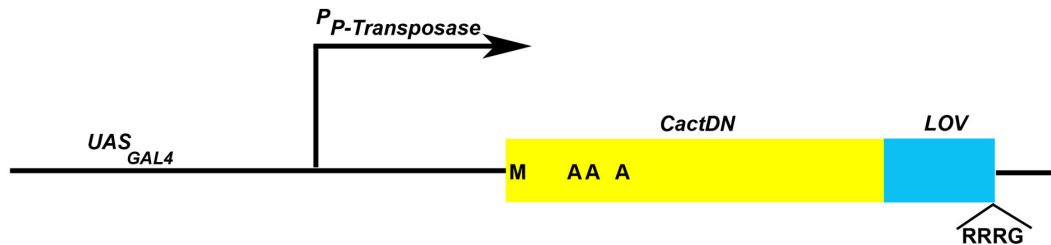


**Fig 6. Schematic diagrams of the transgene constructs encoding PND-, psd- and B-LID domain-tagged versions of the CactDN open reading frame.**

Constructs encoding the three degron-tagged versions of CactDN were introduced into the *Drosophila* genome on the P-element transposon-based expression vector, pUASp [110], downstream of upstream activator sequences for the yeast Gal4 transcription factor ( $UAS_{GAL4}$ ) and the promoter from the P-element transposase gene ( $PP-Transposase$ ).

Expression of the transgenes was accomplished by co-expression of a germline-specific source of the Gal4 transcription factor. (A) PND-HA-CactDN. (B) CactDN-psd. (C) CactDN-B-LID. Labels are as follows: UBI, a single copy of the ubiquitin open reading frame. LOV, encoding the LOV2 domain of plant phototropin I. HA, encoding a single copy of the influenza hemagglutinin (HA) epitope [61]. 3xMyc, sequences encoding three tandem copies of the 9E10 epitope from human c-myc [113]. ODC, an element encoding 23 amino acids from the synthetic ODC-like degron [83]. The single letters A, G, M, and R represent codons encoding individual alanine, glycine, methionine, and arginine. Specifically, M's denote the initiation codons of the open reading frames of the three constructs. The three A's present in the CactDN segments represent 3 serine-encoding codons that were mutated to alanines, rendering the encoded protein insensitive to Toll pathway signal-dependent proteolysis. GGR in PND-HA-CactDN represents codons encoding the two glycine residues at the C-terminus of ubiquitin and the subsequent arginine residue at the N-terminus of the LOV element. Finally, RRRG represents the codons encoding the critical C-terminal residues of the B-LID domain, which are likely to support degradation by the DesCEND mechanism [100,101].

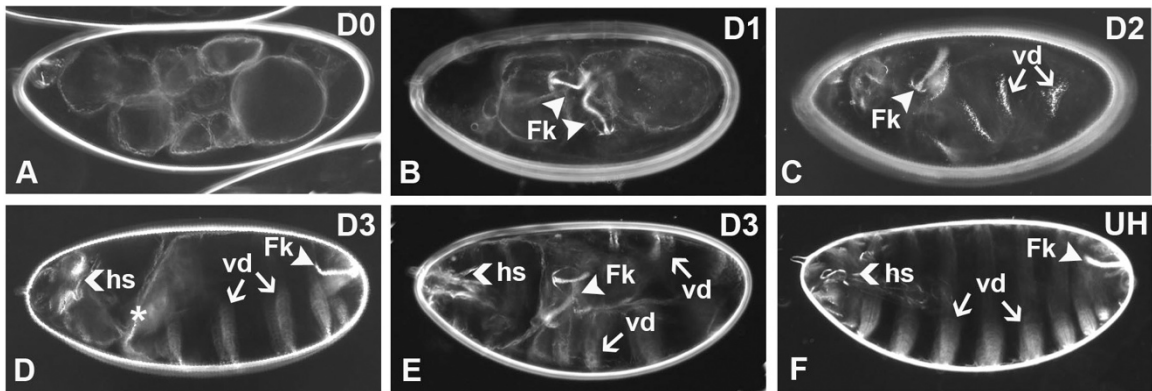


**Fig 7. Representative cuticular phenotypes of embryos expressing maternally provided degron-tagged cactDN constructs.**

Embryos produced by females expressing the degron-tagged versions of CactDN described herein were collected and allowed to complete embryonic development in darkness, then subjected to cuticle preparation [112]. Levels of dorsalization denoted below are indicated at top right of each panel. (A) A completely dorsalized (D0) embryo produced by a female expressing cactDN-psd. (B) A strongly dorsalized (D1) embryo produced by a female expressing cactDN-B-LID. Note the presence of Filzkörper (Fk) structures (= tracheal spiracles). (C) A moderately dorsalized (D2) embryo from a female expressing PND-HA-CactDN. Note the presence of Filzkörper material and narrow ventral denticle (vd) bands. (D) A weakly dorsalized (D3) embryo from a female expressing PND-HA-CactDN, exhibiting the “twisted” phenotype. Note the asterisk marking the twist in the body axis. (E) A weakly dorsalized (D3) embryo, from a PND-HA-CactDN-expressing female, exhibiting the “U-shaped” or “tail-up” phenotype. (F) An apparently normal, unhatched

(UH) embryo produced by a female expressing PND-HA-cactDN. In all panels, arrowheads mark the position of Filzkörper (Fk), arrows mark the position of ventral denticles (vd), and a left pointing angle mark (<) denotes the position of head skeletal (hs) elements. In all panels, anterior is to the left and the dorsal side of the egg is at the top.

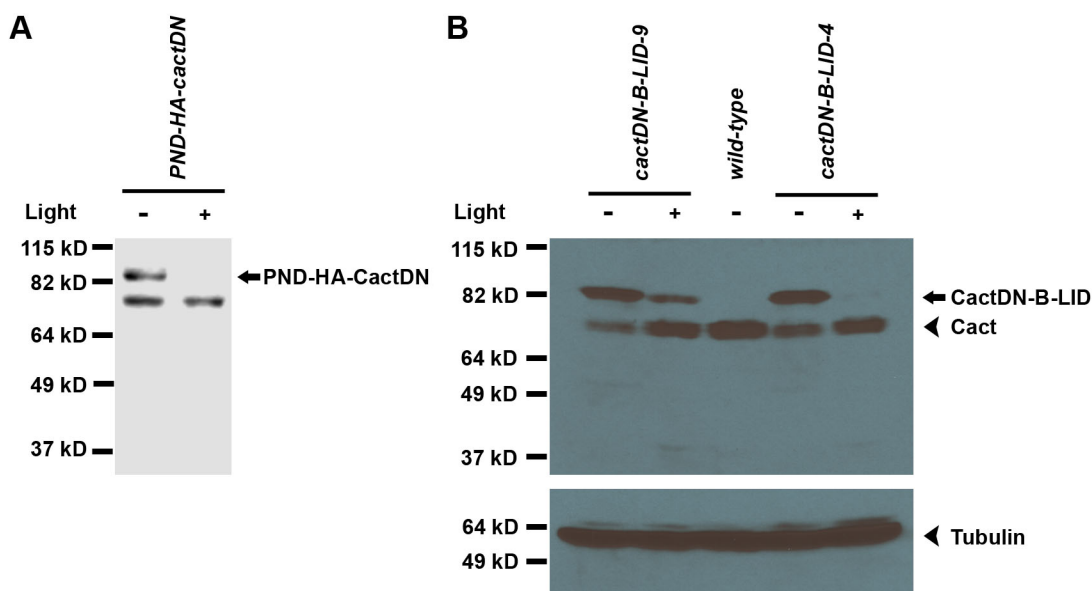


**Fig 8. PND-CactDN and CactDN-B-LID undergo light-dependent loss in *Drosophila* embryos.**

Embryos from females expressing a transgene encoding PND-HA-CactDN (A) or from females expressing two independent transgenic insertions encoding CactDN-B-LID (B), were collected and allowed to develop in either darkness (-) or under blue light illumination (+). Embryonic extracts were prepared from 2–4 hour-old embryos and Western blots of those extracts were probed with antibodies directed against the HA epitope (A) and against Cactus protein (B) are shown. The positions of bands corresponding to PND-HA-CactDN, CactDN-B-LID, and endogenous Cactus (Cact) are shown.

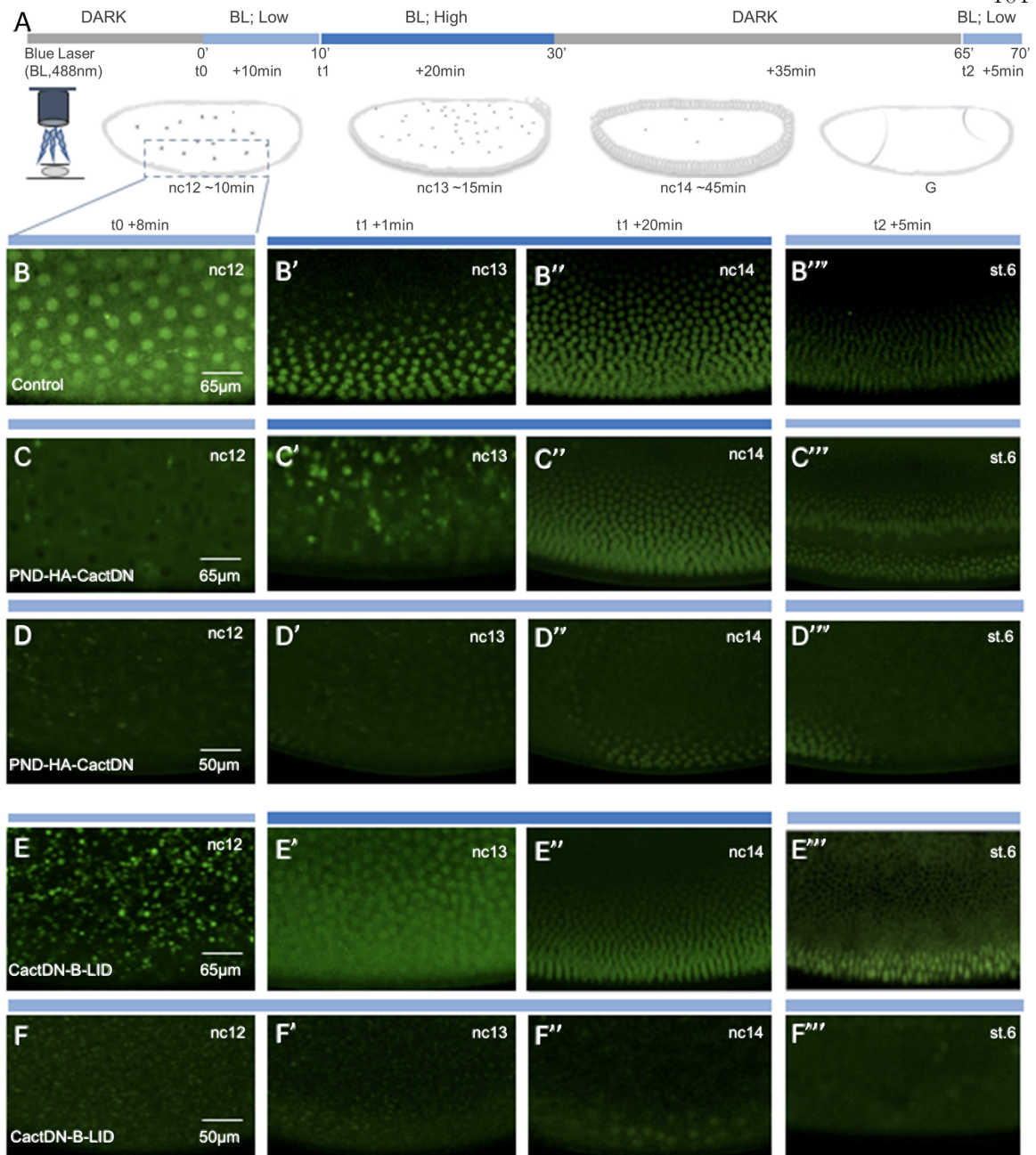


**Fig 9. Laser illumination of live embryos expressing PND-HA-CactDN or CactDN-B-LID induces nuclear accumulation of Dorsal-GFP.**

(A) Schematic showing the imaging setup that was used to visualize Dorsal-GFP in *Drosophila* embryos over a period of ~75 min spanning their development from nuclear

cycle (nc) 12 up to gastrulation (st.6) under conditions that inactivate Cactus-degron fusions. Imaging was initiated at time = 0 (t<sub>0</sub>) and continued for a period of ~10 minutes during nc12 under low power 488 nm laser illumination. Immediately after this treatment (at t<sub>1</sub>) and extending into nc13 (a period of 15 minutes), embryos were illuminated for 20min under high power 488nm laser to initiate degron-mediated loss of CactusDN. After a 30–35' rest in the dark at which point embryos had initiated gastrulation (t<sub>2</sub>), they were again illuminated for 5 min under low power 488nm laser to monitor the Dorsal-GFP gradient and the developmental state of the embryos (t<sub>2</sub> + 5min). The dotted box represents the illuminated area. The remainder of the panels show four snapshots each, taken from movies of embryos containing Dorsal-GFP [85], either expressed alone (B-B<sup>''''</sup>, control; see also S1 Movie) or together with the PND- and B-LID-tagged Cactus variants expressed under the control of the mat- $\alpha$ 4-tub-Gal4:VP16 driver element [108]. The PND-HA-CactDN (C-C<sup>''''</sup>, D-D<sup>''''</sup>; see also S2 and S3 Movies) and the CactDN-B-LID (E-E<sup>''''</sup>, F-F<sup>''''</sup>; see also S4 and S5 Movies) fusion proteins were imaged using conditions outlined in panel A (C-C<sup>''''</sup>, E-E<sup>''''</sup>, S2 and S4 movies) or under low power 488nm laser illumination (light blue bar)(D-D<sup>''''</sup>, F-F<sup>''''</sup>, S3 and S5 Movies). Scale bars represent 65 $\mu$ m or 50 $\mu$ m, as noted; in the absence of Dorsal-GFP nuclear translocation, we used a slightly higher digital magnification (i.e. 50 $\mu$ m), in those cases to increase visibility of empty nuclei.

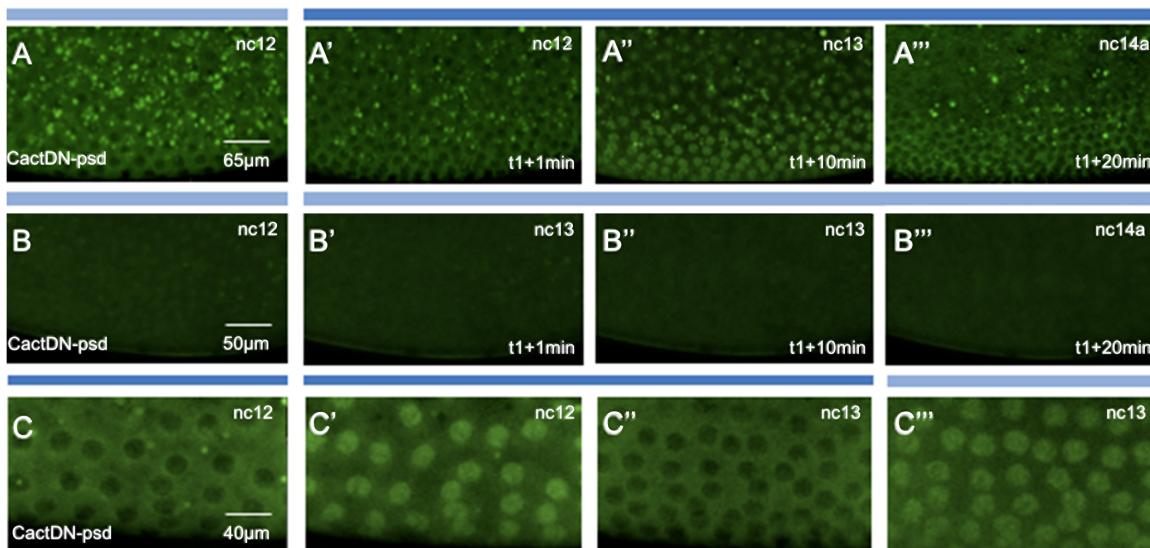


**Fig 10. Laser illumination of live embryos expressing CactDN-psd induces transient cyclical nuclear accumulation of Dorsal-GFP.**

Images shown are four snapshots taken from movies of embryos expressing Dorsal-GFP, together with the photosensitive degron-tagged CactusDN (CactDN-psd) expressed under the control of the *mat-α4-tub-Gal4:VP16* driver element, imaged under different conditions. Panels represent snapshots from respective S6–S8 Movies. (A-A''', B-B''', C-C''') Imaging was initiated at time = 0 ( $t_0$ ) and continued for 10 minutes during nc12 under low power 488 nm, using the scheme diagrammed in Fig 9A. Just after this treatment (i.e.  $t_1$ ) and extending into nc13 ( $t_1+15\text{min}$ ) and nc14a ( $t_1+20\text{min}$ ), embryos were illuminated for 20min at 488nm high power to initiate degron-mediated loss of CactDN-psd (A'-A'''; see also S6 Movie). As a control, embryos were also imaged under low power 488nm only (B-B'''; see also S7 Movie). Scale bars represent 65 $\mu\text{m}$  or 50 $\mu\text{m}$ , as noted; in the absence of Dorsal-GFP nuclear translocation, we used a slightly higher digital magnification (i.e. 50 $\mu\text{m}$ ), to increase visibility of empty nuclei. (C-C''') Embryos were exposed to blue light

earlier for 20 min, initiating at nc12 and into nc13 (blue bar, 488nm), and subsequently imaged under low power 488nm laser illumination. These images show that Dorsal-GFP enters nuclei in a transient manner, entering just before division but relocalize to the cytoplasm after nuclear division; see also S8 Movie.

Maternal Genotype	Hatched Embryos		Unhatched Embryos		N
	%	SEM	%	SEM	
<i>UASp-PND-cactDN</i>	90.4	0.2	9.6	0.2	1099
<i>UASp-cactDN-B-LID</i>	84.8	0.3	15.2	0.3	1485
<i>UASp-cactDN-psd</i>	0	-	100	0	513

<https://doi.org/10.1371/journal.pgen.1009544.t001>

**Table 1. Hatch rates of light-exposed *Drosophila* embryos bearing the three degran-tagged versions of *CactDN*.**

No embryos that were propagated in total darkness hatched.

Maternal Genotype	D0 Embryos		D1 Embryos		D2 Embryos		D3 Embryos		UH Embryos		N
	%	SEM	%	SEM	%	SEM	%	SEM	%	SEM	
<i>UASp-PND-cactDN</i>	0.1	11.1	0.3	11.1	25.0	0.7	71.4	0.9	3.2	0.6	1217
<i>UASp-cactDN-B-LID</i>	13.7	2.2	54.4	0.9	27.6	1.0	4.3	1.2	0	-	1172
<i>UASp-cactDN-psd</i>	98.8	0.1	1.1	1.0	0.1	0.5	0	-	0	-	927
<i>UASp-cactDN-psd</i> (with blue light)	92.7	0.5	6.9	1.7	0.4	1.7	0	-	0	-	466

<https://doi.org/10.1371/journal.pgen.1009544.t002>

**Table 2. Cuticular phenotypes of embryos bearing the three degran-tagged versions of *CactDN*, which had been propagated in total darkness.**

*Chapter 3*TWIST-DEPENDENT RATCHET FUNCTIONING DOWNSTREAM  
FROM DORSAL REVEALED USING A LIGHT-INDUCIBLE DEGRON

This chapter was written with Jihyun Irizarry, Goheun Kim, David Stein, and Angelike Stathopoulos, and published in *Genes Dev.* 2020 Jul 1;34(13-14):965-972.

**ABSTRACT**

Graded transcription factors are pivotal regulators of embryonic patterning but whether their role changes over time is unclear. A light-regulated protein degradation system was used to assay temporal dependence of the transcription factor Dorsal in dorsal-ventral axis patterning of *Drosophila* embryos. Surprisingly, the high-threshold target gene *snail* only requires Dorsal input early but not late when Dorsal levels peak. Instead, late *snail* expression can be supported by action of the Twist transcription factor, specifically, through one enhancer, *sna.distal*. This study demonstrates that continuous input is not required for some Dorsal targets and downstream responses, such as *twist*, function as molecular ratchets.

**INTRODUCTION**

The maternally-deposited transcription factor Dorsal (Dl) is considered a morphogen as it forms a nuclear gradient that specifies distinct cell fates along the dorsal-ventral (DV) axis of *Drosophila* embryos (rev. Reeves and Stathopoulos 2009). How Dorsal nuclear concentration, which varies along the DV axis, impacts target gene expression has been studied, but few studies have focused on the temporal action of this transcription factor on

its targets (Lieberman et al. 2009; Reeves et al. 2012; Rushlow and Shvartsman 2012).

Several recent studies have used optogenetic approaches to study the temporal contributions of other maternal transcription factors, Bicoid (Bcd) and Zelda, finding that they are continuously required in the early embryo to support expression of target genes (McDaniel et al. 2019; Huang et al. 2017). In particular, high-threshold targets of Bcd require continuous input early and late- both preceding and concurrent with cellularization. As Dl levels steadily increase over time, in contrast to Bcd levels which remain relatively constant (rev. Sandler and Stathopoulos 2016b), we hypothesized that target gene dependency on Dl may also be dynamic. In this study, we investigated whether Dl input to target genes is required continuously, as for Bcd, or if instead Dl input is only required at particular timepoints.

## RESULTS

An optogenetic approach was used to examine the temporal action of Dl in supporting target gene expression, initially focusing analysis on the target gene *snail* (*sna*). *sna* is expressed in ventral regions of the embryo in cells that ultimately contain the highest levels of nuclear Dl (Kosman et al. 1991) and is therefore considered a high-threshold target. However, while Dl levels peak in ventral regions of the embryo during nuclear cycle (nc) 14, studies have shown that *sna* is expressed within ventral regions at nc13, suggesting lower levels of Dl are in fact sufficient for this high-threshold target (Reeves et al. 2012).

To assay the temporal dependence on Dl for expression of target genes, including the high-threshold response gene *sna* as well as low-threshold responses including genes *short gastrulation* (*sog*) and *decapentaplegic* (*dpp*) (rev. in Reeves and Stathopoulos 2009), an optogenetic Blue Light-Inducible Degron (BLID) sequence was fused to Dl in-frame at the

C-terminus through modification of the endogenous gene locus using CRISPR/Cas9 technology (Fig. 1A). BLID consists of a LOV2 domain and a degron sequence, such that in the dark, when the alpha-helix of the LOV2 domain interacts with the LOV core domain, the degron is inaccessible; but upon illumination with blue light (~400-500nm), the helix dissociates from the LOV core domain, the degron is exposed, and the entire fusion protein, D1-BLID in this case, is degraded (Bonger et al. 2014).

To assay the degradation efficiency of D1-BLID, embryos laid by homozygous *dl-BLID* mothers were collected and illuminated with blue light for four hours (see Methods). Larval cuticles were examined as (i) a proxy for changes to D1 levels that manifest as DV patterning defects (Roth et al. 1989) and (ii) to assay for any phenotypes induced indirectly by blue light treatment. The majority of *dl-BLID* embryos illuminated for four hours with blue light exhibit cuticles similar in phenotype to dorsalized embryos laid by *dl* null (*dl<sup>1</sup>/dl<sup>4</sup>*) mothers (Fig. 1I, compared with 1K) suggesting that D1-BLID is successfully degraded upon blue light illumination. However, while half the *dl-BLID* embryos that were not subjected to blue light exhibited normal cuticles (Fig. 1B,F), the remaining half exhibited a range of subtle defects including a small number with the more severe, dorsalized cuticle phenotype (Supplemental Fig. S1B-D). In contrast, wildtype and *dl* null mutant embryos appear unaltered when exposed to blue light for four hours (Supplemental Fig. S1A,E), supporting the view that differences in *dl-BLID* cuticles, in the light versus dark, result from light-induced degradation and not indirect effects of blue light exposure. These results suggest that blue light degrades D1, but that the degradation process is likely leaky, occurring to some degree even in the dark.

To directly test if Dl is degraded upon illumination, we stained embryos with anti-Dl antibody and imaged cross-sections to assay for changes to the nuclear concentration gradient. As expected we found that levels of Dl in wildtype embryos containing an unmodified, native *dl* gene are unaltered both for embryos kept in the dark as well as those exposed to blue light for one hour (Fig. 1C,D). In the dark, the Dl gradient signal associated with *dl-BLID* embryos appears qualitatively lower compared to wildtype (Fig. 1C,G). However, when *dl-BLID* embryos were exposed to blue light for one hour almost all of the signal, especially the nuclear gradient, is lost (Fig. 1H). Taken together, Dl-BLID appears to support a relatively normal Dorsal nuclear gradient that is efficiently degradable with blue light illumination but exhibits increased variability in levels/shape compared to wildtype, even in the dark. We use this finding to our advantage, as lower levels of Dorsal initially are likely to be more easily manipulated by short light exposures.

To further confirm that Dl-BLID is being degraded, Dl protein levels in embryos were examined by Western blot using anti-Dl antibodies (Fig. 1E). After 30 min in the blue light, Dl-BLID protein levels were indeed reduced to barely detectable levels (Fig. 1E). For embryos that were kept in the dark, Dl-BLID proteins levels were lower compared to wildtype embryos, possibly due to leaky degradation of the degron (Fig. 1E). This lower Dl level may contribute to the broad range of cuticle phenotypes observed in *dl-BLID* embryos kept in the dark (Supplemental Fig. S1B). The results from the cuticle preparation, Dl antibody staining, and Western suggested that controlling Dl levels using blue light illumination with temporal resolution is feasible.

To directly observe Dl-BLID degradation by blue light, we created and assayed Dl-BLID fluorescent protein fusions. While we find that Dl-mCherry-BLID fusions do not retain Dl function, this fusion does permit visualization of the kinetics of blue light induced degradation. Embryos expressing Dl-mCherry and Dl-mCherry-BLID were imaged live using confocal microscopy. When control embryos are exposed to a high power (40%) blue laser of 488 nm wavelength for 10 min, Dl-mCherry embryos (lacking BLID sequence) exhibit little to no decrease in Dl signal (Fig. 1J,J'; Supplemental Movie S1). On the other hand, Dl-mCherry-BLID embryos undergo a dramatic decrease in Dl signal (Fig. 1L,L'; Supplemental Movie S1) indicating that Dl-BLID degradation is occurring in embryos, with appreciable degradation observable within minutes rather than hours observed in other systems (Baaske et al. 2018). Taken together, these results warrant use of the Dl-BLID system to finely assay temporal dependence of target genes on Dl over time during early embryonic development.

To determine whether high levels of Dl are required continuously throughout early embryonic development, we utilized confocal microscopy to illuminate individual embryos with blue light for either 20 min starting at nc14a (laser early, LE) or 20 min starting at nc14c (laser late, LL) (Fig. 2A). In addition, a triple fluorescent protein (FP) reporter system (H2A-BFP, MCP-GFP, PCP-mCherry) (Bothma et al. 2015) was introduced by genetic crosses into the *dl-BLID* background in order to monitor embryonic development and gene expression responses. The H2A-BFP fusion identifies nuclei, which is useful for monitoring all cells in the developing embryos; whereas the MCP-GFP and PCP-mCherry fusions bind to particular RNA stem-loops, which can be used to monitor nascent transcription.

To start, H2A-BFP signal was used to assay whether blue light illumination affects developmental progression of embryos by observing gastrulation, which involves invagination of the presumptive mesoderm. *dl-BLID* embryos invaginate ventrally and proceed through gastrulation even when illuminated at the low power (0.8%) blue laser needed to image H2A-BFP, despite some low-level degradation of Dl-BLID (“dark”, Fig. 2C; Supplemental Movie S2). Alternatively, when additionally subjected to high power (40%) blue laser illumination during an early time window (“LE”, Fig. 2A), *dl-BLID* embryos fail to ventrally invaginate, and therefore do not gastrulate (Fig. 2D; Supplemental Movie S3). Embryos obtained from females lacking nuclear Dl also fail to undergo gastrulation (Leptin and Grunewald 1990) supporting the idea that the failure of *dl-BLID* embryos illuminated early to gastrulation is due to decrease in Dl levels. In contrast, *dl-BLID* embryos illuminated during a late time window (“LL”, Fig. 2A), surprisingly, are able to invaginate (Fig. 2E; Supplemental Movie S4). These differences in developmental progression between embryos illuminated early or late suggest that high levels of Dl achieved by late nc14 are not necessary for embryos to proceed through gastrulation.

To test how Dl target gene expression is altered by lower Dl levels, we performed fluorescent *in situ* hybridization (FISH) using riboprobes to monitor expressions of the genes *dpp*, *sog*, and *sna*, which span the DV axis (Reeves et al. 2012) comparing expression in the dark to that after illumination. In order to collect enough embryos to carry out FISH experiments, we illuminated embryos *en masse* on plates as opposed to using confocal microscope laser illumination (Fig. 2B; see Methods). *dl-BLID* embryos kept in the dark were analyzed by FISH and show dorsal *dpp* expression at nc14a-b (Fig. 2G) but a narrower

*sna* expression domain with increased variability at the anterior (Fig. 2H, Supplemental Fig. S2). In addition, *sog* expression is repressed in this more narrow domain encompassed by its repressor, Sna (Fig. 2F,H,I; Cowden and Levine 2002). Narrowing of the *sna* domain is likely due to lower levels of total Dl present in the *dl-BLID* background, even in the dark (Fig. 1E,G).

Embryos illuminated for 30 min before being fixed at nc14a (likely illuminated between nc13-nc14a) exhibit ventrally expanded *dpp* (Fig. 2K) but retracted *sog* (Fig. 2J). As *dpp* and *sog* expression share a boundary, where *dpp* is repressed by Dl and *sog* expression is supported by Dl, these genes likely share the same threshold response but with opposite effect (rev. in Reeves and Stathopoulos 2009). Furthermore, *sna* expression is lost in embryos fixed at nc14b (likely illuminated between nc14a-b), but *sog* expression appears unaltered (Fig. 2L; see Discussion). *sog* transcription is absent from ventral-most regions, presumably due to the presence and action of Sna protein despite the lack of *sna* transcripts. As *sna* transcripts have a half-life of ~13 min (Boettiger and Levine 2013), Sna protein made before blue light illumination may perdure and continue to repress *sog* (at least partially) in ventral regions (Bothma et al. 2011).

In contrast, embryos illuminated for 30 min before being fixed at nc14d (likely illuminated later between nc14c-d), express both *sna* and *sog* similar to embryos kept in the dark (Fig. 2I,M). These results support the view that the decrease in Dl levels upon illumination affects multiple target genes, but in a temporally dependent manner. Collectively, these results suggest that embryos exposed to light late (i.e. nc14c to nc14d) can still gastrulate because of maintained expression of target genes including *sna*, a critical

regulator of gastrulation (Leptin and Grunewald 1990); whereas embryos exposed to light early (i.e. nc 14a to nc14b) fail to gastrulate due to loss of *sna*.

To distinguish whether maintenance of *sna* expression at the late timepoint relates to retention of transcripts made earlier or to an ability to produce new transcripts late, even when DI is degraded, we turned to live imaging. The *sna* transcripts identified by *in situ* hybridization within fixed embryos comprise both mature and nascent transcripts; it is difficult to distinguish nascent *sna* transcripts in part because this gene is expressed at high levels and transcripts accumulate. Instead, the MS2-MCP system was used to monitor nascent transcription *in vivo*. Combining the MS2-MCP system with *dl-BLID* allows nascent transcription to be assayed under different illumination schemes. Specifically, transgenic lines containing a previously defined *sna* MS2-based reporter were used to assay *sna* transcriptional activity (Bothma et al. 2015). In these constructs, ~20kB spanning the *sna* locus is used as a reporter in which *sna* is replaced with the *yellow* gene sequence including intronic MS2 RNA stem loop sequences (Fig. 3A; Bothma et al. 2015). When this reporter is actively transcribed, MCP-GFP fusion proteins bind to the stem loops and produce visible nuclear puncta, allowing live monitoring of *sna* expression.

An intermediate power laser setting (5%) was used to image the MS2-MCP signal, while the high power setting was used to degrade DI-BLID (Supplemental Fig. S3A; see Materials & Methods). Again, under these imaging conditions, illumination of *dl-BLID* embryos with high power at the early timepoint (i.e. nc14a-nc14b, “mLE”) leads to gastrulation failure, whereas illumination of embryos later (i.e. nc14c, “mLL”) has no effect on gastrulation despite the use of intermediate laser power to image the MS2-MCP signal for

an extended period of time (Supplemental Fig S3B). We used this scheme, in which MS2-MCP imaging and DI-BLID degradation are compatible, to determine how *sna* transcription is affected by temporal changes in DI levels.

We found that wildtype *sna* MS2-MCP signal (*sna.wt*) was retained when embryos were illuminated with high power laser late (mLL; Fig. 3E,I; Supplemental Movie S7), but was diminished when embryos were illuminated early (mLE; Fig. 3B,H; Supplemental Movie S5). Two enhancers are known to support early *sna* expression during embryogenesis, one proximal (*sna.prox*) and one distal (*sna.dis*) (Ip et al. 1992; Ozdemir et al. 2011; Perry et al. 2010; Dunipace et al. 2011). In order to understand, which cis-regulatory sequences drive *sna* gene expression even when DI is degraded at the late timepoint, we also assayed two reporter variants in which portions of these two early embryonic enhancers had been deleted, constructed in a previous study (Fig. 3A; Bothma et al. 2015). The *sna.Δprox* reporter behaves as the *sna.wt* reporter: embryos illuminated early lose signal, whereas those illuminated late retain it (Fig. 3C,F,H,I; Supplemental Movies S6,S8). In contrast, the *sna.Δdis* reporter loses expression when illuminated at either timepoint (Fig. 3D,G,H,I; Supplemental Movie S6,S8). Thus, the distal enhancer is necessary for late *sna* expression when no or very little DI is present, while the proximal enhancer cannot support late *sna* expression in the absence of DI. This suggests that the proximal *sna* enhancer likely requires high DI levels for activity. Taken together, these results support a model in which DI acts through either enhancer (directly or indirectly) early, but that an additional input is required to sustain late *sna* expression through the *sna.dis* enhancer, specifically.

Another Dl target gene encoding a bHLH transcription factor, *twist* (*twi*), is expressed in ventral regions, and also provides input to *sna* (rev. in Reeves and Stathopoulos 2009). *sna* expression is either lost or greatly diminished in *dl* and *twi* mutants, respectively (Ip et al. 1992). *twi* transcript levels increase rapidly at the onset of nc14 and activation of mesodermal genes follows (Sandler and Stathopoulos 2016a), suggesting that Twi may be an important input into these target genes. Furthermore, peak Dl levels are not required to support *sna* expression as ectopic Twi gradients can support its expression even in conditions of low, but not completely absent, Dl (Stathopoulos and Levine 2002). These previous studies had suggested that Twi may suffice to support *sna* activation at the late timepoint, even in the absence of Dl. However, it was previously not possible to remove Dl but retain Twi as *twi* gene expression is Dl-dependent.

We hypothesized that Twi is responsible for the late expression of *sna*, essentially taking over for Dl. To test this idea, embryos were fixed after 30 min blue LED illumination (Fig. 2B) and assayed for Dl and Twi proteins using antibodies, and for *sna* transcripts by FISH. Embryos exposed to light early or late exhibited low levels or no Dl as expected but, surprisingly, retained Twi expression (Supplemental Fig. S4) demonstrating that even low levels of Dl in nc14 are sufficient to support low levels of Twi expression. *sna* expression is also retained when embryos are illuminated late (Fig. 4A-B''), but not early (Supplemental Fig. 4A-B'') suggesting early nc14 *sna* expression is Dl-dependent. However, when the *twi* mutant is recombined with *dl-BLID*, even when embryos are kept in the dark and high levels of Dl are present, *sna* expression is lost if Twi is absent (Fig. 4C-C''). Taken together, these

results suggested that Twi is a pivotal input for *sna* activation, particularly at late stages when *sna* expression is independent of high Dl levels.

In order to understand the temporal relationship between Dl and Twi transcription factor dynamics, we assayed Twi dynamics with fine time resolution in combination with temporally controlled Dl-BLID levels. Twi levels were detected in *dl-BLID* embryos using a previously described Twi-mCherryLlamaTag fusion protein, which allows early zygotic proteins to be visualized without having to wait for fluorescence maturation (Bothma et al. 2018). When embryos are kept in the dark, mCherry signal intensifies throughout nc14, suggesting exponential production of Twi protein (Fig. 4D,G; Supplemental Movie S9). However, in embryos exposed to high power blue laser illumination at nc14a, no increase in Twi levels is observed (“LE”, Fig. 4E,G; Supplemental Movie S10). In contrast, for embryos illuminated at nc14c, Twi levels increase (“LL”, Fig. 4F,G; Supplemental Movie S10) similarly to embryos without illumination (“dark”, Fig. 4D,G; Supplemental Movie S9). These results support the view that Twi is only responsive to Dl levels early, but is able to maintain its expression late even if Dl levels fall.

To examine how responsive Twi is to Dl levels early, we manipulated Dl levels using various durations of blue laser illumination at nc14b and measured the effect live using the Twi-mCherryLlamaTag as a proxy for Twi levels (see Methods). Short time window illuminations with blue laser (<5 min) early presumably lead to small or negligible changes in Dl-BLID levels and therefore had little or no effect on Twi levels throughout nc14 (Fig. 4H). However, with incremental increase in duration of blue laser illumination (5, 7 or 10min), Twi levels also fail to increase, with severity corresponding to the duration of

illumination. The rate of change for Twi levels decreases substantially, most apparent with the 10 min exposure (Fig. 4H), instead of undergoing the exponential increase observed in dark, laser late, or short time window illuminations of 1 and 3 min (Fig. 4G,H). These results suggest that Twi levels are reflective of the underlying Dl levels early, and that levels of Dl early impact levels of Twi present later.

Interestingly, intermediate exposure of Dl-BLID to blue laser (e.g. 5 to 10 min) results in loss of the late nc14 exponential increase in Twi levels that is normally observed in control embryos (e.g. dark; Fig. 4G) as the rate of change in levels decreases, but it initially remained unclear why (Fig. 4H). In order to explain why Twi levels do not grow exponentially after intermediate duration Dl degradation, we hypothesized that low levels of Dl are retained that continue to support low levels of Twi. In this scenario, a second blue light illumination to knock-down the remaining Dl would be expected to further decrease Twi levels. However, we find that exposure to a second illumination (e.g. 15 min at nc14c) has no effect; Twi is maintained at levels similar to embryos exposed to a single 5 min illumination at nc14b (Fig. 4I). This observation suggests that in late nc14 activation of Twi shifts to a gene regulatory state that is independent of Dl levels. Collectively, these data support the view that a Twi-dependent threshold exists above which Twi can activate its own expression independently of Dl at this late stage and supports a model where levels of Dl in early nc14 determine *twi* expression, but during late nc14, *twi* expression is Dl independent.

## DISCUSSION

In this study, we have examined whether Dl is continuously required to activate target genes in the early embryo by utilizing a Dl-BLID fusion. Dl is required early for the initiation

of expression of the *sna* target gene in ventral regions, but surprisingly is not needed late to maintain its expression. Like *sna*, expression of *htl*, *mes3*, and *netA* are sustained in *dl-BLID* embryos illuminated with blue LED light late (Supplemental Fig. S7) suggesting that other target genes are similarly regulated. In contrast, we found that the lateral gene *sog* is still expressed no matter when Dl degradation occurs during nc14. This unexpected result appears to contradict the model where the *sog* dorsal boundary is formed by limiting levels of nuclear Dorsal. Although, one possible explanation that is consistent with this model is that low levels of Dorsal remain after illumination and are enough to activate *sog*. However, this should result in either a narrow *sog* expression domain or requires asymmetrical degradation of Dorsal, neither of which is observed (Supplemental Fig. S2, Fig. 1H, and Supplemental Movie S1). Another explanation is that once the *sog* domain is established by lower levels of Dl, *sog* does not require Dl to remain active because another factor acts to retain its expression. A simpler explanation is that *sog* transcripts are long and the detected signal could be from *sog* transcripts that were initiated at an earlier timepoint, when Dorsal was present. These possible explanations for how *sog* transcription fails to respond to Dorsal degradation upon illumination are not mutually exclusive. Addressing how *sog* transcription becomes Dl independent in future studies will be an important step forward in our understanding of how the *sog* dorsal boundary is set.

Our results also provide insight into how a transcriptional network may buffer changes in levels of a maternal patterning morphogen. In the case of *sna*, high levels of Dl are required early to activate *sna* gene expression. Dl acts both directly and indirectly by controlling *twi* expression, as Twi is also an input to *sna* (Fig. 4J, left). In contrast, Dl is

dispensable for *sna* activation at later timepoints. When DI levels are reduced *sna* expression remains (Fig. 4J, right), likely maintained by Twi once Twi is expressed. The ability to retain expression of a morphogen target gene despite a decrease in morphogen levels has been termed a “ratchet-reponse”, and was demonstrated for targets of the activin morphogen in *Xenopus* (Gurdon et al. 1995). Twi can maintain its own expression through autoregulation (Kosman et al. 1991; Crews and Pearson 2009), and we propose this autoregulatory feedback serves to support this ratchet response that is able to buffer against decreases in DI levels. However, simple Twi autoregulatory feedback would predict a single steady-state concentration for Twi. Instead, we observed that Twi levels increase exponentially or reach intermediate levels of Twi when varying the length of illumination. While this result would not support simple autoregulatory feedback as a mechanism for maintaining Twi expression in the absence of high DI, it requires Twi levels to be at steady-state. It is possible the observed responses have not reached steady-state, and if given enough time they might all converge to the same steady-state concentration (i.e. a single response supported by autoregulation). It is likely that other factors contribute to *twi* regulation, however these results support the model that DI activates *twi*, and Twi is able to maintain its own expression through autoregulation.

Taken together, we propose that once Twi reaches sufficient levels to support its own auto-activation, DI is no longer required to support *sna* expression (Fig. 4J, right). This is in sharp contrast to the Bcd morphogen which patterns the anterior-posterior (AP) axis and to the early maternal pioneer factor Zelda (Huang et al. 2017; McDaniel et al. 2019). Both Bcd and Zelda have been found to be required continuously; perturbations at any stage cause

loss of gene expression. Alternatively, the DV gene regulatory network shifts from a state of high Dl-dependence to a state of Dl-independence for several target genes expressed in the presumptive mesoderm. It is possible that this ratchet-response relates to the ability of *twi* gene expression to buffer changes in Dl-concentration, and allows the DV-patterning network to respond only to increasing Dl levels. Taken together, ratchet-like responses are crucial steps during animal development not only because they support morphogen-dependent patterning, but also they may serve to buffer expression of target genes against fluctuations in morphogen levels due to genetic and environmental changes.

## **MATERIALS & METHODS**

### *Fly stocks/ husbandry and plasmids*

All flies were kept at 18°C, unless otherwise noted. *yw* was used as wildtype. Fly stocks used: *dl<sup>4</sup>/CyO* (#7096, Bloomington *Drosophila* Stock Center, BDSC), *dl<sup>1</sup>/CyO* (#3236, BDSC), *twi<sup>1</sup>/CyO* (#2381, BDSC), *nos>MCP-GFP*, *nos>mCherry-PCP*, *His2Av-eBFP2* (from Michael Levine, Princeton University, US; Lim et al. 2018), *snailBAC>MS2* with both proximal and distal enhancers (WT, *sna.wt*), proximal deletion (NoPrimary, *sna.Δprox*), or distal deletion (NoShadow, *sna.Δprox*) (from Michael Levine, Princeton University, US; Bothma et al. 2015), *vasa-mCherry* and *Tw-mCherryLlamaTag* (from Hernan Garcia, UC Berkeley, US; Bothma et al. 2018). For details regarding fly crosses, see supplemental methods.

### *Genome editing*

CRISPR was performed as described previously (Gratz et al. 2014). Briefly, the gRNA fly line (targeting before the c-term and after the 3'UTR of Dorsal, see supplemental methods and Table S1) and the Cas9 line *Sp/CyO, P{nos-Cas9}2A*, (NIG-FLY, CAS-0004) were mated. Embryos were collected and the homology-directed repair (HDR) template containing the C-term of *dl* fused to *BLID* (see supplemental methods) was injected into these embryos. Flies were screened for DsRed. The integration was confirmed by PCR and sequencing.

### *Blue light illumination*

Embryos were collected at 18°C for 1 hr followed by 4 hr incubation for aging and illuminated with blue light using either a set of LEDs (2501BU Blue 225 LED 13.8 Watt Square Grow Light Panel 110) or the 488nm laser on a Zeiss LSM 800 confocal microscope. For blue LED light illumination, embryos on agar plates were placed 6.5 cm below the LED light panel and illuminated for appropriate time lengths. After blue light exposure, the embryos were fixed. For 488 nm blue laser illumination, the embryos were dechorionated and mounted on a heptane glued slide. The embryos were immersed in water, and a blue laser was applied using a 25x water immersion objective. All the embryos were prepared under red filtered light to avoid possible DI-BLID degradation by light coming from microscopes or other ambient sources.

### *Cuticle preparations*

Embryos were collected at 18°C for 2 hours, aged 1.5 hours in the dark, and illuminated with blue LEDs for 4 hours. Subsequently, embryos were aged for an additional 36-40 h in the dark and then processed by standard cuticle preparation using lactic acid.

### *Western blot analysis*

Aged embryos were dechorionated and mounted in Halocarbon 27 oil (Sigma-Aldrich). Embryos at nc14b were manually selected and illuminated for 30 min with LED blue light. After light exposure, embryos at nc14c were prepared for standard Western blot.

### *Immunostaining and fluorescent in situ hybridization (FISH)*

Immunostaining and FISH protocols were followed as previously described (Kosman et al. 2004). Sheep anti-digoxigenin (Life Technology PA185378), or rabbit anti-FITC (Invitrogen A889), mouse anti-Dl (1:10; Developmental Studies Hybridoma Bank 7A4) or guinea pig anti-Twi (1:200; Trisnadi and Stathopoulos 2014) were used together with Alexa conjugate secondaries (1:400; Thermo Fisher). DAPI staining (1:10,000 Molecular Probes) was used to mark nuclei.

### *Live imaging and quantification*

To test efficiency of Dl-BLID degradation upon blue laser illumination, 488nm blue laser with 40% laser power (high power) was applied to the embryos heterozygous for either *dl-mCherry* or *dl-mCherry-BLID*; while also applying 555nm laser to monitor mCherry signal.

To examine the continuous requirement of high level of Dl at blastoderm stage, *dl-BLID* embryos were illuminated by 488nm blue laser with 40% laser power (high power) for 20 min, starting at the appropriate developmental stage. Early embryonic development was examined by live imaging of H2A-BFP (i.e. His2Av.eBFP2) using 405nm blue laser with 0.8% laser power (low power) (Lim et al. 2018).

To test *sna* transcriptional activities, the MS2-MCP system was used (Bothma et al. 2015) in combination with *dl-BLID* to optogenetically manipulate Dl levels and assay target gene expression live. To both detect *sna*.MS2-MCP.GFP signals and degrade Dl-BLID, a 488nm blue laser was used for both purposes but using different laser power: 5% (intermediate level) and 15% (high power), respectively. To distinguish this MS2-MCP imaging scheme from standard approach (i.e. Fig. 2A), we refer to MS2-MCP imaging laser early and laser late as “mLE” and “mLL” with exact conditions outlined in Fig. S3A.

To image Twi protein dynamics, Twi-mCherryLlamaTag system, which recognizes maternally-deposited mature mCherry fluorescent protein, was utilized (Bothma et al. 2018). mCherry was imaged live from the onset of *nc14a* to gastrulation while Dl-BLID was degraded by 488nm blue laser at 40% laser power (high power) with varying lengths of time at appropriate developmental stages. All images were taken using a 25x water immersion objective. For additional details regarding imaging and quantification, see Supplemental Methods.

## ACKNOWLEDGEMENTS

We are grateful to Mike Levine and Hernan Garcia for providing fly stocks, Leslie Dunipace for injections and guidance, Theodora Koromila for help with imaging strategy, and Susan Newcomb for edits to manuscript. This study was supported by funding from NIH grants R21HD095639 and R35GM118146 to A.S. and R21OD017964 to D.S.

Author contributions: A.S., D.S., J.I., and J.M. conceived the project and planned the experimental approach. A.S. directed the project. J.I. performed all imaging. J.M. performed all quantitative analysis of the imaging data, Crispr/Cas9 genomic engineering, western analysis, and viability studies. J.I. and J.M. performed stainings. D.S. and G.K. validated the use of BLID for studies in *Drosophila* and helped to develop protocols for its use. J.I., J.M., and D.S. developed the protocol for fixed embryo analysis, whereas J.I. and J.M. develop protocols for BLID live imaging. Data were analyzed by J.I., J.M., and A.S. The manuscript was written by J.I., J.M., and A.S. with edits provided by D.S.

## REFERENCES

- Baaske J, Gonschorek P, Engesser R, Dominguez-Monedero A, Raute K, Fischbach P, Müller K, Cachat E, Schamel WWA, Minguet S, et al. 2018. Dual-controlled optogenetic system for the rapid down-regulation of protein levels in mammalian cells. *Sci Rep* **8**: 15024.
- Boettiger AN, Levine M. 2013. Rapid transcription fosters coordinate snail expression in the *Drosophila* embryo. *Cell Rep* **3**: 8–15.
- Bonger KM, Rakhit R, Payumo AY, Chen JK, Wandless TJ. 2014. General method for regulating protein stability with light. *ACS Chem Biol* **9**: 111–115.
- Bothma JP, Garcia HG, Ng S, Perry MW, Gregor T, Levine M. 2015. Enhancer additivity and non-additivity are determined by enhancer strength in the *Drosophila* embryo. *Elife* **4**. <http://dx.doi.org/10.7554/eLife.07956>.
- Bothma JP, Magliocco J, Levine M. 2011. The snail repressor inhibits release, not

- elongation, of paused Pol II in the *Drosophila* embryo. *Curr Biol* 21: 1571–1577.
- Bothma JP, Norstad MR, Alamos S, Garcia HG. 2018. LlamaTags: A Versatile Tool to Image Transcription Factor Dynamics in Live Embryos. *Cell* 173: 1810–1822.e16.
- Cowden J, Levine M. 2002. The Snail repressor positions Notch signaling in the *Drosophila* embryo. *Development* 129: 1785–1793.
- Crews ST, Pearson JC. 2009. Transcriptional autoregulation in development. *Current Biology* 19: R241–R246. <http://dx.doi.org/10.1016/j.cub.2009.01.015>.
- Dunipace L, Ozdemir A, Stathopoulos A. 2011. Complex interactions between cis-regulatory modules in native conformation are critical for *Drosophila* snail expression. *Development* 138: 4075–4084.
- Ferguson EL, Anderson KV. 1992. Decapentaplegic acts as a morphogen to organize dorsal-ventral pattern in the *Drosophila* embryo. *Cell* 71: 451–461.
- Gratz SJ, Ukken FP, Rubinstein CD, Thiede G, Donohue LK, Cummings AM, O'Connor-Giles KM. 2014. Highly specific and efficient CRISPR/Cas9-catalyzed homology-directed repair in *Drosophila*. *Genetics* 196: 961–971.
- Gurdon JB, Harger P, Mitchell A, Lemaire P. 1994. Activin signalling and response to a morphogen gradient. *Nature* 371: 487–492.
- Gurdon JB, Mitchell A, Mahony D. 1995. Direct and continuous assessment by cells of their position in a morphogen gradient. *Nature* 376: 520–521. <http://dx.doi.org/10.1038/376520a0>.
- Huang A, Amourda C, Zhang S, Tolwinski NS, Saunders TE. 2017. Decoding temporal interpretation of the morphogen Bicoid in the early embryo. *Elife* 6. <http://dx.doi.org/10.7554/eLife.26258>.
- Ip YT, Park RE, Kosman D, Yazdanbakhsh K, Levine M. 1992. Dorsal-twist interactions establish snail expression in the presumptive mesoderm of the *Drosophila* embryo. *Genes Dev* 6: 1518–1530.
- Kosman D, Ip YT, Levine M, Arora K. 1991. Establishment of the mesoderm-neuroectoderm boundary in the *Drosophila* embryo. *Science* 254: 118–122.
- Kosman D, Mizutani CM, Lemons D, Cox WG, McGinnis W, Bier E. 2004. Multiplex detection of RNA expression in *Drosophila* embryos. *Science* 305: 846.
- Leptin M, Grunewald B. 1990. Cell shape changes during gastrulation in *Drosophila*. *Development* 110: 73–84.

- Liberman LM, Reeves GT, Stathopoulos A. 2009. Quantitative imaging of the Dorsal nuclear gradient reveals limitations to threshold-dependent patterning in *Drosophila*. *Proc Natl Acad Sci U S A* 106: 22317–22322.
- Liberman LM, Stathopoulos A. 2009. Design flexibility in cis-regulatory control of gene expression: synthetic and comparative evidence. *Dev Biol* 327: 578–589.
- Lim B, Heist T, Levine M, Fukaya T. 2018. Visualization of Transvection in Living *Drosophila* Embryos. *Mol Cell* 70: 287–296.e6.
- McDaniel SL, Gibson TJ, Schulz KN, Fernandez Garcia M, Nevil M, Jain SU, Lewis PW, Zaret KS, Harrison MM. 2019. Continued Activity of the Pioneer Factor Zelda Is Required to Drive Zygotic Genome Activation. *Mol Cell* 74: 185–195.e4.
- Ozdemir A, Fisher-Aylor KI, Pepke S, Samanta M, Dunipace L, McCue K, Zeng L, Ogawa N, Wold BJ, Stathopoulos A. 2011. High resolution mapping of Twist to DNA in *Drosophila* embryos: Efficient functional analysis and evolutionary conservation. *Genome Research* 21: 566–577. <http://dx.doi.org/10.1101/gr.104018.109>.
- Ozdemir A, Ma L, White KP, Stathopoulos A. 2014. Su(H)-Mediated Repression Positions Gene Boundaries along the Dorsal-Ventral Axis of *Drosophila* Embryos. *Developmental Cell* 31: 100–113. <http://dx.doi.org/10.1016/j.devcel.2014.08.005>.
- Perry MW, Boettiger AN, Bothma JP, Levine M. 2010. Shadow enhancers foster robustness of *Drosophila* gastrulation. *Curr Biol* 20: 1562–1567.
- Port F, Chen H-M, Lee T, Bullock SL. 2014. Optimized CRISPR/Cas tools for efficient germline and somatic genome engineering in *Drosophila*. *Proc Natl Acad Sci U S A* 111: E2967–76.
- Reeves GT, Stathopoulos A. 2009. Graded dorsal and differential gene regulation in the *Drosophila* embryo. *Cold Spring Harb Perspect Biol* 1: a000836.
- Reeves GT, Trisnadi N, Truong TV, Nahmad M, Katz S, Stathopoulos A. 2012. Dorsal-ventral gene expression in the *Drosophila* embryo reflects the dynamics and precision of the dorsal nuclear gradient. *Dev Cell* 22: 544–557.
- Roth S, Stein D, Nüsslein-Volhard C. 1989. A gradient of nuclear localization of the dorsal protein determines dorsoventral pattern in the *Drosophila* embryo. *Cell* 59: 1189–1202.
- Rushlow CA, Shvartsman SY. 2012. Temporal dynamics, spatial range, and transcriptional interpretation of the Dorsal morphogen gradient. *Curr Opin Genet Dev* 22: 542–546.
- Sandler JE, Stathopoulos A. 2016a. Quantitative Single-Embryo Profile of *Drosophila* Genome Activation and the Dorsal–Ventral Patterning Network. *Genetics* 202: 1575–1584. <http://dx.doi.org/10.1534/genetics.116.186783>.

- Sandler JE, Stathopoulos A. 2016b. Stepwise Progression of Embryonic Patterning. *Trends Genet* 32: 432–443.
- Stathopoulos A, Levine M. 2002. Linear signaling in the Toll-Dorsal pathway of *Drosophila*: activated Pelle kinase specifies all threshold outputs of gene expression while the bHLH protein Twist specifies a subset. *Development* 129: 3411–3419.
- Trisnadi N, Stathopoulos A. 2014. Ectopic expression screen identifies genes affecting *Drosophila* mesoderm development including the HSPG Trol. *G3* 5: 301–313.
- Zeitlinger J, Zinzen RP, Stark A, Kellis M, Zhang H, Young RA, Levine M. 2007. Whole-genome ChIP-chip analysis of Dorsal, Twist, and Snail suggests integration of diverse patterning processes in the *Drosophila* embryo. *Genes & Development* 21: 385–390. <http://dx.doi.org/10.1101/gad.1509607>.

FIGURE 1

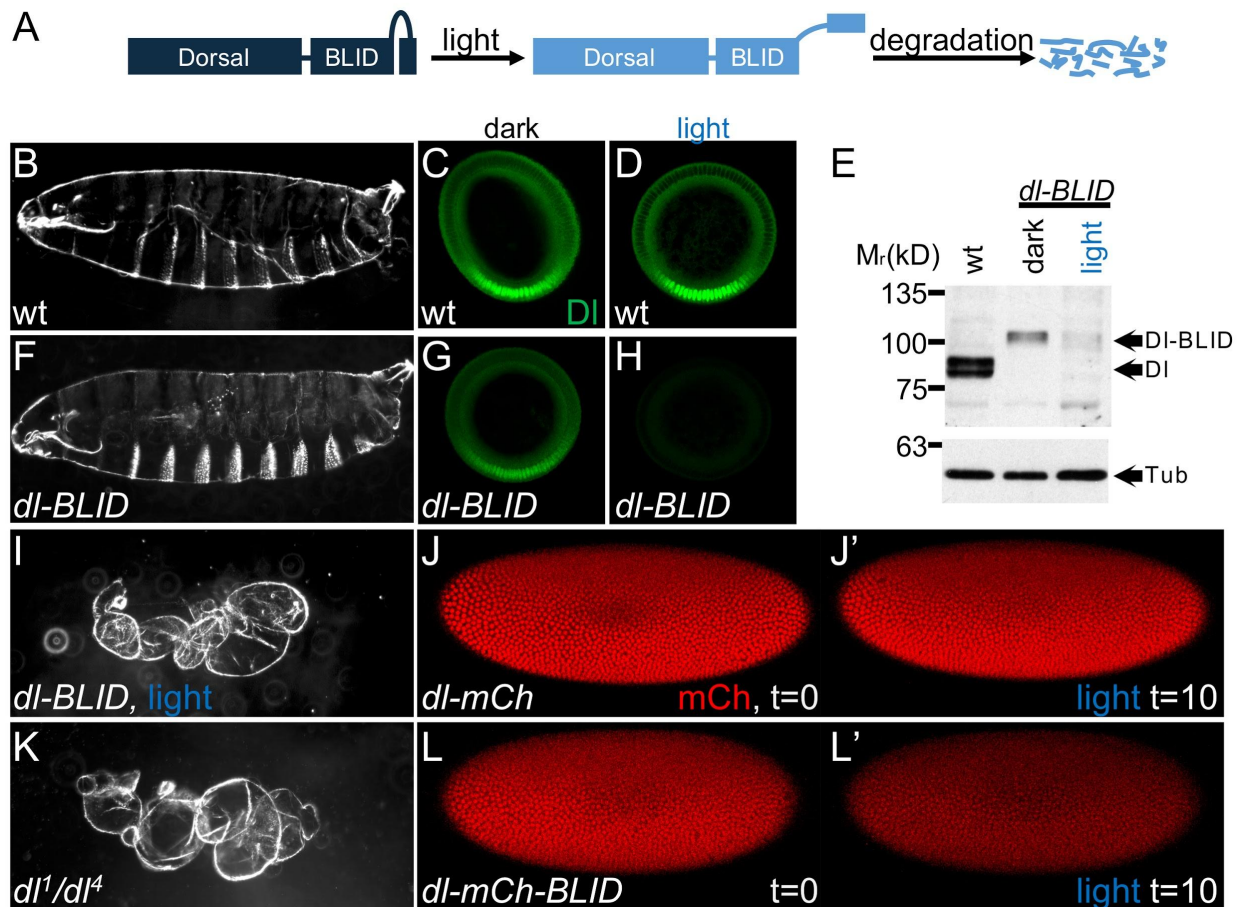


**Figure 1. Illumination with blue light induces degradation of DI-BLID fusion proteins.**

(A) The DI-BLID construct. Blue light illumination causes a degradation sequence to be exposed, resulting in the degradation of the entire fusion protein. (B,F,I,K) Cuticle preparations of embryos derived from wildtype mothers without illumination (B, n=181/190), *dl-BLID* mothers without illumination (F, n=147/310), *dl-BLID* mothers with four hours of blue LED illumination (I, n=31/36), and *dl* null mutant (*dl<sup>1</sup>/dl<sup>4</sup>*) mothers without illumination (K, 142/142). (C,D,G,H) Manually cross sectioned embryos stained with anti-DI antibody (green) derived from wildtype mothers without illumination (C, n=5/5), wildtype

mothers with 1 hour of blue LED illumination (D, n=5/5), *dl-BLID* mothers without illumination (G, n=5/5), and *dl-BLID* mothers with one hour of blue LED illumination (H, n=4/5). All embryos in C,D,G,H were imaged at the same settings, demonstrating a clear decrease in D1 levels in H. (E) Western blot of wildtype (lane 1), *dl-BLID* without illumination (lane 2), and *dl-BLID* with 30 min blue LED illumination (lane 3). Top blot is probed with anti-D1 antibody. Bottom blot is probed with anti-Tubulin antibody to serve as a loading control. Arrows indicate the approximate locations of D1, D1-BLID, and Tubulin bands. (J,J',L,L') Snapshots from live imaging movies of *dl-mCherry* (n=1) and *dl-mCherry-BLID* (n=3) at the start (J, L t=0) and after 10 min of 40% power blue laser illumination (J', L' t=10). All embryos/larval cuticles are oriented with anterior to left and dorsal up, except cross sections which are oriented with the ventral side at the bottom and the dorsal side at the top.

FIGURE 2

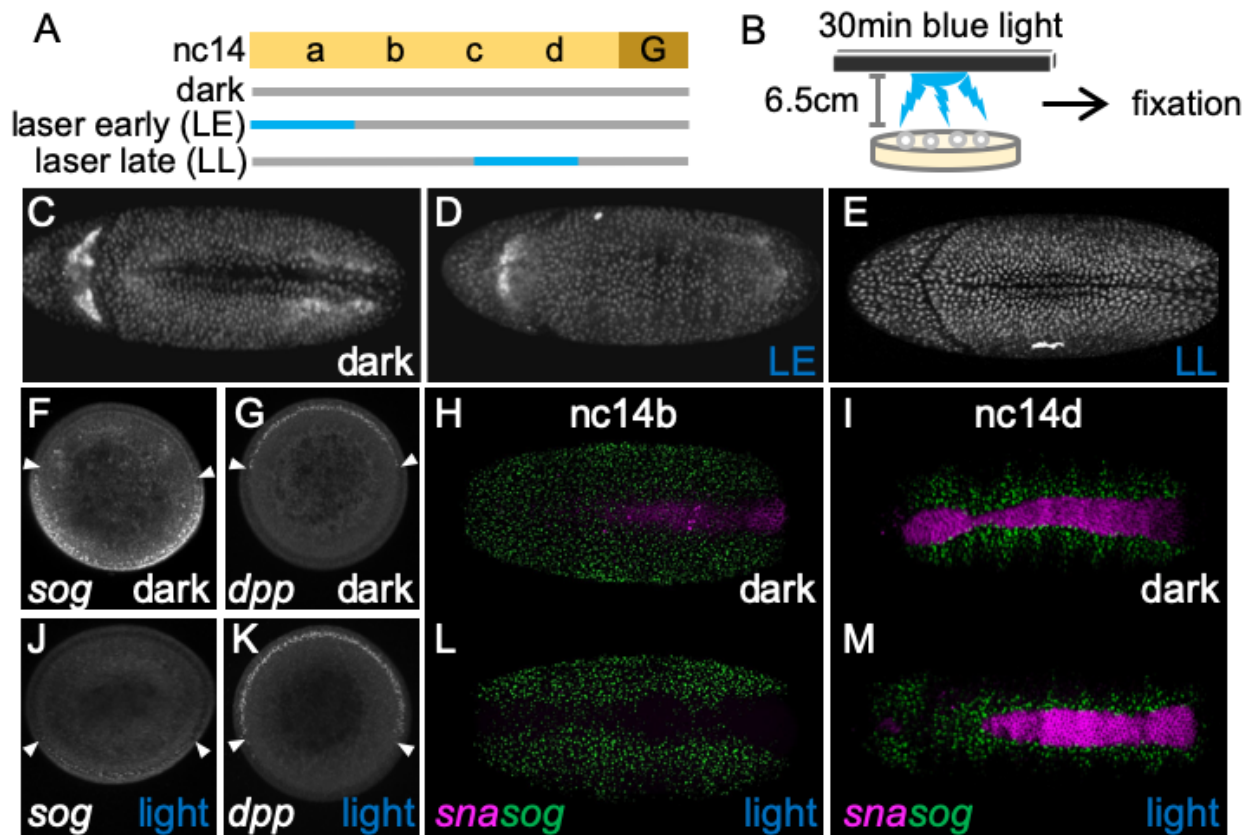


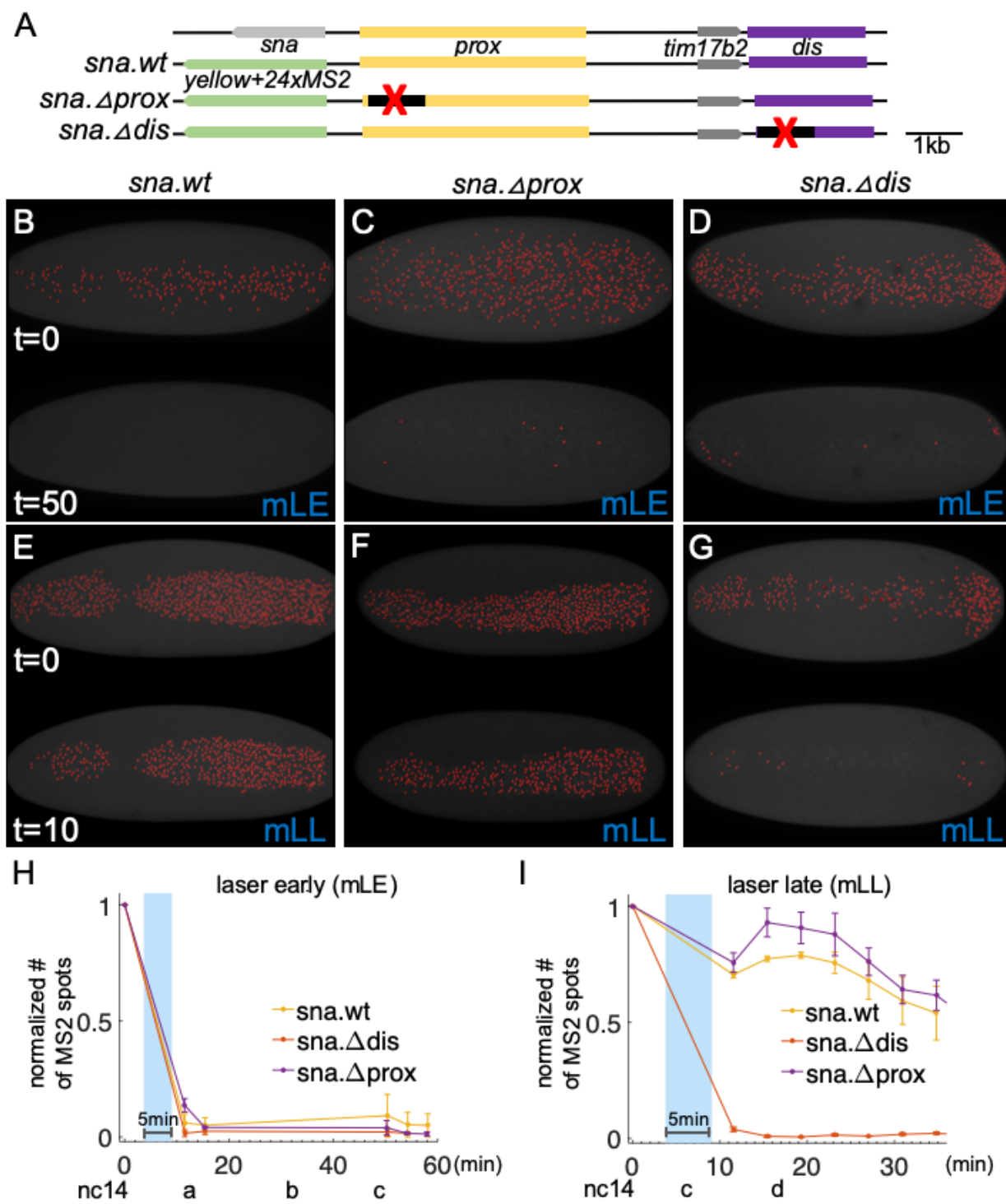
**Figure 2. High levels of DI at late stages are not required to support *sna* or gastrulation.**

(A) Scheme of 20 min 40% blue laser illumination on single embryos using a confocal microscope. Gray bar: 0.8% (low power) 405nm laser to image H2A.BFP. Blue bar: 0.8% 405nm laser and 20 min 40% (high power) 488nm laser. (B) Scheme of 30 min blue LED illumination on a batch of embryos, which was followed by immediate fixation. (C-E) *dl-BLID* embryos at stage 6 illuminated using a laser (see A). Embryos (C) kept in the dark (“dark”, n=2), (D) with 20 min blue laser early illumination (“LE”, n=3), and (E) with 20 min blue laser late illumination (“LL”, n=3). (F,G,J,K) Manually cross-sectioned *nc14a* embryos stained for *sog* (F,J) or *dpp* (G,K) transcripts kept in the dark (F,G), or with 30 min

blue LED illumination (“light”, J,K). White arrowheads mark the expression boundaries.

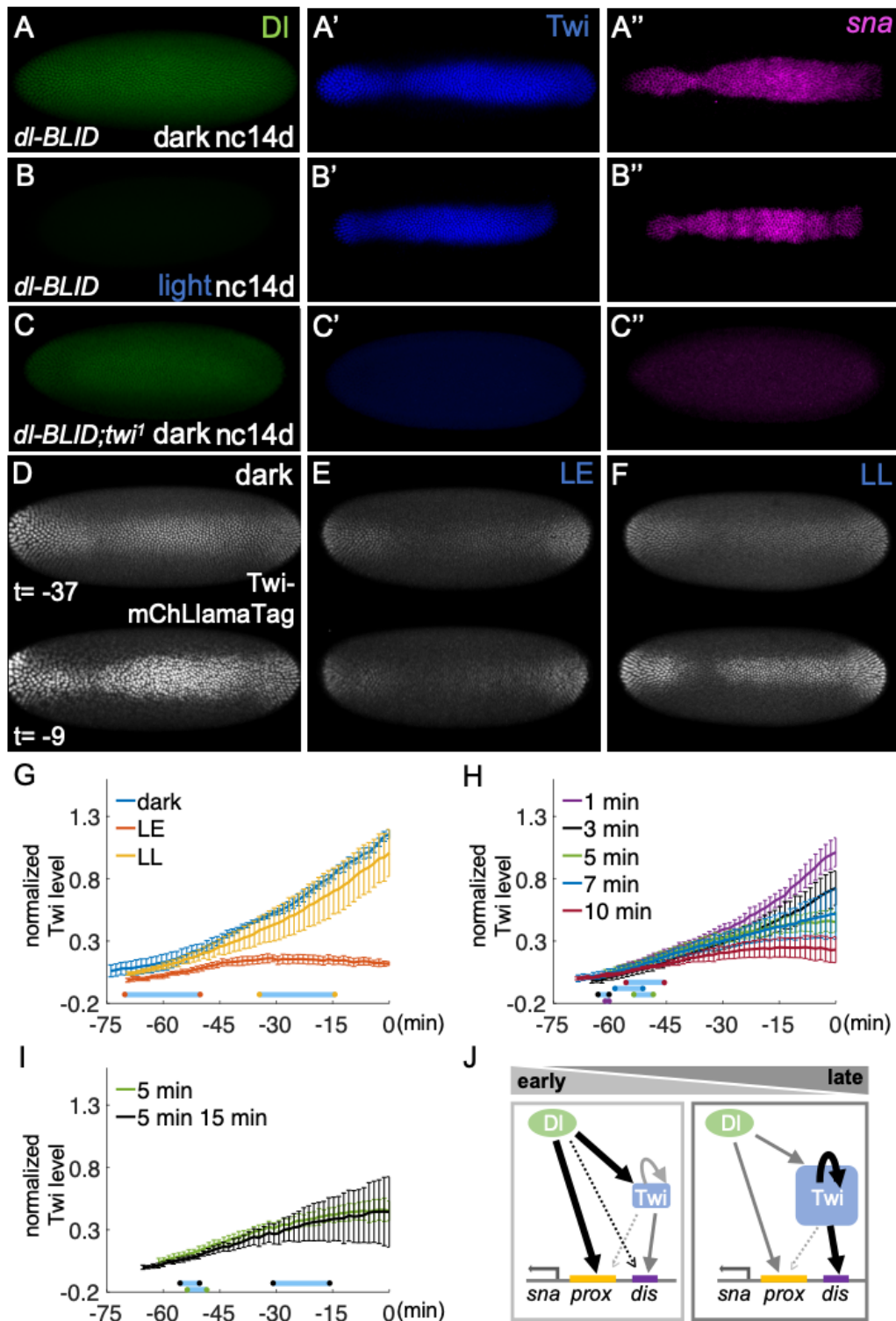
(H,I,L,M) *sna* (purple) and *sog* (green) transcript expressions were assayed in *dl-BLID* embryos kept in the dark (H: n=4,L: n=6) or illuminated with a blue LED (see B) for 30 min (I: n=7,M: n=6). The stages of embryos at fixation were nc14b (H,L) and nc14d (I,M). All whole mount images are a ventral view with anterior to the left. Cross-sectioned embryos are aligned with the ventral side at the bottom and the dorsal side at the top.

FIGURE 3



**Figure 3. High level of DI is required for *sna* activation only at early stages, but not at late stages, in which *sna* expression is predominantly supported by the *sna* distal enhancer.** (A) Scheme of large reporter constructs used to assay *sna* transcriptional activities by MS2-MCP system (Bothma et al. 2015). (B-G) MCP.GFP signals associated with the *sna* MS2 reporter were imaged (false-colored red dots) in *dl-BLID* with early (B-D) or late (E-G) blue laser illumination that is MS2-MCP imaging compatible (“mLE” and “mLL”, respectively; see also Fig. S3) in various *sna* regulatory conditions including wildtype (*sna.wt* B,E), proximal enhancer deletion (*sna.Δprox* C,F), and distal enhancer deletion (*sna.Δdis* D,G). Images are snapshots from movies, before illumination (top) and after illumination (bottom) of each panel. Three movies were taken for each condition. Ventral views of embryos are shown with anterior oriented to the left. (H,I) Quantitative analysis of the number of MCP.GFP dots associated with the *sna* MS2 reporter in *dl-BLID* embryos with *sna.wt*, *sna.Δprox*, or *sna.Δdis* *sna* regulatory condition. Number of MS2-MCP.GFP spots are counted in each time frame, and the values are normalized to the initial value detected in the first frame (before 5min blue laser illumination with 15% laser power) with early laser (H) or late laser (I) illumination. Blue shade indicates a time frame of 5min 15% blue laser illumination. Error bars represent standard error of the mean. For individual traces, see Supplemental Fig. S5. For details for detection of *sna*.MS2-MCP.GFP and blue laser illumination, see Supplementary Fig. S3.

FIGURE 4



**Figure 4. Twi suffices to support *sna* expression at late stages in the absence of high levels of Dl.** (A-C) Expression of Dl proteins (green), Twi proteins (blue), and *sna* transcripts (pink) were examined in *dl-BLID* embryos with *twi* wildtype (A,B) or *twi<sup>l</sup>* mutant background at nc14d without (A,C) or with (B, n=11) 30min blue LED illumination. (D-F) Snapshots from movies showing mCherry signal associated with the Twi-mCherryLlamaTag (Twi-mChLlamaTag; Bothma et al. 2018) under various confocal 40% blue laser illumination conditions: (D) no illumination (dark), (E) 20min early illumination at nc14a (LE), and (F) 20min late illumination at nc14c (LL). Time indicates the time length preceding the germband extension. (G-I) Quantitative analysis of the levels of mCherry associated by Twi-mChLlamaTag with varying 40% blue laser illumination conditions: (G) no illumination (dark, blue), 20 min early illumination at nc14a (LE, red), and 20 min late illumination at nc14c (LL, yellow); (H) illumination at nc14b for: 1 min (purple), 3min (black), 5min (green), 7min (blue), and 10min (red); and (I) the 5 min (green) data replotted from H to compare with 5min at nc14b followed by additional 15 min illumination at nc14c (black). Three movies were taken for each condition. For the individual traces, see Supplemental Fig. S6. (J) A model of regulatory shift, such as from high level of Dl to high level of Twi dependent regulatory states, to support *sna* expression throughout early embryonic development. Dl proteins (green circle), Twi proteins (Blue square), *sna* proximal enhancer (yellow bar), and *sna* distal enhancer (purple bar). All embryo images are ventral views with anterior to the left. Blue bars in G-I represent the average time window of confocal blue laser illumination to their respective curves. Error bars represent standard error of the mean.

*Chapter 4*A SUBSET OF TARGET GENES REQUIRES DORSAL  
TRANSCRIPTION FACTOR NUCLEAR RETENTION

This chapter was written with Virginia Pimmett, Antonio Trullo, Mounia Lagha, and Angelike Stathopoulos.

**SUMMARY**

While the spatial response to morphogen gradients has been well studied, less is known regarding the temporal aspects of morphogen inputs including the duration necessary to elicit a transcriptional response. Across the dorsal-ventral (DV) axis of *Drosophila* embryos, changing nuclear levels of the transcription factor Dorsal (DL), the NF $\kappa$ B homolog, controls target gene expression, but whether DL's nuclear retention also plays a role is unknown<sup>1,2</sup>. We devised an optogenetic approach fusing DL to two genetically encoded tags to temporally manipulate its levels while using the MS2-MCP imaging system<sup>3</sup> to assay dynamics associated with five representative genes expressed in ventral, ventrolateral, lateral, and dorsal regions<sup>4,5</sup>. Using DL-LEXY to support blue light-inducible nuclear export<sup>6,7</sup>, we identified critical temporal windows of DL input for ventral- and ventrolaterally-expressed genes. Genes expressed in the lateral and dorsal regions were refractory to export of DL, likely because low level nuclear-cytoplasmic shuttling persists during blue light. Only when DL was eliminated through blue light-induced degradation using DL-BLID<sup>8,9</sup> did the boundary of lateral gene *short gastrulation (sog)* shift ventrally. Furthermore, mutation of serines within a previously

characterized nuclear export sequence (NES) located at the DL C-terminus<sup>10,11</sup> resulted in the width of ventral gene *snail* (*sna*) either being reduced (Ser>Ala) or unaffected (phosphomimetic Ser>Asp). *sog* was unaffected by either mutation. Collectively, these results demonstrate that DL nuclear retention is important for particular morphogen responses and suggest that regulation of DL nuclear export contributes to differential gene expression along the DV axis.

## RESULTS & DISCUSSION

To develop a system where we could control nuclear Dorsal levels, we used CRISPR/Cas9 genome editing to construct in-frame fusions of DL and DL-mCherry to a genetically-encoded LEXY (light-inducible nuclear export system<sup>6</sup>) tag, generating *Drosophila* stocks *dl-LEXY* and *dl-mCh-LEXY* (Figure 1B). These stocks are homozygous viable, fertile and healthy in the dark, but embryos reared under blue light result in ~95% failure to hatch, suggesting this perturbation has a large effect on DL function (Figure S1A). When embryos expressing DL-LEXY are treated with blue light, it results in eviction of the fusion protein from the nucleus detected by anti-DL antibody staining after fixation (Figure S1B-D) or by following the mCherry signal associated with DL-mCh-LEXY with live imaging (Figure 1A,C,D, Movie S1). After the blue light is removed, DL-mCh-LEXY again enters nuclei within ~5 minutes (Figure 1E, Movie S1). This process of eviction and return can be repeated multiple times (Movie S1) allowing the possibility to test target genes for critical windows of time when DL is required using live imaging. Our previous study used a DL-BLID (Blue Light Inducible Degron<sup>2</sup>) fusion to temporally control DL degradation (Figure 1A) but the process was irreversible by

design<sup>8</sup>, because *dl* transcripts are maternally deposited so presumably little to no new protein is made once it is degraded. With these two means to perturb DL levels, either transiently using DL-LEXY or irreversibly using DL-BLID, our aim was to compare how target gene dynamic expression is affected.

DL forms a nuclear concentration gradient and regulates gene expression along the dorsal-ventral (DV) axis of *Drosophila* embryos<sup>12,13</sup> (Figure 1F). It activates expression of an array of target genes including high threshold targets *snail* (*sna*) and *twist* (*twi*) in the ventral region, intermediate threshold target *ventral neuroblasts defective* (*vnd*) in ventrolateral regions, and low threshold *short gastrulation* (*sog*) broadly in lateral regions. The transcriptional repressor Sna represses *sog* and *vnd* in the ventral domain, refining expression of these genes to two lateral stripes. DL also acts directly as a repressor to limit the expression of the gene *zerknüllt* (*zen*) to dorsal regions, inverse to the *sog* pattern. To monitor expression of these DL target genes, we used several previously published MS2 reporters that relate to reporter genes inserted at exogenous locations (*sna-MS2*, *vnd-MS2*)<sup>14,15</sup> and created three new reporters of endogenous expression by inserting MS2 at each gene locus (*twi-MS2*, *sog-MS2*, and *zen-MS2*) (Figure 1G; see Methods). The MS2 array presumably does not perturb the expression of these genes, as homozygous stocks are viable. Using the MS2-MCP imaging system, we were able to observe expression of these DL target genes in different locations along the DV-axis over time (e.g. Figure 1H).

The early stages of embryogenesis consist of rapid DNA replication and nuclear divisions, called nuclear cycles (nc). DL nuclear levels are dynamic during these early

stages<sup>4,16</sup> (Figure 2A). We examined DL's role during nc14, the longest nuclear cycle during these early stages, and the time at which many zygotic genes are activated. Nc14 can be broken into four ~15-20 min periods depending on temperature and are referred to as nc14a, nc14b, nc14c, and nc14d. To test the effect of removing DL transiently at nc14c, when nuclear concentration of DL in ventrally-positioned nuclei is highest<sup>4</sup>, embryos from *dl-LEXY* mothers were illuminated with blue light for 10 min and compared to embryos that were kept in the dark during a similar period of time (Figure 2A). In the dark, *sna* is continuously expressed in the ventral domain during nc14c (Figure 2B, Movie S2). After 10 min of blue light exposure, *sna* nascent transcription is undetectable in most nuclei (Figure 2D 00:11, Movie S2) but reinitializes after returning to the dark (Figure 2D 00:22, Movie S2). Similar effects were observed with *twi*, although expression after recovery is difficult to detect as levels of *twi* are normally low at this point (Figure 2C,E Movie S3). These results demonstrate that in *dl-LEXY*, DL is always required to maintain *sna* and *twi* expression at nc14.

We previously showed that *sna* transcription at later stages of nc14 is independent of DL, as expression is retained in the presence of blue light in embryos laid by *dl-BLID* mothers<sup>7</sup>, an apparent contradiction to the experiment using *dl-LEXY* (Figure 2D 00:11, Movie S2). To test this discrepancy, we repeated the experiment using *dl-BLID* under the same imaging conditions as *dl-LEXY* (Figure 2I,K, Movie S2). *sna* transcription initially decreases after 10 min of blue light illumination in *dl-BLID* and partially recovers when returned to the dark, in agreement with our previous results<sup>7</sup> (Figure 2K, Movie S2). To test if *sna* could recover under a longer illumination, we illuminated for 20 min. *sna*

recovers in *dl-BLID* even in the presence of light (Figure 2M, Movie S2) but, in contrast, *sna* expression remains inhibited in *dl-LEXY* (Figure 2F, Movie S2). The number of detected foci, which reflects the number of detected active sites of transcription, was quantified over time and showed the same trend (Figure 2G,H). In *dl-BLID*, *sna* transcription recovers with similar dynamics regardless of whether the embryo was exposed to blue light for 10 min or 20 min (Figure 2H). Importantly, these results suggest that despite both approaches reducing nuclear DL levels under blue light illumination, DL-LEXY has a negative effect on *sna* transcription under blue light, possibly due to the transient nature of DL-LEXY shuttling in and out of the nucleus.

To test whether a ventrolateral gene responsive to intermediate levels of DL would also be affected by the same intensity light for 10 min, we tested *vnd*. Similar to *sna*, *vnd* is expressed continuously at nc14. It is repressed ventrally by *sna*, restricting its expression to two lateral stripes of which only one is visible in a ventral-lateral view (Figure 2J, Movie S3). As with *twi* and *sna*, *vnd* expression is lost during the 10 min blue light exposure and recovers after returning to the dark (Figure 2L, Movie S3).

While the previous results suggest that DL input is required continuously in *dl-LEXY*, they do not demonstrate whether DL input at nc14 alone is sufficient to properly express DL target genes. To test this, we illuminated embryos at nc13 and then allowed DL to recover in the dark during nc14 (Figure 3A). In the dark, *sna* transcription is detected in nc12, nc13, and nc14 (Figure 3B, Movie S4). At the end of nc14 embryos successfully undergo gastrulation (Figure 3C, Movie S4). When we illuminate at nc13, *sna* transcription is lost at nc13 during the illumination (Figure 3D, -00:15, Movie S4). In

addition, *sna* levels are reduced and transient or even absent at nc14 for five of six embryos examined, even though DL levels are allowed to recover (Figure 3D, 00:06 and 00:26, Movie S4). Furthermore, embryos illuminated at nc13 do not undergo gastrulation (Figure 3E, Movie S4), suggesting that both *sna* and *twi* cumulative expression levels are below what is required for gastrulation to occur<sup>17</sup>. To test whether nc13 is critical, or if only total exposure to DL is critical, we also illuminated during nc12 and nc14a, and allowed the embryos to recover in the dark during nc13 and nc14b through gastrulation (Figure 3F, Movie S4). During the blue light exposure, *sna* expression is very low or undetectable (Figure 3F, -00:31 and 00:06, Movie S4). The recovery of *sna* expression in nc13 showed distinct variability. If *sna* transcription at nc13 was strong (Figure 3F, -00:15, Movie S4), *sna* expression appeared to recover later in nc14b-d (Figure 3F, 00:26, Movie S4) and embryos were able to invaginate, albeit somewhat defectively compared to wild type or *dl-LEXY* in the dark (Figure 3G, Movie S4). If *sna* expression was weak at nc13, *sna* expression at nc14 was weak or absent (Figure S2E). We quantified the number of spots between conditions and observed that embryos illuminated at nc13 do not recover *sna* expression at nc14 (Figure 3L). These data suggest that nc13 is a critical window for DL to properly activate *sna*.

To determine if there are any differences between how high threshold and intermediate threshold targets respond to DL at nc13, we also observed *vnd-MS2* expression when illuminated during nc13. In the dark, *vnd* is detected at nc12, nc13, and nc14 (Figure 3H). Similar to *sna*, *vnd* expression is greatly reduced by illumination during nc13 (Figure 3J, -00:15). However, unlike *sna*, *vnd* appears to recover at nc14 (Figure 3J, 00:06 and

00:26). These embryos also fail to undergo gastrulation, as expected (Figure 3K, compare with 3E). We quantified *vnd* expression at nc14 and found it appears largely unaffected by removal of DL at nc13 (Figure 3M).

These experiments demonstrated how DL input is important for expressing high and intermediate threshold target genes, but we also wanted to test how low threshold target genes are affected by the removal of DL. In initial studies, when we illuminated *dl-LEXY* at nc13 or nc14, we did not notice any obvious changes in *sog* or *zen* expression. Previously, changes in the *sog* boundary in fixed samples were only detected if we illuminated *dl-BLID* embryos for a prolonged period<sup>8</sup>. Thus, we illuminated continuously from the end of nc12 until germ-band extension was observed (i.e. all of nc13 and nc14, Figure 4A). For *sog-MS2*, transcription was rarely detected at nc12 in the dorsal-lateral view, however, low levels of signal were detected at nc13 and nc14 in the dark (Figure 4D, Movie S5). When illuminated during nc13 and nc14, there was not a noticeable difference in the position of the dorsal boundary of the *sog* domain (Figure 4D,F, Movie S5). To quantify this we calculated the area of expression for all the time points in nc13 and the first 100 time points of nc14 (~40 min) and then computed the difference between nc14 and nc13. When comparing the change in area at nc14 and nc13, we saw no significant difference between the light and dark in *dl-LEXY* (Figure 4B). To test another low-threshold target, we looked at *zen*, which is expressed in an inverse pattern to *sog*. In the dark, *zen-MS2* was detected at nc12, nc13, and nc14, with retraction during nc14 as described previously<sup>4,18</sup> (Figure 4E, Movie S6). When illuminated during nc13 and nc14, similar to *sog*, no significant difference was detected for *zen* in the expression

area at nc14 compared to the area in nc13 in the dark or light with *dl-LEXY* (Figure 4C,E,G, Movie S6).

To determine the effect of blue light illumination on the boundaries of *sog* and *zen* in *dl-BLID*, we also examined *sog-MS2* and *zen-MS2* dynamics in embryos laid by *dl-BLID* mothers when illuminated from nc13 through nc14. In the dark, *sog* expression is similar to *dl-LEXY* and the dorsal boundary at nc13 and nc14 appears in a similar location (Figure 4H, Movie S5). However, when illuminated from nc13 through nc14, the dorsal boundary of *sog* retracts (Figure 4B and 4J, compare -00:12 and 00:08, Movie S5). This retraction is detected by a change in area between nc13 and nc14, where the area is smaller at nc14 (Figure 4B). The light condition is significantly different from the dark condition in *dl-BLID* for *sog* ( $p=0.002$ ). Under similar imaging conditions, *zen* expression in *dl-BLID* remains unchanged (Figure 4C,I,K, Movie S6) as seen by comparing the change in area at nc14 relative to nc13 between dark and light (Figure 4C).

Since *sog* and *zen* are unaffected by blue light in *dl-LEXY*, this suggests that the low levels of nuclear DL-LEXY are sufficient to correctly pattern these genes. In *dl-BLID*, *sog* expression retracts in response to a decrease in DL levels, but *zen* does not expand. This could be because we are unable to detect a change in the *zen* boundary between nc12 and nc13, *zen* responds to a lower threshold than *sog*, or *zen* responds to DL at an earlier time, such as nc12. Taken together, these experiments demonstrate that *dl-LEXY* and *dl-BLID* behave differently for the low threshold target *sog*.

As stated previously, the critical difference between *dl-LEXY* and *dl-BLID* is that in *dl-LEXY* the protein is still present but cytoplasmic, while in *dl-BLID* the protein is degraded under blue light illumination. It is known that DL shuttles in and out of nuclei in ventral and lateral regions where Toll signaling is active and drives DL nuclear accumulation but also in dorsal nuclei without Toll signaling<sup>11</sup>. The major role of Toll signaling is to remove Cactus, an inhibitor of DL that prevents nuclear accumulation of DL<sup>19</sup>. However, *cactus Toll* double mutant embryos exhibit a lateralized phenotype, likely because they still retain the ability of DL to enter the nucleus but cannot reach peak levels<sup>20</sup>. For these reasons, it is reasonable to assume that during blue light illumination DL-LEXY continues to shuttle in and out of the nucleus but with a strong bias towards being exported. These experiments with DL-LEXY suggest that the rapid shuttling of DL-LEXY into and out of the nucleus is enough to support the low threshold gene *sog* (Figure 4B,D,F); whereas this same activity actively prevents *sna* from being expressed (Figure 2F). In contrast, when DL-BLID is degraded, the levels of DL fall below the threshold necessary to support *sog*, resulting in a shift of the dorsal boundary (Figure 4B,H,J) and loss of DL disrupts activation of *sna*. However, the system is able to reinitialize in a DL-independent manner, which we have previously shown to be mediated by Twi<sup>8</sup>.

To further explore what role nuclear export plays in the levels of nuclear DL, we generated mutations in a known nuclear export sequence (NES) in the C-terminal end of DL<sup>11</sup>. We mutated four serine residues, one of which has been observed to be phosphorylated in the C-terminal NES<sup>21</sup>, to either alanine residues (*dl-AAAA*) that cannot

be phosphorylated or to aspartic acid residues (*dl-DDDD*) that could mimic a constitutively phosphorylated state. These mutations were made in the context of *dl-Venus* rescue transgenes that were then introduced into a *dl* mutant background (Figure 4L; see Methods). We performed *in situ* hybridization using riboprobes for *sna*, *ind*, *sog*, and *zen* (Figure 4M,O). In *dl-AAAA*, *sna* is narrow, but *sog* and *zen* do not appear to change boundaries at early nc14b when *ind* is not expressed. The expression patterns of the target genes in the *dl-DDDD* background qualitatively appear normal. In late nc14, *sna* is again narrow in *dl-AAAA*, but *ind*, *sog*, and *zen* are relatively unperturbed. We also performed an antibody staining for DL in these mutants and found that the levels of nuclear DL on the ventral side are lower in the *dl-AAAA* mutant (Figure S3A-D). The narrow *sna* domain in *dl-AAAA* (Figure 4M,O) supports the idea that DL nuclear levels can be modulated by affecting nuclear export and suggests that phosphorylation of the NES might be a way of controlling export and thus DL nuclear levels.

In summary, this study identified the temporal requirements for targets of the morphogen DL, which controls patterning along the DV axis, and suggests that regulation of DL nuclear export may act to support different threshold outputs. Our data show that high threshold targets (*sna*, *twi*) require DL input during a critical window. This result echoes the similar temporal requirement of the Bicoid morphogen for high threshold target genes but differs in that DL is not required until nc13 whereas Bicoid is required earlier at nc11<sup>22</sup>. Furthermore, while *sna* expression can switch to a DL-independent mode late in nc14<sup>8</sup>, this can only occur when DL is entirely degraded via DL-BLID mediated degradation. Export to the cytoplasm via DL-LEXY likely allows some transient DL in

the nucleus, which is incompatible with promoting *sna* expression, suggesting that *sna* requires sustained DL-input. On the other hand, low threshold target genes (*sog*, *zen*) are supported even in the presence of blue light with DL-LEXY suggesting that even transient exposure suffices. In support of this, perturbations of the DL C-terminal NES also differentially influence target gene expression, showing effects on high threshold targets (*sna*) but having little to no effect on low threshold targets (*sog*). We suggest that DL-morphogen gradient outputs are differentially sensitive to DL nuclear retention and also that nc13 is a critical time in which DL is required to support high threshold targets such as *sna*. It is possible this window is important for establishing sustained DL nuclear levels to support high threshold target genes and may relate to preparations during nc13 for the midblastula transition (MBT) <sup>23-25</sup>. This study provides general insights into the timing of action of morphogens through the regulation of nuclear import-export kinetics providing support for recently generated models<sup>2,26</sup>.

## ACKNOWLEDGMENTS

We are grateful to Norbert Perrimon and Richelle Sopko for sharing unpublished data, Sarah Bray, Mike Levine, and Julia Zeitlinger for sharing fly stocks and antibodies, Leslie Dunipace for comments on the manuscript, and Theodora Koromila, Kimberley Muchenje, Anil Ozdemir, and David Stein for technical support and helpful discussions. We warmly thank Eileen Furlong and Alessandro Dulja for sharing their optogenetic box and related advice. This study was supported by funding from National Institutes of Health grants R03HD101961 and R35GM118146 to A.S.; M.L. and A.T. are supported by CNRS and V.P. by ERC SyncDev grant to M.L.

## **AUTHOR CONTRIBUTIONS**

A.S. and J.M. conceived the project. J.M. and V.P. planned the experimental approach. A.S. directed the project. J.M. performed all experiments with the exception of the hatching assay and DL quantifications with the optogenetic box, performed by V.P. J.M. conducted all the computational work used to analyze live imaging data. A.T. developed the code to quantify DL eviction in fixed embryos. J.M., V.P., and A.T. analyzed the data with input from A.S. and M.L. The manuscript was written by J.M. and A.S. with input from V.P., A.T., and M.L.

## **DECLARATION OF INTERESTS**

The authors declare no competing interests.

## FIGURES AND LEGENDS

Figure 1

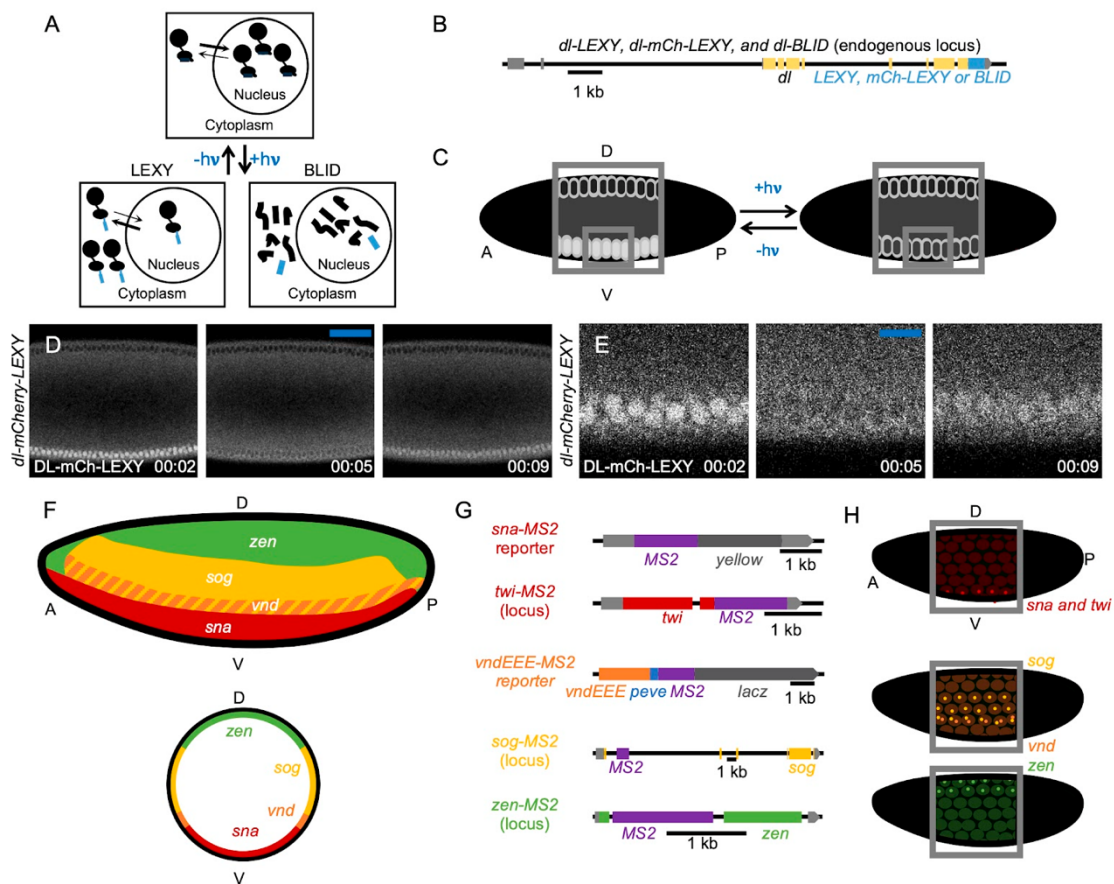


**Figure 1. DL-LEXY is rapidly exported using blue light and is reversible.**

(A) In LEXY, blue light reveals a NES, leading to nuclear export. In BLID, blue light reveals a degron, leading to degradation. (B) The DL-LEXY, DL-mCh-LEXY, and DL-BLID constructs were inserted endogenously using CRISPR/Cas9, shown in blue. Exons are yellow/gold, and the 5' and 3' UTR are gray. (C) A model of DL export when DL-LEXY and DL-mCh-LEXY, in white, are exposed to blue light. The large gray box represents the field of view and the area of blue light illumination. The small gray box represents the zoomed area. (D) DL-mChery-LEXY before (00:02), during (00:05), and

after (00:09) blue light exposure. The blue bar represents images taken under blue light. (E) The same images as in D, only zoomed in. (F) DL target gene expression along the DV axis in a lateral view and cross section. Target genes are colored based on threshold: high threshold targets (*sna* and *twi*) are red, intermediate threshold targets (*vnd*) are orange, low threshold targets (*sog*) are yellow/gold, and repressed targets (*zen*) are green. (G) *MS2* constructs used to assay target gene expression. The gene body matches the threshold color, *MS2* is purple, UTRs are gray, and introns and untranscribed regions are black. (H) *MS2* foci depicting *sna* and *twi* (red), *vnd* (orange), *sog* (yellow/gold), and *zen* (green). Embryos are oriented with the anterior (A) to the left, posterior (P) to the right, dorsal (D) at the top, and ventral (V) at the bottom.

Figure 2

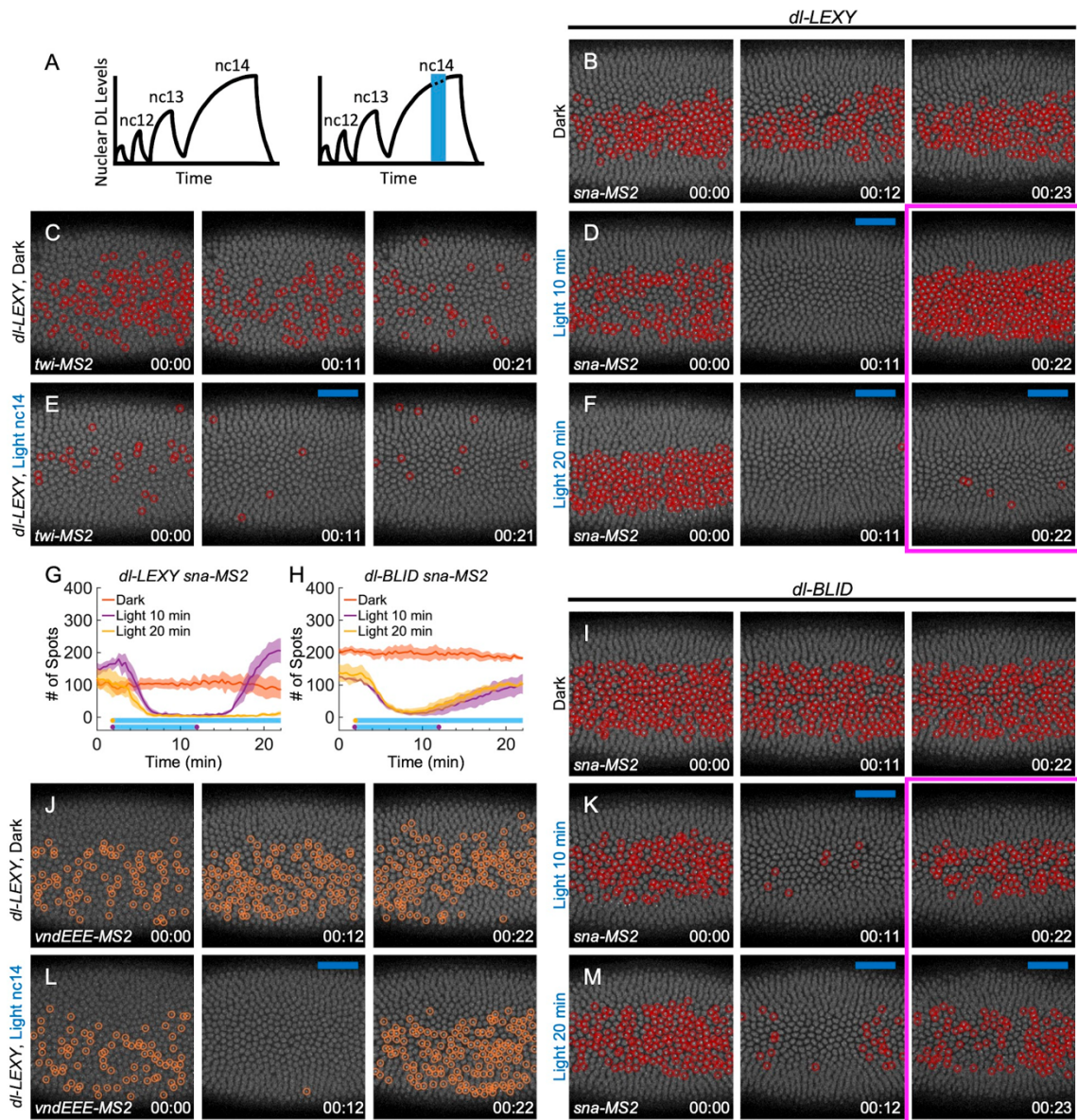


**Figure 2. Expression for *twi*, *sna*, and *vnd* is lost in DL-LEXY, but *sna* expression recovers in DL-BLID, when illuminated with blue light at *nc14*.**

(A) Schematic of DL nuclear concentration trends over time from previously quantified data<sup>4</sup> without blue light (left) and with 10 min blue light exposure during *nc14* (right). (B,

D, F) *sna-MS2* in *dl-LEXY* during late nc14, when kept in the dark (B), illuminated for 10 min (D), or illuminated for 20 min (F), at 0 min (00:00), 11 min (00:11 and 00:12), and 22 min (00:22 and 00:23). (C, E) *twi-MS2* during nc14, when kept in the dark (C) or illuminated for 10 min (E) at 0 min (00:00), 11 min (00:11), and 21 min (00:21). (G) The mean number of spots (mean  $\pm$  SEM, n = 3 for each) detected for *sna-MS2* in *dl-LEXY* over time. Red is in the dark, purple is 10 min illumination, and yellow is 20 min illumination. The blue bars represent the average illumination window for the matching condition. (H) Similar to G, except for *dl-BLID*. (I, K, M) Similar conditions to B, D, and F, except for *dl-BLID*. (J, L) *vndEEE-MS2* in *dl-LEXY* during nc14, when kept in the dark (J) or illuminated for 10 min (L) at 1 min (00:00), 12 min (00:12), and 22 min (00:22). Foci are circled in red (*sna* and *twi*) or orange (*vnd*), blue bars represent frames under blue light, and time stamps are hours:minutes.

Figure 3

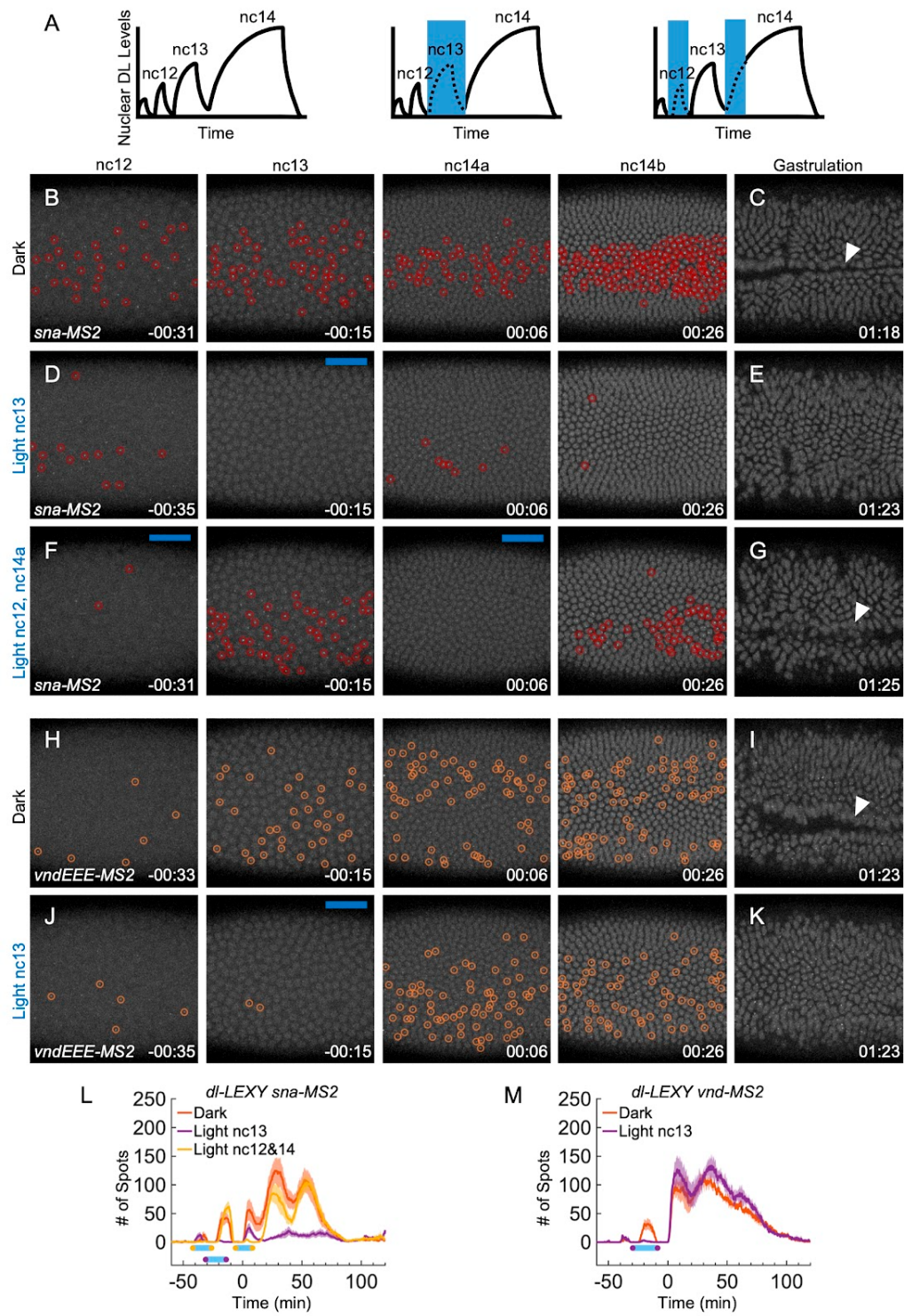


**Figure 3. *sna* expression is reduced, while *vnd* expression is not, at nc14 when DL-*LEXY* is illuminated at nc13.**

(A) Schematic of DL nuclear concentration trends over time without blue light (left), with blue light during nc13 (center), or with blue light during nc12 and early nc14a. (B) *sna-MS2* in *dl-LEXY* in the dark at nc12 (-00:31), nc13 (-00:15), nc14a (00:06) and nc14b (00:26). (C) Mesoderm invagination when kept in the dark. (D) Similar to B, except with illumination at nc13. (E) Failed mesoderm invagination when illuminated at nc13. (F) Similar to D and E, except with illumination at nc12, and nc14a. (G) Mesoderm invagination when illuminated at nc12 and nc14a. (H) *vndEEE* expression in the dark. (I) Same as C. (J) *vndEEE* expression when illuminated with blue light at nc13. (K) Same as E. (L) The average number of spots (mean  $\pm$  SEM) for *sna-MS2*. Red is in the dark (n=5/5), purple is blue light illumination at nc13 (n=5/6, other shown in Figure S2E), and yellow is blue light illumination at nc12 and nc14a (n=5/8, others shown in Figure S2E). The blue bars represent the average illumination window for the matching condition. (M) Similar to L, except for *vnd* (mean  $\pm$  SEM, n = 3 for each). For all images, foci are circled in red (*sna*) or orange (*vnd*), t = 0 is set as the beginning of nc14, blue bars represent frames under blue light, white arrowheads point to mesoderm invagination, and time stamps are hours:minutes.

Figure 4

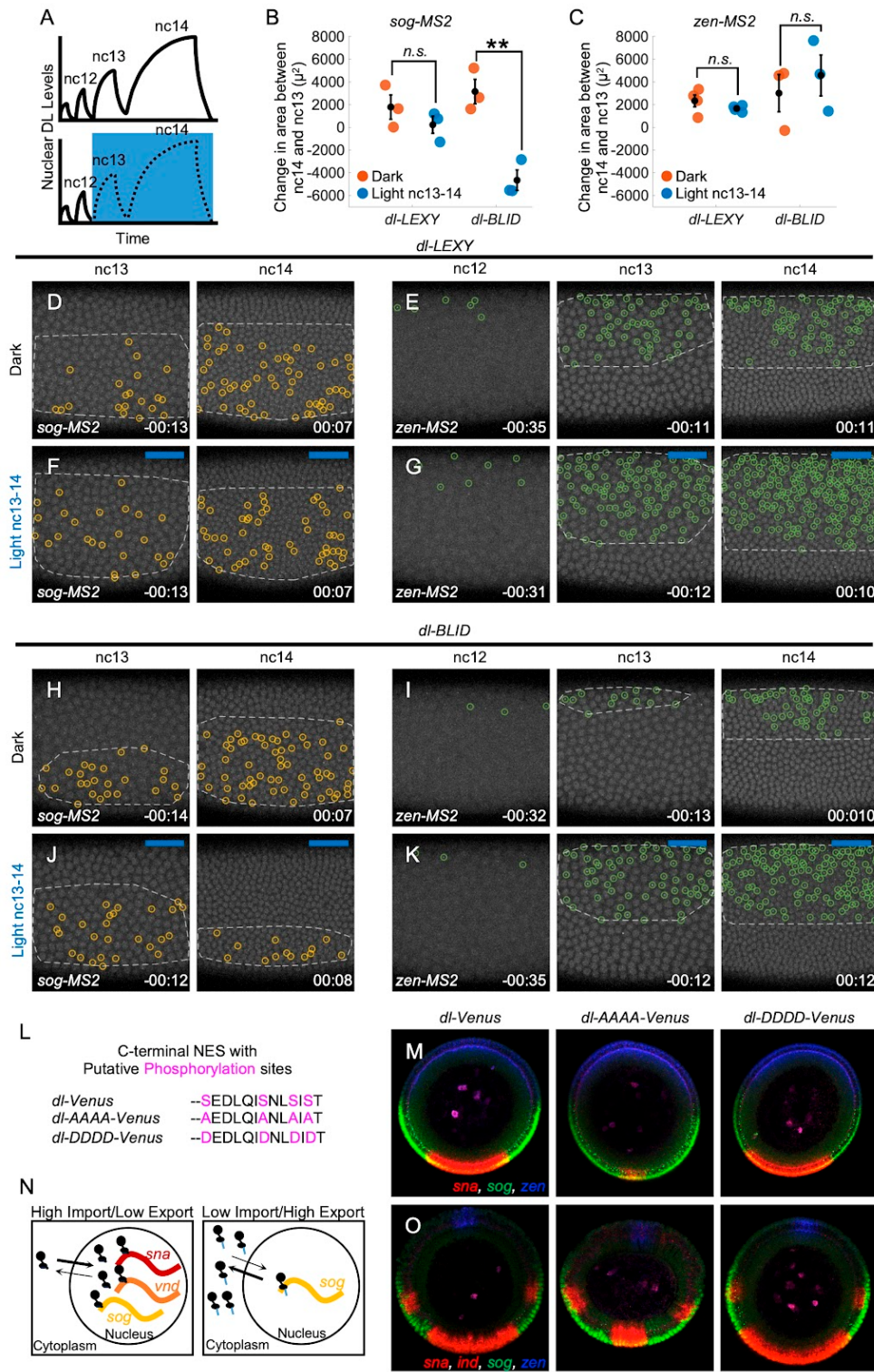


**Figure 4. Transient levels of DL are enough to support *sog* and *zen* expression.**

(A) Schematic of DL nuclear concentration trends over time without blue light (left) and with continuous blue light in nc13 through nc14 (right). (B, C) Quantification of the change in area between nc14 and 13 for *sog-MS2* in *dl-LEXY* and *dl-BLID* (B) and for *zen-MS2* in *dl-LEXY* and *dl-BLID* (C). Red/orange markers are in the dark and blue markers are with illumination from nc13-14 (in black, mean  $\pm$  SEM, n = 3 for each, except for DL-LEXY *zen-MS2*, n=4). When comparing dark to light at nc13-14, only *dl-BLID* is significantly different, p = 0.002, for *sog-MS2* (Tukey's HSD). There is no significant difference for *dl-LEXY* and *dl-BLID* for *zen-MS2* when comparing dark to light. (D, F) *sog-MS2* in *dl-LEXY* when kept in the dark at nc13 (-00:13) and nc14a (00:07) (D) or when illuminated continuously from nc13 through nc14 (F). (E, G) *zen-MS2* in *dl-LEXY*, when kept in the dark at nc12 (-00:32 and -00:35), nc13 (-00:13 and -00:11), and nc14a (00:04 and 00:08) (E) or when illuminated continuously from nc13 through nc14 (G). (H, I, J, K) Similar to D, E, F, and G, except for *dl-BLID*. (L) Mutations of known or putative phosphorylation sites in the C-terminal NES of DL, with alanine substitutions blocking phosphorylation and increasing nuclear export and aspartic acid substitutions potentially mimicking a constitutively phosphorylated state and decreasing nuclear export. (M, O) Transverse cross sections of in situ hybridization for DL target genes in *dl-Venus*, *dl-AAAA-Venus*, and *dl-DDDD-Venus* rescue constructs in a *dl* null background, where *sna* and *ind* are in red, *sog* is in green, and *zen* is in blue. M is nc14b and O is nc14c/d. (N) If export of DL out of the nucleus is low, DL levels are high,

and *sna* (red), *vnd* (orange), and *sog* (yellow) can be activated by DL. If export of DL out of the nucleus is high, DL levels are low, and only *sog* (yellow) can be activated by DL. Foci are circled in yellow (*sog*) or green (*zen*), areas calculated from detected MS2 spots are depicted by white dashed lines, blue bars represent frames under blue light, and time stamps are hours:minutes.

## STAR METHODS

### RESOURCE AVAILABILITY

#### Lead contact

Further information and requests for resources and reagents should be directed to and will be fulfilled by the lead contact, Angelike Stathopoulos ([angelike@caltech.edu](mailto:angelike@caltech.edu)).

#### Materials availability

*Drosophila* strains and other reagents generated in this study will be available upon request from the lead contact, or the commercial sources listed in the key resources table.

#### Data and code availability

Two github repositories with the codes for quantitative analyses were generated and are publically available: ([https://github.com/StathopoulosLab/MS2\\_quantification](https://github.com/StathopoulosLab/MS2_quantification)) and ([https://github.com/ant-trullo/FixedLEXY\\_Analyzer](https://github.com/ant-trullo/FixedLEXY_Analyzer)). Any additional information required to reanalyze the data shown in this paper is available from the lead contact upon request.

## EXPERIMENTAL MODEL AND SUBJECT DETAILS

### Fly stocks and husbandry

All *D. melanogaster* stocks were kept at 22°C in standard medium. Experimental crosses were kept in cages with apple juice agar plates supplemented with yeast paste and were kept at 18°C. *w; dl-LEXY/CyO; PrDr/TM3* and *w; dl-BLID/CyO; PrDr/TM3* were crossed to *Sp/Cyo; MCP-mCherry (w+, NLS)/TM3* to generate *w; dl-LEXY/CyO; MCP-*

*mCherry* (*w*<sup>+</sup>, *NLS*)/*TM3* and *w*; *dl-BLID*/*CyO*; *MCP-mCherry* (*w*<sup>+</sup>, *NLS*)/*TM3*, which were grown in bottles, and virgin *dl-LEXY*; *MCP-mCherry* (*w*<sup>+</sup>, *NLS*)/*TM3* or *dl-BLID*; *MCP-mCherry* (*w*<sup>+</sup>, *NLS*)/*TM3* were selected. These virgins were crossed to males bearing the MS2. MS2 lines included *sna-MS2 BAC* (III), *vndEEE-peve-MS2-lacZ/CyO* (II), *twi-MS2*, *sog-MS2*/ (I); *Sp/CyO*, and *Sp/CyO*; *zen-MS2/TM3* (III). *sna-MS2* is a large reporter construct of ~25kB with MS2 inserted at the 5' end of the transcript following the 5'UTR and the coding sequence replaced by the gene *yellow*<sup>15,27</sup>. The *vnd-MS2* reporter is a small reporter construct with a single enhancer, *vndEEE*, positioned upstream of a heterologous promoter driving MS2<sup>14</sup>. On the other hand, *twi-MS2* contains an insertion of MS2 sequence at the 3' end of the *twi* coding sequence; whereas *sog-MS2* and *zen-MS2* contain insertion of MS2 within introns. In addition, *dl-mCherry-LEXY/CyO* was grown in bottles and added to experimental cages. *y*<sup>2</sup> *cho*<sup>2</sup> *v*<sup>1</sup> *P*{*nos-phiC31*\int.NLS}X; *attP2* (III) (NIG-FLY TBX-0003) was used to make *y*<sup>2</sup> *cho*<sup>2</sup> *v*<sup>1</sup> *P*{*nos-phiC31*\int.NLS}X; *P*{*dl-gRNA*}*attP2* (III). *y*<sup>2</sup> *cho*<sup>2</sup> *v*<sup>1</sup>; *Sp/CyO*, *P*{*nos-Cas9*, *y*<sup>+</sup>, *v*<sup>+</sup>}2A (NIG-FLY CAS-0004) virgins were crossed to *y*<sup>2</sup> *cho*<sup>2</sup> *v*<sup>1</sup> *P*{*nos-phiC31*\int.NLS}X; *P*{*dl-gRNA*}*attP2* (III) for injection.

A 25 kB *dl-Venus* rescue transgene was previously generated and demonstrated that the addition of *Venus* fluorescent protein fusion does not significantly change the extent of the DL nuclear-cytoplasmic gradient<sup>4</sup>. In the course of the current study, we used recombineering mediated gap repair<sup>28</sup> to introduce changes that modify the sequence of the NES. The *dl-AAAA* and *dl-DDDD* mutations were created by introducing the following changes into the DL NES (lowercase):

TGCGCCTCAATgctGAAGATCTGCAGATAgcgAACCTGgcgATAgctACG and TGCGCCTCAATgatGAAGATCTGCAGATAgacAACCTGgacATAgatACG, respectively. The resulting two mutated *dl* constructs fused to a fluorescent protein were inserted into the 86Fb landing site on the third chromosome<sup>29</sup>, as done previously for the *dl-Venus* control<sup>4</sup>. Transgenic lines were obtained, insertions confirmed by sequencing, and crossed using standard genomic crosses into a *dl* null background, transheterozygous for *dl*<sup>1</sup> and *dl*<sup>4</sup> alleles (Bloomington stock center), and assayed at one copy: *dl*<sup>1</sup>/*dl*<sup>4</sup>; *dl-Venus*/+ (wildtype NES), *dl*<sup>1</sup>/*dl*<sup>4</sup>; *dl-AAAA-Venus*/+ (NES Ser>Ala), and *dl*<sup>1</sup>/*dl*<sup>4</sup>; *dl-DDDD-Venus*/+ (NES Ser>Asp).

## METHOD DETAILS

### Homologous Repair Template Cloning

*LEXY*<sup>2</sup> was codon optimized and, along with *MS2*<sup>30</sup>, synthesized by GenScript in pUC57. The *dl-LEXY*, *dl-mCh-LEXY*, *sog-MS2* and *zen-MS2* homologous repair templates were generated by editing *pHD-DsRed*<sup>31</sup>. The *twist-MS2* homologous repair template was generated in pBlueScript II (SK)+. The right homology arm for *dl-LEXY* and *dl-mCh-LEXY* was generated by PCR using a *dl-Venus-BAC*<sup>4</sup> as a template, and was inserted into *pHD-DsRed* downstream of the *DsRed* using BglIII and XhoI sites. The left homology arm was generated by overlap PCR, combining three fragments, the C-term of *dl*, the *LEXY* domain, and the *dl* 3'UTR. The left homology arm of *dl-mCh-LEXY* was made by overlap PCR, combining PCR products that used *dl-mCherry* HDR and the *dl-LEXY* HDR as a template. This PCR product was inserted into *pHD-DsRed* upstream of the *DsRed* using EcoRI and NheI sites. The *sog-MS2* homologous repair template was made

by PCR, using a BAC as the template (BacPac Resource Center BACR25D05).

Overlap PCR was used to mutate the gRNA binding site in the repair template. The left homology PCR product was cut with *NheI* and *AseI* and the *pHD-DsRed* plasmid was cut with *NheI* and *NdeI* to make compatible sticky ends, which were ligated together. The right homology arm PCR product and the *pHD-DsRed* were digested with *AscI* and *XhoI* and ligated. The *zen-MS2* homologous repair template was made the same way as the *sog-MS2* template, but used *NheI* and *NdeI* on both the insert and the backbone, and the right homology arm also used overlap PCR to mutate the gRNA sequence. The *MS2* sequence was added using *NotI* and *AvrII*, which were added to the reverse primer used to generate the left homology arm of both *sog-MS2* and *zen-MS2*.

The *twist-MS2* homologous repair construct was made by PCR using genomic DNA from *yw* flies as a template for the homology arms and *pHD-dsRed* as a template for the screening marker. The left homology arm was inserted between *KpnI* and *BamHI* sites while introducing mutations in the gRNA cut site using overlap PCR as well as introducing a *SpeI* site for *MS2* insertion after the stop codon in the 3' UTR. The 24x*MS2*, 3' UTR and 3xP3-dsRed were introduced in the *SpeI* site, followed by the left homology arm insertion into the *SacI* site with the gRNA cut site being disrupted by the 3xP3-dsRed cassette. The *twist-MS2* gRNA were cloned separately into pCFD3 by oligo annealing followed by insertion into a *BbsI* site. The *zen-MS2* gRNA was made by *BbsI* digestion of pCFD5 and Gibson assembly was used to combine the vectorized backbone and the PCR product. In both *sog-MS2* and *zen-MS2*, the *MS2* sequence was inserted into the first intron, as annotated on Flybase.

## CRISPR/Cas9 Genome Editing

For *dl-LEXY* and *dl-mCh-LEXY*,  $y^2 cho^2 v^l$ ; *Sp/CyO*,  $P\{nos-Cas9, y+, v+\}2A$  virgins were crossed to  $y^2 cho^2 v^l P\{nos-phiC31\int int.NLS\}X$ ;  $P\{dl-gRNA\}attP2$  (III). The HDR template for *dl-LEXY* and *dl-mCh-LEXY* were injected into embryos from this cross. The *sog-MS2* HDR was co-injected with a previously made gRNA<sup>32</sup> into  $w[1118]$ ;  $PBac\{y[+mDint2]=vas-Cas9\}VK00027$  (Bloomington #51324). For *zen-MS2* and *twist-MS2*, gRNAs were found using flyCRISPR Target Finder<sup>31</sup>. The *zen-MS2* HDR was co-injected into  $y^2 cho^2 v^l$ ;  $attP40\{nos-Cas9\}/CyO$  (NIG-FLY CAS-0001). For both *sog-MS2* and *zen-MS2*, Rainbow Transgenics performed the injections. For *twist-MS2*, a mix of HDR template and gRNA-containing plasmids was injected into  $y^l M\{w[+mC]=nanos-Cas9.P\}ZH-2A w[*]$  embryos (Bloomington #54591) by the *Drosophila* Transgenesis Service at the Centro de Biología Molecular Severo Ochoa (Madrid, ES). All HDR templates included DsRed as a selectable marker, and transgenics were screened for DsRed expression.

## Hatching Assay

Embryos from *dl-LEXY* homozygous flies and *yw* controls were collected for one hour in the dark at RT on apple juice agar plates supplemented with yeast. Embryos were aged for 24h in the dark or under blue LED illumination (30% power with 2 seconds of illumination/1 second dark; gift of Eileen Furlong, EMBL) at 25°C, followed by a 24 hour recovery period in the dark. After recovery, plates were scored for the total number of eggs laid and the number of unhatched eggs. Statistical significance was determined using Tukey's HSD.

### **Live Imaging**

Embryos from crosses between *dl-LEXY* and the *MS2* lines were collected for four hours or overnight, both at 18°C. To prepare the embryos for live imaging, embryos were hand dechorionated in the dark, using a red film (Neewer, 10087407). Embryos were transferred to an agar square and oriented so that the face that would be imaged was facing the agar. Preprepared slides were made by adding heptane glue (heptane plus double sided tape) to a coverslip that was taped to the slide and allowing it to sit overnight. This slide was used to pick the embryos up from the agar. Embryos were then checked to make sure the orientation had not been disrupted and oriented again if necessary. Water from the lab faucet was then added to prevent desiccation of the embryos. Embryos were transferred to the microscope in a covered box. Imaging occurred on a Zeiss LMS 800 using a 25x immersible objective at 1.7 zoom. The MCP-mCherry signal was detected using a 561 nm laser at 1% laser power. The 488 nm laser at 4.5% laser power was used to perform blue light illumination. Z-stacks were taken, with 30 z-planes per timepoint at 1  $\mu\text{m}$  thickness. Images were taken every ~25 seconds, starting as soon as the previous z-stack finished. Images were captured as 16 bit images, and each z-slice was 512 by 512 pixels, with each pixel being 0.29  $\mu\text{m}$  in length and width. For *sna-MS2*, eight movies were taken using slower settings. Images were taken every ~2 min and each z-slice was 1024 by 1024 pixels with each pixel being 0.15  $\mu\text{m}$  long. Imaging was terminated after observing gastrulation or movement of the nuclei congruent with germ band extension when gastrulation was absent or not observable.

### **Fixed Imaging**

For fixed sample preparation of the *dl-Venus*, *dl-AAAA-Venus*, and *dl-DDDD-Venus*, embryos were dechorionated in bleach, fixed in 4 mL of 9.25% formaldehyde and 4 mL of heptane for 20 minutes and then rinsed and stored in methanol at -20°C. For in situ hybridization, protocols were followed as described previously<sup>33</sup> using riboprobes generated for *sna*, *ind*, *sog*, and *zen*. Sheep anti-digoxigenin (Life Technology PA185378), rabbit anti-FITC (Invitrogen A889), and Mouse anti-Biotin (Invitrogen 03-3700) were used. Fluorescently conjugated secondaries, Alexa 555, 488, and 647, from ThermoFisher were used (1:400).

For Dorsal antibody staining, embryos were fixed in 10% formaldehyde:heptane for 25 minutes as previously described<sup>33</sup> followed by storage in methanol at -20°C. To quantify Dorsal eviction in the hatching assay, fixed embryos were stained with 1:100 mouse anti-Dorsal (7A4, Drosophila Studies Hybridoma Bank) and 1:250 rabbit anti-Snail (gift of Julia Zeitlinger), followed with 1:500 donkey anti-mouse AF488, 1:500 donkey anti-rabbit AF647 (Invitrogen) and DAPI.

Embryos in mid-nc14 were imaged using an Zeiss LSM880 with Airyscan using a 40x Plan Apo oil lens (NA=1.3) and sequential channel acquisition. Excitation was performed with a 405nm laser for DAPI, an argon 488 nm laser for AF488, and a He/Ne laser for AF647 coupled with detection on a GaAsP-PMT array coupled to an Airyscan detector. Image processing was performed in Zen Black (Zeiss) prior to analysis. For each embryo, single Z-planes in the dorsal and ventral domains were acquired as 16-bit images at zoom 3x with a pixel size of 0.069 $\mu\text{m}^2$  and an image size of 1024 by 1024 pixels. A tile scan of

3072 by 2048 pixels was also acquired to indicate relative orientation of the dorsoventral axis for each analyzed embryo.

## **QUANTIFICATION AND STATISTICAL ANALYSIS**

To quantify the number of MS2 foci, or spots, in the images/movies captured, three custom MATLAB functions were used. The first function opens the image, including relevant metadata, and performs the spot detection. First “salt and pepper” noise is removed using a median filter. The background is subtracted by using a median filter over a larger area to blur the image, and then subtracting the blurred image from the original. After background subtraction, the image is blurred with a Gaussian filter. The image is then thresholded by a user defined threshold, tiny objects of only one pixel are removed, and objects detected on the edge are removed. The entire embryo is segmented by projecting all the time points together, blurring the image with a Gaussian filter, and using thresholding. The detected embryo is then morphologically closed to smooth the edges and small objects less than 100 pixels are discarded so only one object, the embryo, is detected. Any spot detected outside the embryo is removed. We observed that the background intensity of nuclei increased over time, and so to account for this, we increased the threshold by a small amount using a user defined value that increases logarithmically during nc14. To increase the detection of spots, we segmented the unprocessed image a second time using a user defined threshold, and retained only the spots detected with both thresholds. The algorithm works by setting the first threshold low, detecting both real spots and noise, and then removing the noise based on a second, higher threshold. The centroid coordinates for these spots are saved for further analysis.

A second function displays the images in a GUI and allows overlapping the mask of the segmented foci on the image. In addition to overlaying, the centroids can be used to plot points at the detected spots. These were used to evaluate the success of the thresholding. Comparable imaging conditions used the same empirically determined threshold. Specifically, when comparing dark and light or *dl-LEXY* and *dl-BLID* the same threshold was used. The threshold was only changed for different MS2 signals (i.e. *sna* versus *sog*) or different lengths of imaging (i.e. nc12-nc14 versus 25 min of nc14). A third function was used to quantify the number of spots and plot the results. To plot the averages, the data was interpolated using MATLAB's built in `interp1` function and the Modified Akima cubic Hermite interpolation method. The mean number of spots and standard error of the mean were calculated from the interpolated data and plotted. In addition, this function also approximated the area of expression. This was done by concatenating all the centroids in given time windows corresponding to nc13 or the first 100 time points of nc14, and removing spots that were two median absolute deviations (MAD) from the median for the centroids of all spots detected. We used a conservative approach because this removed points that tended to be isolated, were not detected in multiple frames, or were actually noise and not a real spot. To determine the area, a convex hull was drawn around the remaining points and the area for this convex hull was determined. The area at nc13 was then subtracted from the area at nc14 to determine the change in nc13 to nc14 and account for potential discrepancies in the orientation of the embryo. This was only done for *sog-MS2* and *zen-MS2*.

To determine if the differences in area were statistically significant, we performed one way ANOVA and Tukey's honestly significant difference (HSD) test to compare *dl-LEXY* dark, *dl-LEXY* light, *dl-BLID* dark, and *dl-BLID* light. We performed this analysis for the areas determined for both *sog-MS2* and *zen-MS2*. A p-value less than 0.05 was considered statistically significant.

*LEXY* fixed images were analyzed with a Python™ custom developed routine. The DAPI channel was used to define the nuclear area and to define the area surrounding the nuclei itself. Both masks were used to measure the Dorsal intensity in the nuclear and cytoplasmic spaces. The DAPI signal was filtered with a Gaussian filter with kernel 5 as pre-smoothing followed by non-linear transformation. We took the square of the filtered images and we used the Otsu algorithm to define a first threshold value. We recovered nuclear shapes by automatically tuning the inferred threshold value, knowing that the nuclear area covered about 10% of the image. The cytoplasmic space was then defined using a dilation algorithm on the detected nuclei. Average intensity in the Dorsal channel was then retrieved by masking. Statistical significance was established using Tukey's HSD.

## REFERENCES

1. Sandler, J.E., and Stathopoulos, A. (2016). Stepwise Progression of Embryonic Patterning. *Trends Genet.* 32, 432–443.
2. Schloop, A.E., Bandodkar, P.U., and Reeves, G.T. (2020). Formation, interpretation, and regulation of the *Drosophila* Dorsal/NF- $\kappa$ B gradient. *Curr. Top. Dev. Biol.* 137, 143–191.

3. Fernandez, C., and Lagha, M. (2019). Lighting Up Gene Activation in Living *Drosophila* Embryos. *Methods Mol. Biol.* 2038, 63–74.
4. Reeves, G.T., Trisnadi, N., Truong, T.V., Nahmad, M., Katz, S., and Stathopoulos, A. (2012). Dorsal-ventral gene expression in the *Drosophila* embryo reflects the dynamics and precision of the dorsal nuclear gradient. *Dev. Cell* 22, 544–557.
5. Stathopoulos, A., and Levine, M. (2002). Dorsal gradient networks in the *Drosophila* embryo. *Dev. Biol.* 246, 57–67.
6. Niopek, D., Wehler, P., Roensch, J., Eils, R., and Di Ventura, B. (2016). Optogenetic control of nuclear protein export. *Nat. Commun.* 7, 10624.
7. Kögler, A.C., Kherdjemil, Y., Bender, K., Rabinowitz, A., Marco-Ferreres, R., and Furlong, E.E.M. (2021). Extremely rapid and reversible optogenetic perturbation of nuclear proteins in living embryos. *Dev. Cell* 56, 2348–2363.e8.
8. Irizarry, J., McGehee, J., Kim, G., Stein, D., and Stathopoulos, A. (2020). Twist-dependent ratchet functioning downstream from Dorsal revealed using a light-inducible degron. *Genes Dev.* 34, 965–972.
9. Bonger, K.M., Rakhit, R., Payumo, A.Y., Chen, J.K., and Wandless, T.J. (2014). General Method for Regulating Protein Stability with Light. *ACS Chemical Biology* 9, 111–115. 10.1021/cb400755b.
10. Xylourgidis, N., Roth, P., Sabri, N., Tsarouhas, V., and Samakovlis, C. (2006). The nucleoporin Nup214 sequesters CRM1 at the nuclear rim and modulates NFkappaB activation in *Drosophila*. *J. Cell Sci.* 119, 4409–4419.
11. DeLotto, R., DeLotto, Y., Steward, R., and Lippincott-Schwartz, J. (2007). Nucleocytoplasmic shuttling mediates the dynamic maintenance of nuclear Dorsal levels during *Drosophila* embryogenesis. *Development* 134, 4233–4241.
12. Reeves, G.T., and Stathopoulos, A. (2009). Graded dorsal and differential gene regulation in the *Drosophila* embryo. *Cold Spring Harb. Perspect. Biol.* 1, a000836.
13. Stein, D.S., and Stevens, L.M. (2014). Maternal control of the *Drosophila* dorsal-ventral body axis. *Wiley Interdiscip. Rev. Dev. Biol.* 3, 301–330.
14. Faló-Sanjuan, J., and Bray, S. (2022). Notch-dependent and -independent transcription are modulated by tissue movements at gastrulation. *Elife* 11. 10.7554/eLife.73656.

15. Bothma, J.P., Garcia, H.G., Ng, S., Perry, M.W., Gregor, T., and Levine, M. (2015). Enhancer additivity and non-additivity are determined by enhancer strength in the *Drosophila* embryo. *eLife* 4. 10.7554/elife.07956.
16. Rushlow, C.A., and Shvartsman, S.Y. (2012). Temporal dynamics, spatial range, and transcriptional interpretation of the Dorsal morphogen gradient. *Curr. Opin. Genet. Dev.* 22, 542–546.
17. Leptin, M., and Grunewald, B. (1990). Cell shape changes during gastrulation in *Drosophila*. *Development* 110, 73–84. 10.1242/dev.110.1.73.
18. Rushlow, C., Colosimo, P.F., Lin, M.C., Xu, M., and Kirov, N. (2001). Transcriptional regulation of the *Drosophila* gene *zen* by competing Smad and Brinker inputs. *Genes Dev.* 15, 340–351.
19. Belvin, M.P., Jin, Y., and Anderson, K.V. (1995). Cactus protein degradation mediates *Drosophila* dorsal-ventral signaling. *Genes Dev.* 9, 783–793.
20. Roth, S., Hiromi, Y., Godt, D., and Nüsslein-Volhard, C. (1991). *cactus*, a maternal gene required for proper formation of the dorsoventral morphogen gradient in *Drosophila* embryos. *Development* 112, 371–388.
21. Hilger, M., Bonaldi, T., Gnad, F., and Mann, M. (2009). Systems-wide analysis of a phosphatase knock-down by quantitative proteomics and phosphoproteomics. *Mol. Cell. Proteomics* 8, 1908–1920.
22. Huang, A., Amourda, C., Zhang, S., Tolwinski, N.S., and Saunders, T.E. (2017). Decoding temporal interpretation of the morphogen Bicoid in the early embryo. *Elife* 6. 10.7554/eLife.26258.
23. Yuan, K., Seller, C.A., Shermoen, A.W., and O'Farrell, P.H. (2016). Timing the *Drosophila* Mid-Blastula Transition: A Cell Cycle-Centered View. *Trends Genet.* 32, 496–507.
24. Chen, K., Johnston, J., Shao, W., Meier, S., Staber, C., and Zeitlinger, J. (2013). A global change in RNA polymerase II pausing during the *Drosophila* midblastula transition. *Elife* 2, e00861.
25. Blythe, S.A., and Wieschaus, E.F. (2016). Establishment and maintenance of heritable chromatin structure during early embryogenesis. *Elife* 5. 10.7554/eLife.20148.
26. Barros, C.D.T., Cardoso, M.A., Bisch, P.M., Araujo, H.M., and Lopes, F.J.P. (2021). A reaction-diffusion network model predicts a dual role of Cactus/I $\kappa$ B to regulate

- Dorsal/NF $\kappa$ B nuclear translocation in *Drosophila*. *PLoS Comput. Biol.* 17, e1009040.
27. Perry, M.W., Boettiger, A.N., Bothma, J.P., and Levine, M. (2010). Shadow enhancers foster robustness of *Drosophila* gastrulation. *Curr. Biol.* 20, 1562–1567.
  28. Venken, K.J.T., He, Y., Hoskins, R.A., and Bellen, H.J. (2006). P[acman]: a BAC transgenic platform for targeted insertion of large DNA fragments in *D. melanogaster*. *Science* 314, 1747–1751.
  29. Bischof, J., Maeda, R.K., Hediger, M., Karch, F., and Basler, K. (2007). An optimized transgenesis system for *Drosophila* using germ-line-specific phiC31 integrases. *Proc. Natl. Acad. Sci. U. S. A.* 104, 3312–3317.
  30. Yamada, S., Whitney, P.H., Huang, S.-K., Eck, E.C., Garcia, H.G., and Rushlow, C.A. (2019). The *Drosophila* Pioneer Factor Zelda Modulates the Nuclear Microenvironment of a Dorsal Target Enhancer to Potentiate Transcriptional Output. *Curr. Biol.* 29, 1387–1393.e5.
  31. Gratz, S.J., Ukken, F.P., Rubinstein, C.D., Thiede, G., Donohue, L.K., Cummings, A.M., and O'Connor-Giles, K.M. (2014). Highly specific and efficient CRISPR/Cas9-catalyzed homology-directed repair in *Drosophila*. *Genetics* 196, 961–971.
  32. Dunipace, L., Ákos, Z., and Stathopoulos, A. (2019). Coacting enhancers can have complementary functions within gene regulatory networks and promote canalization. *PLoS Genet.* 15, e1008525.
  33. Kosman, D., Mizutani, C.M., Lemons, D., Cox, W.G., McGinnis, W., and Bier, E. (2004). Multiplex detection of RNA expression in *Drosophila* embryos. *Science* 305, 846.

*Chapter 5*

## DISCUSSION

**The role of phosphorylation of Dorsal**

Since Dorsal has been shown to be unevenly distributed in *cactus* mutants but is even in *cactus toll* double mutants (Roth et al. 1991; Bergmann et al. 1996) it is reasonable to assume that Toll signaling provides an additional cue besides degrading Cactus. As we have stated previously, this could be a post-translational modification of Dorsal, specifically phosphorylation. Thus, a reasonable next step would be to test the distribution of Dorsal in the serine mutation lines we made in the C-terminal NES of Dorsal in *cact*, *toll*, and *cact toll* double mutants. One would expect that in the alanine mutant line, which removes phosphorylation, Dorsal would be evenly distributed in a *cact* mutant, likely at low levels. Similarly, in the aspartic acid mutant, one would expect Dorsal to be uniform in a *cact* mutant, but at high levels, similar to a constitutively active Toll allele, Toll10b. In the *cact toll* double mutant, both lines should look like they did in a *cact* mutant. In a *toll* mutant, both should be at low levels because Cact is still present.

If Dorsal is in fact phosphorylated, which there is strong evidence for (Norris and Manley 1992; Whalen and Steward 1993; Gillespie and Wasserman 1994; Drier, Huang, and Steward 1999), the kinase that phosphorylates Dorsal remains elusive. PKA has been shown to phosphorylate Dorsal (Briggs et al. 1998), although this is disputed (Drier, Huang, and Steward 1999). In addition, using bioinformatics, S665 is predicted to be phosphorylated by CHKI/Grapes, which could indicate that it is regulated by cell cycle

and the DNA damage checkpoint. Another possibility is Raf, which has been shown to be important in Dorsal gradient formation ([Lusk et al. 2022](#)), and could be revealed to directly phosphorylate Dorsal. How Dorsal phosphorylation plays a role in affecting target gene expression, and which kinases or phosphatases might play a role, remains an open question.

### **The role of Dorsal at nc13**

We found that nc13 was important for the correct expression of *sna*. When Dorsal is lost at nc13, not only is *sna* not expressed at nc13, but expression at nc14 is also disrupted. It is unclear what is mediating this change at nc13. Dorsal is clearly not sufficient to reverse what occurs at nc13. To uncover a mechanism for this loss of *sna*, one approach would be to screen for potential repressors that act at nc13. The screen could be done by blind mutagenesis, although this would be difficult to do. A targeted screen of known repressors could be undertaken. One likely repressor is Su(H) which is known to play a role in establishing the boundary of *sna* and which has many binding sites in the distal enhancer of *sna* ([Ozdemir et al. 2014](#)). This would suggest a model where Dorsal is necessary to block this repressor, and if it does not, an irreversible event occurs, potentially through chromatin modification. One could also perform ATACseq when illuminating an embryo at nc13 to detect changes in chromatin conformation.

### **The role of enhancers in Dorsal mediated transcription**

In addition to looking for the mechanism controlling Dorsal's requirement at nc13, the role of *sna*'s enhancers in this phenomenon could shed light on what is occurring. Specifically, one could test the removal of Dorsal using blue light when the proximal or

distal *sna* enhancer is deleted. One would expect that deleting the distal enhancer could possibly remove this requirement for Dorsal at nc13, as repressors such as Su(H) are known to bind to the *sna* distal enhancer ([Ozdemir et al. 2014](#)). Another possibility is that *sna* expression when the distal enhancer is deleted will look exactly like *sna* expression when Dorsal is removed at nc13, if a key role for Dorsal is to prevent repressors from binding to the distal enhancer. Removing the proximal enhancer when removing Dorsal at nc13 may exacerbate the effect. Since the proximal enhancer has been shown to have many Dorsal binding sites, it is likely that loss of the proximal would reduce *sna* expression, and if the distal enhancer is repressed, *sna* could completely turn off in nc14. Regardless of the outcome, performing such an experiment would likely help elucidate how Dorsal at nc13 is important for *sna*.

We have shown that in DL-BLID, Dorsal is not necessary for continued expression of *sna* in late nc14, but in DL-LEXY, *sna* is lost whenever Dorsal is removed through blue light illumination. We also observed that *sog* boundaries shift in *dl-BLID*, but do not shift in *dl-LEXY*. Since DL-BLID is likely to drive total Dorsal levels to be very low through degradation, while DL-LEXY simply prevents Dorsal from accumulating in the nucleus through strong nuclear export, it is likely that Dorsal in *dl-LEXY* is constantly entering and exiting the nucleus. Since *sog* and *zen* boundaries do not shift in *dl-LEXY* under blue light, we theorize that this constant movement of Dorsal into and out of the nucleus is sufficient to activate low level targets like *sog* and *zen*. Our data supports this model, since we observe *sog* and *zen* not changing in *dl-LEXY* under blue light. We further extend this model to theorize that these low levels of Dorsal from constant import and

export is able to block *sna* transcription. One possible explanation is that Dorsal is involved in the formation of enhancer promoter complexes. When Dorsal levels are high, it is able to stably form these complexes and initialize *sna* transcription. When Dorsal is constantly being shuttled in and out of the nucleus, this structure tries to form but is unable to and thus prevents *sna* transcription from being activated. However, when Dorsal is completely removed, at first this structure is lost and *sna* transcription is lost, but then is able to reform in a Dorsal-independent manner. Since we have found that Twist (Twi) is necessary for *sna* to be expressed at late nc14 in a Dorsal independent manner we would expect Twi to mediate this function.

To further test this idea, we could image *sna* transcription at late nc14 in embryos that have a proximal or distal deletion, in both *dl-BLID* and *dl-LEXY*. We have shown deleting the distal enhancer causes a loss of *sna* transcription at late nc14 in *dl-BLID* and would expect that it would behave similarly in *dl-LEXY*. When the proximal is deleted in *dl-BLID* with illumination, *sna* can recover. We predict that in *dl-LEXY*, the proximal deletion would alleviate whatever is preventing *sna* transcription from becoming Dorsal independent. Thus, in this model Dorsal removal acts through the proximal enhancer and the constant flux of Dorsal prevents the distal enhancer from stably interacting with the promoter.

### **Modeling the Dorsal gradient and downstream genetic circuit**

The Dorsal gradient has been modeled previously (Kanodia et al. 2009; Ambrosi et al. 2014; O'Connell and Reeves 2015; Carrell et al. 2017) to understand how the gradient forms. These models can include modeling the downstream genetic circuits, but simple

models for these circuits can also be derived using mass action kinetics and differential equations. This can be done for both the Dorsal gradient and the downstream genetic circuits, either individually or in conjunction. Simple models can capture the general behavior of the system but may not replicate all the observed behaviors. In addition, these models can be updated to include blue light inducible degradation (BLID) or export (LEXY), which would allow predictions to be made from the model or experimental data to be used to validate the model.

Modeling could be used to test how the differences between BLID and LEXY affect target gene expression. If the rates of degradation and nuclear export under blue light are quantified for Dorsal, this information could be combined with mathematical modeling to determine how BLID and LEXY result in differences in target gene expression.

Frequently, enhancers and transcription factor binding are grouped into single terms, such as Hill equations. Modeling BLID and LEXY using Hill equations would need to be tested but is unlikely to properly capture the difference in target gene expression. Thus, modeling of enhancer activity likely needs to be refined to better explain transcription dynamics.

Another use of modeling would be to look directly at the coherent feedforward loop of Dorsal, Twi, and Sna. Coherent feedforward loops have been shown to result in bistable switches ([Kalir, Mangan, and Alon 2005](#)), which we have shown experimentally to occur upon removal of Dorsal. Insights could be gained by modeling this loop using data collected for Dl, Twi, and Sna, to inform the parameters of the model. The model could be validated using data already collected, such as for Dl-BLID and Dl-LEXY and could

also be used to make future predictions. These models could also be applied to the dynamics from live imaging but would require quantification of individual transcription spots.

Combining modeling and optogenetics provides a unique and powerful tool, as modeling can be used to make predictions that the use of optogenetics is able to test that previously could not be tested. In turn, this data can be used to validate the model, and these cycles can be repeated. For example, testing that Twi can support the correct expression of *sna*, a prediction that could be made from modeling the circuit, was previously very difficult to test because removing Dorsal also caused a loss of Twi. However, with optogenetics, one could selectively remove Dorsal and test what effect this has on *sna* expression when Twi remains. Thus, the use of optogenetics can lead to solving problems posed by modeling that were previously difficult or impossible to test.

### **Optogenetics as a useful tool for dissecting gene regulatory networks**

The work presented here supports that optogenetics can be incredibly useful for helping to dissect complex regulatory networks. One can imagine that these tags could be used on a wide array of different proteins to understand temporal dynamics. This work also demonstrates that careful interpretation of the results is required, as unexpected effects can occur, likely due to how the optogenetic tags work. It would be interesting to see if LEXY and BLID can work for all types of proteins, or if they do not work for some, like repressors which are thought to bind DNA more tightly. In this case, LEXY might fail, but perhaps BLID would still work, but this requires further testing to determine what the effect would be.

## References

- Ambrosi, Priscilla, Juan Sebastian Chahda, Hannah R. Koslen, Hillel J. Chiel, and Claudia Mieko Mizutani. 2014. "Modeling of the Dorsal Gradient across Species Reveals Interaction between Embryo Morphology and Toll Signaling Pathway during Evolution." *PLoS Computational Biology* 10 (8): e1003807.
- Bergmann, A., D. Stein, R. Geisler, S. Hagenmaier, B. Schmid, N. Fernandez, B. Schnell, and C. Nüsslein-Volhard. 1996. "A Gradient of Cytoplasmic Cactus Degradation Establishes the Nuclear Localization Gradient of the Dorsal Morphogen in *Drosophila*." *Mechanisms of Development* 60 (1): 109–23.
- Briggs, L. J., D. Stein, J. Goltz, V. C. Corrigan, A. Efthymiadis, S. Hübner, and D. A. Jans. 1998. "The cAMP-Dependent Protein Kinase Site (Ser312) Enhances Dorsal Nuclear Import through Facilitating Nuclear Localization Sequence/importin Interaction." *The Journal of Biological Chemistry* 273 (35): 22745–52.
- Carrell, Sophia N., Michael D. O'Connell, Thomas Jacobsen, Amy E. Pomeroy, Stephanie M. Hayes, and Gregory T. Reeves. 2017. "A Facilitated Diffusion Mechanism Establishes the Dorsal Gradient." *Development* 144 (23): 4450–61.
- Drier, E. A., L. H. Huang, and R. Steward. 1999. "Nuclear Import of the *Drosophila* Rel Protein Dorsal Is Regulated by Phosphorylation." *Genes & Development* 13 (5): 556–68.
- Gillespie, S. K., and S. A. Wasserman. 1994. "Dorsal, a *Drosophila* Rel-like Protein, Is Phosphorylated upon Activation of the Transmembrane Protein Toll." *Molecular and Cellular Biology* 14 (6): 3559–68.
- Kalir, Shiraz, Shmoolik Mangan, and Uri Alon. 2005. "A Coherent Feed-Forward Loop with a SUM Input Function Prolongs Flagella Expression in *Escherichia Coli*." *Molecular Systems Biology* 1 (March): 2005.0006.
- Kanodia, Jitendra S., Richa Rikhy, Yoosik Kim, Viktor K. Lund, Robert DeLotto, Jennifer Lippincott-Schwartz, and Stanislav Y. Shvartsman. 2009. "Dynamics of the Dorsal Morphogen Gradient." *Proceedings of the National Academy of Sciences of the United States of America* 106 (51): 21707–12.
- Lusk, Jay B., Ellora Hui Zhen Chua, Prameet Kaur, Isabelle Chiao Han Sung, Wen Kin Lim, Vanessa Yuk Man Lam, Nathan Harmston, and Nicholas S. Tolwinski. 2022. "A Non-Canonical Raf Function Is Required for Dorsal-Ventral Patterning during *Drosophila* Embryogenesis." *Scientific Reports* 12 (1): 7684.

- Norris, J. L., and J. L. Manley. 1992. "Selective Nuclear Transport of the *Drosophila* Morphogen Dorsal Can Be Established by a Signaling Pathway Involving the Transmembrane Protein Toll and Protein Kinase A." *Genes & Development* 6 (9): 1654–67.
- O’Connell, Michael D., and Gregory T. Reeves. 2015. "The Presence of Nuclear Cactus in the Early *Drosophila* Embryo May Extend the Dynamic Range of the Dorsal Gradient." *PLoS Computational Biology* 11 (4): e1004159.
- Ozdemir, Anil, Lijia Ma, Kevin P. White, and Angelike Stathopoulos. 2014. "Su(H)-Mediated Repression Positions Gene Boundaries along the Dorsal-Ventral Axis of *Drosophila* Embryos." *Developmental Cell* 31 (1): 100–113.
- Roth, S., Y. Hiromi, D. Godt, and C. Nüsslein-Volhard. 1991. "Cactus, a Maternal Gene Required for Proper Formation of the Dorsoventral Morphogen Gradient in *Drosophila* Embryos." *Development* 112 (2): 371–88.
- Whalen, A. M., and R. Steward. 1993. "Dissociation of the Dorsal-Cactus Complex and Phosphorylation of the Dorsal Protein Correlate with the Nuclear Localization of Dorsal." *The Journal of Cell Biology* 123 (3): 523–34.

*Appendices*

## A. SUPPLEMENTARY MATERIALS FOR CHAPTER 2

**SUPPORTING INFORMATION****Movie Captions****S1 Movie. Dorsal-GFP entry into nuclei in the absence of degron-tagged CactDN under the conditions of laser illumination used in this study.**

A single embryo expressing Dorsal-GFP was imaged from nuclear cycle (nc) 12 until gastrulation (st.6), demonstrating the formation of a normal ventral-to-dorsal gradient of nuclear accumulation in the absence of CactDN expression. In brief, the embryo was imaged under three conditions as outlined in Fig 9A: (i) imaging was initiated at nc12 using the low power (3.1%) 488nm laser; (ii) 10min later (nc13) high power (10%) 488nm was applied for a period of 20min; finally, after a resting period of 35min, imaging was reinitiated at low power (3.1%) 488nm, extending until gastrulation. The movie is a compilation of these 3 imaging sessions taken over time, and due to lack of CactDN serves as a control for the movies of embryos expressing the various degron-tagged versions of CactDN. Snapshots from the movie are shown in Fig 9B, 9B', 9B'', and 9B'''.

**S2 Movie. Blue laser light induces nuclear accumulation of Dorsal-GFP expressed together with PND-HA-CactDN.** The movie shows an embryo expressing Dorsal-GFP and PND-HA-CactDN imaged using the same conditions as described for S1 Movie from nc12

to nc14/gastrulation; importantly, including 20 min high power blue light (i.e. 488nm, 10%) illumination used to initiate degron-mediated loss of PND-HA-CactusDN activity at nc13/14, resulting in Dorsal-GFP nuclear localization. Snapshots from the movie are shown in Fig 9C, 9C', 9C'', and 9C'''.

**S3 Movie. Perturbation of nuclear localization of Dorsal-GFP expressed together with PND-HA-CactDN under low intensity light.**

The movie shows an embryo expressing Dorsal-GFP together with PND-HA-CactDN fusion protein, imaged under low power blue light only (488 nm, 3.1%) initiating at nc12 and continuing until late nc14/gastrulation over a period of ~75 min. Snapshots from the movie are shown in Fig 9D, 9D', (D''', and 9D'''.

**S4 Movie. Blue laser light induces nuclear accumulation of Dorsal-GFP expressed together with CactDN-B-LID.** The movie shows an embryo expressing Dorsal-GFP and CactDN-B-LID using the same conditions described for S1 Movie, from nc12 to nc14/gastrulation, importantly including 20 min high power blue light illumination (488nm, 8.6%) to initiate degron-mediated loss of CactDN-B-LID activity at nc13/14, resulting in Dorsal-GFP nuclear localization. Snapshots from the movie are shown in Fig 9E, 9E', 9E'', and 9E'''.

**S5 Movie. Perturbation of nuclear localization of Dorsal-GFP expressed together with CactDN-B-LID under low intensity light.** The movie shows an embryo expressing Dorsal-GFP together with CactDN-B-LID, imaged under low power blue light only (488 nm, 2%)

initiating at nc12 and continuing until nc14/gastrulation. Snapshots from the movie are shown in Fig 9F, 9F', 9F'', and 9F'''.

**S6 Movie. Laser illumination of live embryos expressing CactDN-psd induces transient cyclical nuclear accumulation of Dorsal-GFP (low mag).** The movie shows an embryo expressing Dorsal-GFP together with CactDN-psd from nc12 up to nc14. In brief, embryos were imaged under two conditions: (i) first, imaging was initiated at nc12 using the low power 488nm laser; (ii) after mitotic division (nc13), high power 488nm laser light was applied for a period of 20min. Importantly, high power blue light (488nm) illumination was used to initiate degron-mediated loss of CactDN-psd activity during nc13, resulting in transient Dorsal-GFP nuclear localization just before the onset of nuclear mitosis. The movie is a compilation of these 2 imaging sessions taken over time. Snapshots from the movie are shown in Fig 10A, 10A', 10A'', and 10A'''.

**S7 Movie. Dorsal-GFP expressed together with CactDN-psd fails to accumulate in nuclei under low intensity light.**

The movie shows an embryo expressing Dorsal-GFP together with CactDN-psd imaged under low power 488 nm laser light, 3.1% from nc12 to nc14. Snapshots from the movie are shown in Fig 10B, 10B', 10B'', and 10B'''.

**S8 Movie. Laser illumination of live embryos expressing CactDN-psd induces transient cyclical nuclear accumulation of Dorsal-GFP (higher mag).** The movie shows an embryo expressing Dorsal-GFP together with CactDN-psd which was exposed to high power blue

light (488nm, 10%) for 20 min, initiating at nc12 and extending into nc13, and subsequently imaged with low power light (488 nm, 3.1%) until the end of nc13. Snapshots from the movie are shown in Fig 10C, 10C', 10C'', and 10C'''.

**B. SUPPLEMENTARY MATERIALS FOR CHAPTER 3****SUPPLEMENTAL MATERIALS**

- I. Supplemental Materials & Methods**
- II. Supplemental Figures with Legends**
- III. Supplemental Movie Legends**

**I. SUPPLEMENTAL MATERIALS & METHODS***Genetic crosses*

To generate *dl* mutants, virgin *dl<sup>4</sup>/CyO* (#7096, Bloomington *Drosophila* Stock Center, BDSC) were crossed *dl<sup>1</sup>/CyO* (#3236, BDSC). For the cuticle preparation in *dl* mutant, female *dl<sup>1</sup>/dl<sup>4</sup>* were crossed with *yw* males. To test continuous requirements of high levels of D1 at blastoderm stage, first, *dl-BLID* flies were recombined with *MCP-GFP*, *mCherry-PCP*, *His2Av-eBFP2* (from Michael Levine, Princeton University, US; Lim et al. 2018), and then *dl-BLID/CyO;MCP-GFP*, *mCherry-PCP*, *His2Av-eBFP2* male was crossed with *dl-BLID/CyO* virgin females to generate *dl-BLID/dl-BILD; MCP-GFP*, *mCherry-PCP*, *His2Av-eBFP2*. Female *dl-BLID/dl-BILD; MCP-GFP*, *mCherry-PCP*, *His2Av-eBFP2* flies were crossed with *yw* males to image nuclei to observe overall development upto gastrulation. Furthermore, virgin *dl-BLID/dl-BILD; MCP-GFP*, *mCherry-PCP*, *His2Av-eBFP2* flies were crossed male *snailBAC>MS2* with both proximal and distal enhancers (WT), proximal deletion (NoPrimary), or distal deletion (NoShadow) (from Michael Levine, Princeton

University, US; Bothma et al. 2015). To examine Twi dynamics, first, *dl-BLID* flies were recombined with *vasa-mCherry* (from Hernan Garcia, UC Berkeley, US). Virgin *dl-BLID;vasa-mCherry* flies were crossed with male *Twi-mCherryLlamaTag* (from Hernan Garcia, UC Berkeley, US; Bothma et al. 2018). To recombine *dl-BLID* with *twi<sup>l</sup>*, *dl-BLID/CyO* females were crossed with male *twi<sup>l</sup>/CyO*. Individual *dl-BLID/twi<sup>l</sup>* virgin female was crossed with male double balancer flies. Recombinants were identified by examining brown eye color, crossing putative recombinant *dl-BLID,twi<sup>l</sup>/CyO* with *bw<sup>l</sup>*. Once recombinants were identified, virgin *dl-BLID* flies were crossed with male *dl-BLID,twi<sup>l</sup>/CyO* to generate *dl-BLID, twi<sup>l</sup>/dl-BLID*. Finally, virgin *dl-BLID,twi<sup>l</sup>/dl-BLID* flies were crossed with *twi<sup>l</sup>/CyO* males, and the embryos were collected and fixed.

#### *Generation of gRNAs and homologous repair template construct*

The guide RNAs (gRNA) were designed using the flyCRISPR Target Finder (Gratz et al. 2014). gRNAs that were upstream of the D1 stop codon and downstream of the 3'UTR were chosen (see Table S1 for sequences). The gRNAs were cloned into pCFD4 (Addgene Plasmid #49411) as done previously (Port et al. 2014). Briefly, primers were designed with the gRNA sequence, cut with BspI, and ligated into pCFD4. This plasmid was injected into *P{nos-phiC31}X;attP2 (III)* (NIG-FLY, TBX-0003). Integration of the gRNA was screened using *v<sup>+</sup>*.

The *dl-BLID* homologous repair template was made by editing pHD-DsRed (Gratz et al. 2014). An 1160bp sequence was inserted using BglII and XhoI sites, and served as the right homology arm. 984bp upstream of the stop codon were fused to BLID sequence from

plasmid pBMN HAYFP-LOV24 (Addgene #49570; Bongger et al. 2014) and the 3'UTR using overlap PCR including a 6x Gly linker. This PCR product was inserted using EcoRI and NheI sites and serves as the left homology arm plus the insert.

#### *dl-BLID viability*

*dl-BLID* viability is severely reduced when allowed to develop at 25°C, as no larva hatch. All experiments were carried out at 18°C, where the viability is improved but roughly less than 50%.

#### *In situ hybridization*

Antisense RNA probes labeled with digoxigenin or FITC-UTP were utilized to examine *sna*, *sog*, *htl*, *mes3*, or *netA* transcripts. For *sna* probes, *sna* was transcribed from cDNA subcloned into pGEM-T vector. For *sog*, *htl*, *mes3*, and *netA* probes, primers were designed to target coding sequence of each gene.

#### *Live imaging and quantification*

To stage embryos for live imaging, individual embryos were manually dechorionated and mounted on a slide with heptane glue. Once embryos were immersed in water, nuclear morphology was observed live under a confocal microscope brightfield with 25x objective lens. To minimize possible degradation of DI-BLID during staging, the light was filtered by red film (Newer, 10087407).

To test efficiency of DI-BLID degradation upon blue laser illumination, 488nm blue laser with 40% laser power (high power) was applied to the embryos heterozygous for either *dl-mCherry* or *dl-mCherry-BLID*; while also applying 555nm laser with 1.8% laser power to monitor mCherry signal. Images were taken in 14 Z-planes of interval distance 2.28 $\mu$ m.

To test whether high levels of DI are continuously required at blastoderm stage, staging embryos and overall development of embryos were tested by imaging His2Av-eBFP2 excited at 0.8% of 405nm laser power (low power) between 28 Z-planes separated by 2.28 $\mu$ m. For 488nm laser illumination (high power, e.g. early illumination started at nc14a, whereas late illumination started at nc14c), 40% of laser power was utilized with 33 Z-planes separated by 2.28 $\mu$ m while imaging His2Av-eBFP2 for 20 minutes. After blue laser illumination, His2Av-eBFP2 was imaged with the initial His2Av-eBFP2 settings up to gastrulation. For the dark condition, the embryos were imaged with His2Av-eBFP2 setting without 488nm laser illumination from the onset of nc14 to gastrulation.

To test *sna* transcriptional activities, the MS2-MCP system was utilized. To minimize DI-BLID degradation while imaging MS2-MCP activities, we started by imaging MS2-MCP.GFP at a single timepoint with 5% of 488nm laser power, then illuminated with 15% of laser power (intermediate power) for five minutes to sufficiently degrade DI-BLID and then lowered the laser power to 5% to allow imaging of MS2-MCP.GFP. All the images were taken 30 Z-planes separated by 3 $\mu$ m. While MS2-MCP.GFP activities were being imaged, overall embryo morphology were examined by imaging His2Av-eBFP2 with 1.5%

of 405nm laser power. Imaris Bitplane software was used to identify the thresholded data only for presentation purposes by replacing GFP positive dots with a red sphere (Fig. 3B-G).

To image Twi dynamics, Twi-mCherryLlamaTag system, which recognizes maternally deposited mCherry proteins, was utilized (Bothma et al. 2018). To image mCherry proteins bound by Twi-mCherryLlamaTag, the fluorescent proteins were excited at 555nm with 5% of laser power. Images were taken in 30 Z-planes separated by 3 $\mu$ m. For Dl degradation, 488nm blue laser at high power (40%) was used to illuminate embryos while also imaging mCherry signal.

MS2-MCP.GFP foci were quantified using custom MATLAB functions. Images of MS2-MCP.GFP were first Z-projected and then segmented using a gaussian filter to smooth the image (standard deviation of 1 was used), then using Top-hat filtering to remove background (a disk structuring element with a radius of 3 pixels was used). The resulting image was then segmented using a threshold. The threshold was determined using otsu's method on several of the images acquired, and then choosing a threshold that gave the best segmentation under different conditions. A threshold of 0.06 (on a scale of 0 to 1) was used, however threshold of 0.04 and 0.08 were also tested. Segmentation was verified manually. A threshold of 0.04 generally captured all foci but also included numerous regions where no real signal was present. A threshold of 0.08 generally did not include any regions without real signal, but also failed to include regions with clear signal. A threshold of 0.06 generally included most regions with real foci and the fewest regions without real foci. The number of foci or spots was determined by counting the number of unique (non-touching) regions detected. Although the segmentation is not perfectly accurate (including false positives, false

negatives, and any foci that could not be separated), the differences in the number of spots detected between conditions were quite large, and any error introduced by false positives or negatives is likely negligible. The time of each acquisition was determined from the metadata of the image file. The number of spots detected was averaged for replicates. Blue light illumination time frames were noted manually and the time was determined from the corresponding time frames. The start and end timepoints of blue light illumination were averaged among all lines appearing on a single plot. Individual plots are listed in Supplementary Fig. S4.

Levels of mCherry associated with Twi-mCherryLlamaTag were quantified using custom MATLAB functions by first making a Z-projection, and then drawing a ROI within the Twi domain. The raw signal was calculated by taking the mean intensity of the ROI for each timepoint using the same ROI. Background levels were calculated by taking the mean of an ROI drawn outside of the Twi domain. The raw signal was normalized by first subtracting the background levels and then dividing by the background levels. The time of each acquisition was determined from the metadata of the image file. To align the timepoints for all images taken, the frame where germ band elongation is observed was determined manually, and this timepoint was set to zero for each line by subtracting the time at that timepoint from all the other timepoints. This was done individually for each image series. The quantifications from replicates were averaged together by taking the mean of the normalized intensity values at each timepoint. Since the time for similar timepoints were not completely identical, but were very similar, the time was averaged as well. Standard error of the mean was determined and plotted as error bars. The frames where the embryo was

undergoing blue light illumination were determined manually for each image series, and the time window of blue light was calculated as the starting time of the first frame where the embryo was illuminated to the start of the first frame after illumination ended. The time window of blue light illumination for the averaged normalized intensities were taken as the average of the start and end points of blue light illumination for the individual image series. Individual plots are listed in Supplementary Fig. S5.

## II. SUPPLEMENTARY FIGURES

## FIGURE S1

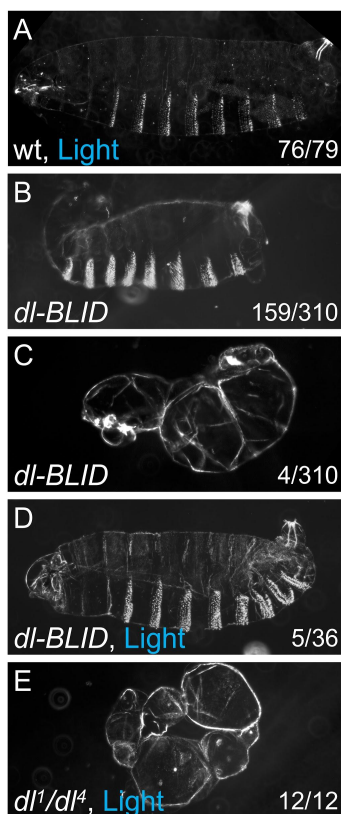


**Figure S1. Blue light has no effect on the cuticles of wildtype or *dl* mutant.** Larval cuticles with anterior to the left and dorsal side up. (A) Larval cuticles from wildtype mothers after four hours of blue LED illumination (n = 76/79). (B) An example of cuticle from *dl-BLID* mothers without illumination that exhibit abnormal cuticles (n=159/310). (C) Cuticles from *dl-BLID* mothers without illumination that appear lateralized or dorsalized (n=4/310). (D) A representative image of cuticles from *dl-BLID* mothers with four hours of blue LED illumination that did not exhibit lateralized or dorsalized cuticles (n=5/36). (E) Cuticles from *dl¹* (*dl¹/dl⁴*) mothers with four hours of blue LED illumination that are dorsalized (n = 12/12).

FIGURE S2

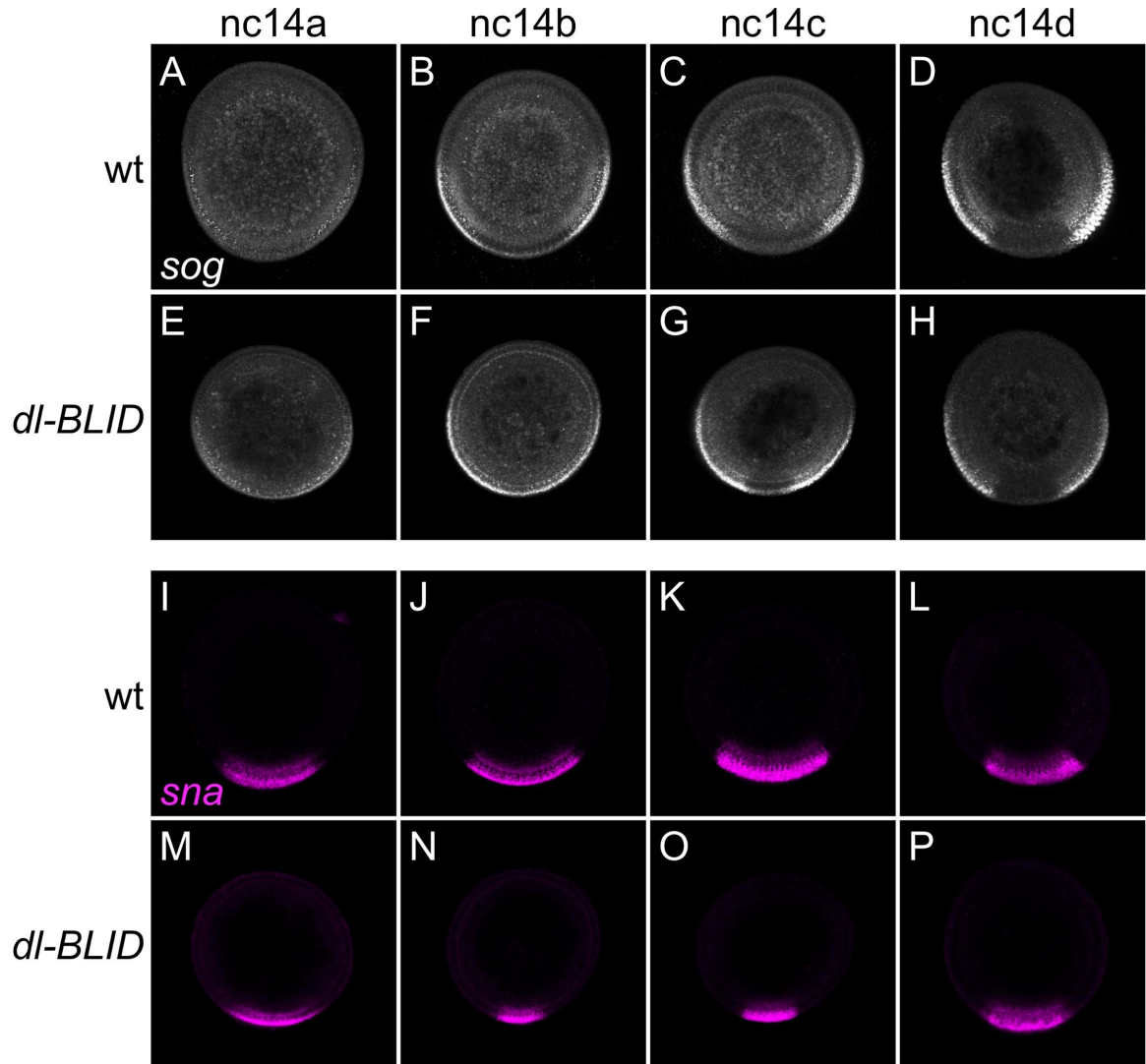


**Figure S2. Expression of *sog* and *sna* transcripts during nc14 for wt and *dl-BLID* embryos kept in the dark.** Manually cross sectioned embryos co-stained for *sog* and *sna* transcripts using FISH. (A-D) *sog* expression in wt embryos kept in the dark at 14a (A), 14b (B), 14c (C), 14d (D). (E-H) *sog* expression in *dl-BLID* embryos kept in the dark at

approximately the same stage as those in A-D. (I-L) *sna* expression in wt embryos kept in the dark, from the same embryos in A-D. (M-P) *sna* expression in *dl-BLID* embryos kept in the dark, from the same embryos in E-H. Note the variability in the width of *sna* expression in *dl-BLID*, and also the differences in *sna* width between wt and *dl-BLID* (J compared with N). *sog* expression appears similar between wt and *dl-BLID*.

FIGURE S3

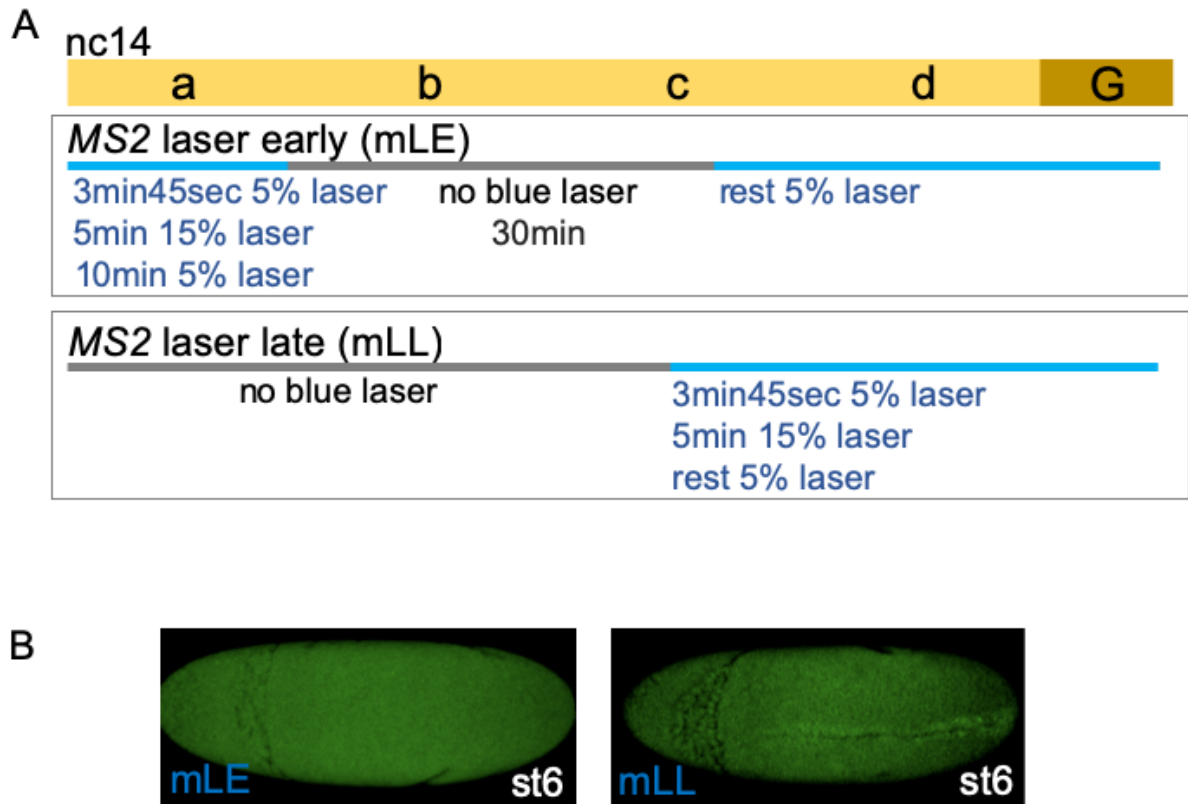


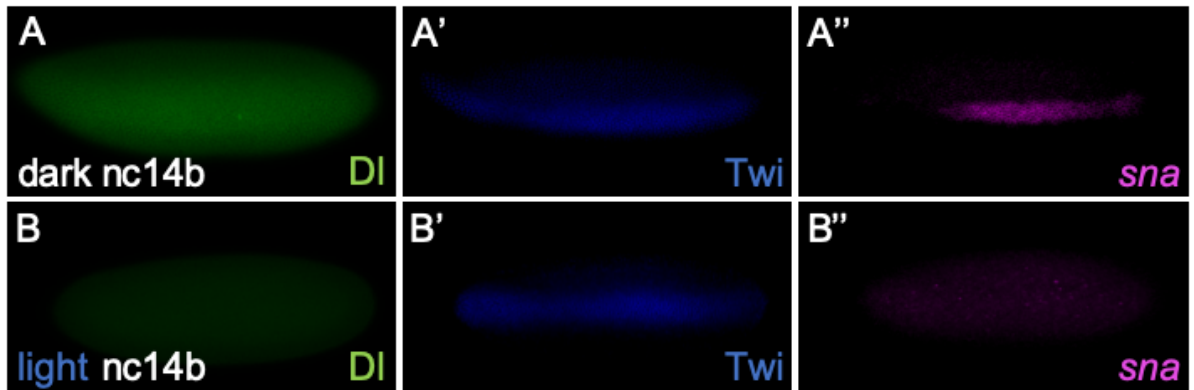
**Figure S3. Scheme of early laser exposure or late laser exposure to degrade DI-Blid while detecting *sna* transcriptional activities using MS2-MCP.GFP system.**

(A) Scheme of “MS2-MCP.GFP compatible Laser Early” (mLE) or “MS2-MCP.GFP compatible Laser Late” (mLL) exposures in *dl-BLID* recombined with *sna.MS2*. 5% laser power (intermediate power) was used to image MCP.GFP signals associating *sna.MS2*, while 15% (high power) laser power was used to degrade most DI-BLID. In mLE scheme, at nc14a, signals of MCP.GFP associating *sna.MS2* were imaged with 5% laser power during the first time frame to image the initial state of *sna* transcriptional activities. Then, a blue laser with 15% power was applied to the embryo to degrade DI-BLID for 5 min, followed by imaging

MCP.GFP signals with 5% laser power for the next ten min. To avoid further DI-BLID degradation while imaging MCP.GFP signals, imaging with blue laser was stopped for 30 min. Finally, MCP.GFP signals were imaged using 5% laser power for the rest. In the mLL scheme, *dl-BLID* embryos recombined with *sna.MS2* were aged upto nc14c. First, MCP.GFP signal interacting with *sna.MS2* were imaged using blue laser with 5% laser power. Then, a blue laser with 15% power was applied to the embryo for 5min to degrade DI-BLID, followed by imaging MCP.GFP associated with *sna.MS2* using a blue laser with 5% power for the rest of development.

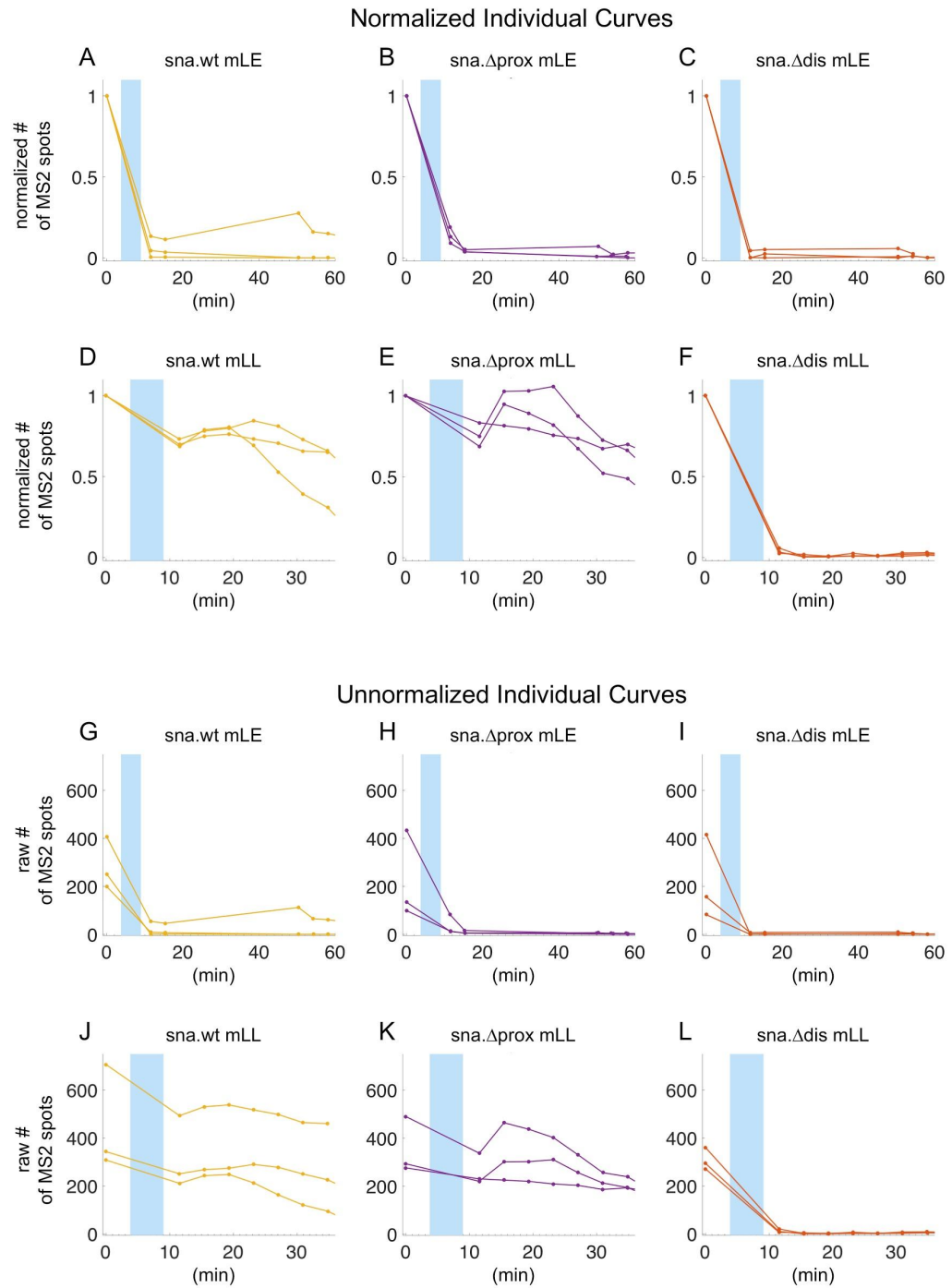
(B) Embryos at st6 to assay gastrulation defects after mLE (left) or mLL (right) blue laser illumination. Images of embryos in (B) are ventral views with anterior oriented to the left.

FIGURE S4



**Figure S4. Expression of D1 proteins, Twi proteins, and *sna* transcripts in nc14b *dl-BLID* embryos with or without 30 min blue LED illumination.** (A,B) *In situ* hybridization combined with immunostaining of nc14b *dl-BLID* embryos in the absence (dark, A-A'') or presence (light, B-B'') of 30 min of blue LED illumination to detect D1 protein (green), Twi protein (blue) and *sna* transcripts (pink). Images of embryos are ventral views with anterior oriented to the left.

FIGURE S5



**Figure S5. Individual plots for the number of spots detected using MS2-MCP system**

**for each of three assayed *sna* reporter genes.** (A-C) individual plots for the number of spots detected using MS2-MCP for the *sna* transcriptional reporters: (A) *sna.wt* (gold), (B) *sna.Δprox* (purple), and (C) *sna.Δdis* (red) with blue laser illumination applied early (mLE) and normalized by the number of spots detected in the first frame. (D-F) the same reporters and same normalization with blue laser illumination applied late (mLL). (G-I) The same data as in A-C but using the unnormalized number of spots. (J-L) The same data as in D-F but using the unnormalized number of spots. The blue windows represent the average of the start and end of blue light illumination for the lines on the respective plots, which are approximately 5 min in duration.

FIGURE S6

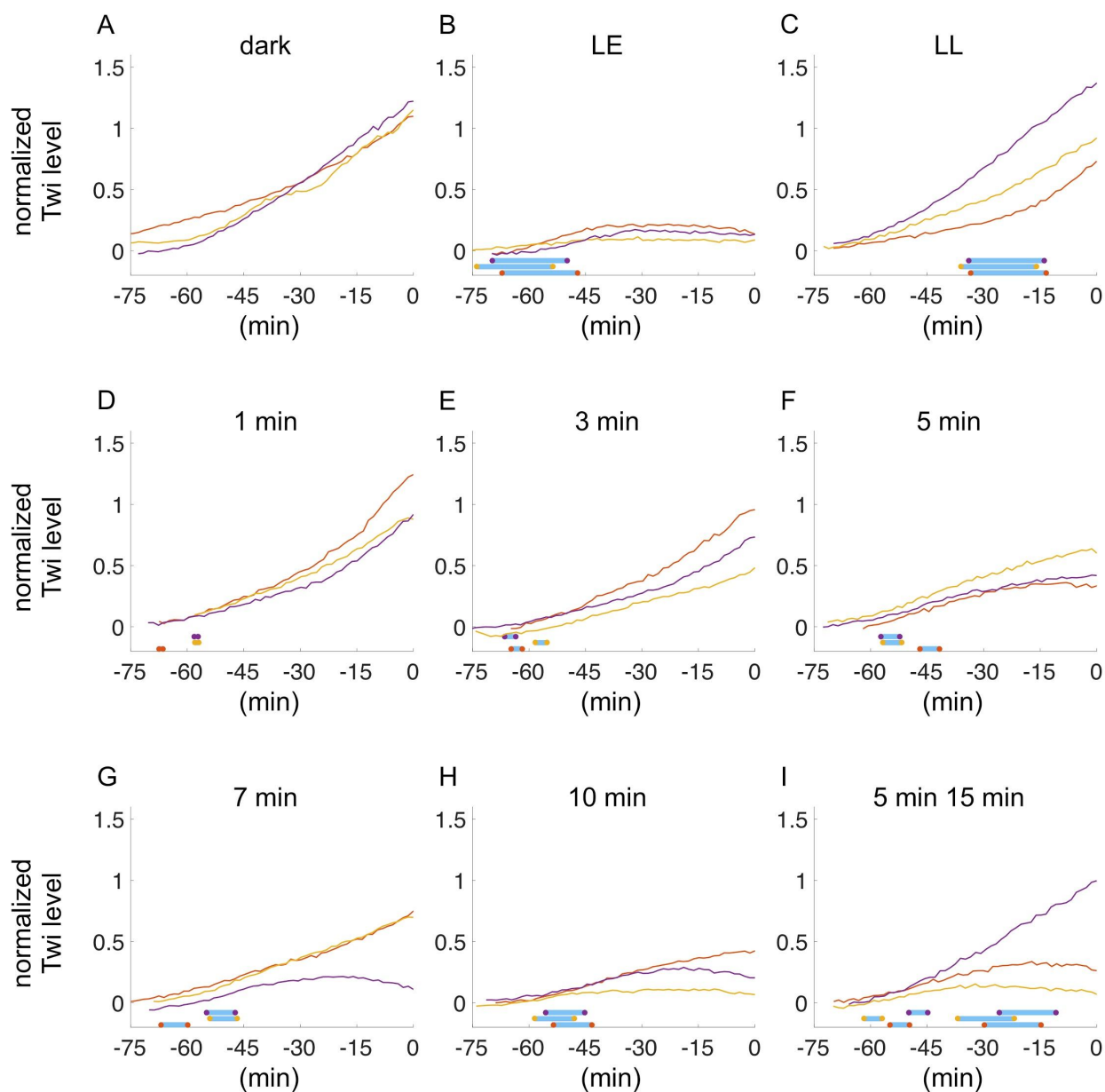


**Figure S6. Individual plots for the quantification of Twi using Twi-mChLlamaTag.** (A-I) individual plots for the quantification of Twi when embryos are (A) kept in the dark, (B) illuminated early (LE), (C) illuminated late (LL), (D) illuminated for 1min at nc14b, (E)

illuminated for 3min at nc14b, (F) illuminated for 5min at nc14b, (G) illuminated for 7min at nc14b, (H) illuminated for 10min at nc14b, and (I) illuminated for 5min at nc14b and illuminated again for 15min at nc14c. Gold, purple, and red lines represent individual embryos. Colors are repeated for each condition. Blue bars represent the time when embryos are illuminated with blue light, and correspond to the line matching the color of the two dots at the end of the blue bar.

FIGURE S7

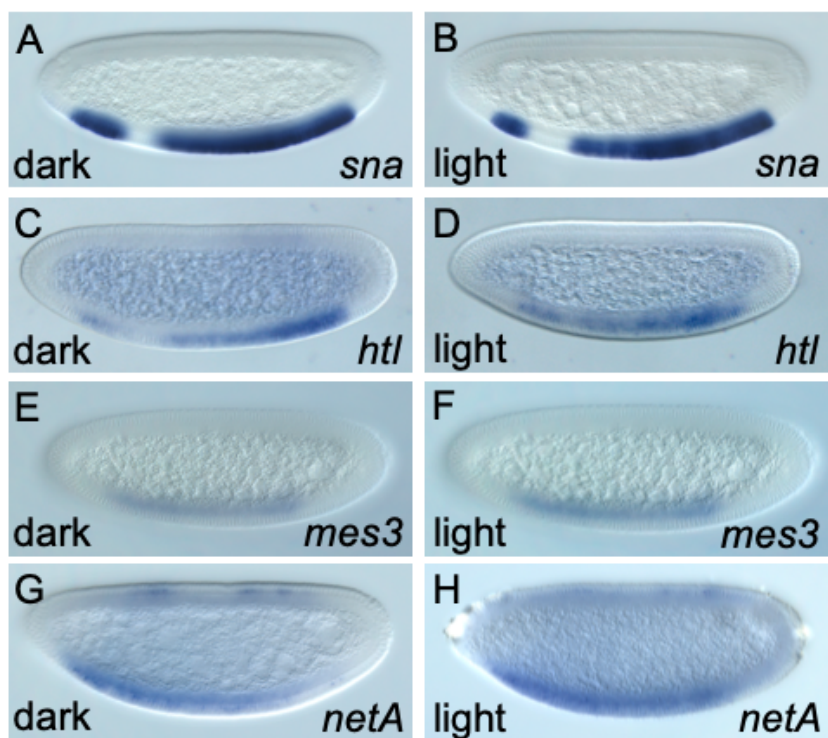


**Figure S7. Target gene expression in ventral regions of *nc14d dl-BLID* embryos with or without 30 min blue LED illumination.** Lateral view of *nc14d* embryos stained for mesoderm targets without (left column, dark) or with 30 min blue LED illumination (right column, light). (A,B) *sna*, (C,D) *htl*, (E,F) *mes3*, and (G,H) *netA*. Expression remains for each gene tested. Embryos are oriented with anterior to the left and dorsal side up.

**Table S1**

NAME	SEQUENCE	COMMENTS
	gRNA	gRNA uppercase
gRNA F	tatataggaagatatccgggtgaacttcgAATCTGCTTAGCTTCGATAGgttttagagctagaatagcaag	
gRNA R	attttaacttgctatttctagctctaaacACGTTCCAGATTTCACAACGcgacttaattgaaaataggtc	
	HDR Left Homology (LH) Primers	dl uppercase
LH dl F	ATTgaattcCTCGCTTCGCTTTGTAGATA	EcoRI lowercase
LH dl R	ATTgctagcAAAATTTAATTTGCAATAAGATCG	NheI lowercase
dl R	acccccaccgctctcccCGTGGATATGGACAGGTTTCG	6x Gly linker lowercase; with LH dl F
	dl-BLID	BLID uppercase
dl-BLID 1 F	ggaggagcggtgggggtTTCTTGGCTACTACACTTGAACG	6x Gly linker lowercase
dl-BLID 1 R	gtttgaaaaaggtactAACCTCGCCGCTTGC	dl lowercase
dl-BLID 2 F	GCAAGGCGGCGAGGTTAGtaccttttcacaacgaacc	dl lowercase; with LH dl R
	dl-mCherry	mCh uppercase
dl-mCh 1 F	ggaggagcggtgggggtATGGTGAGCAAGGGCGAGGA	6x Gly linker lowercase
dl-mCh 1 R	ggttcggtgaaaaaggtactTACTTGTACAGCTCGTCCATGC	dl lowercase
dl-mCh 2 F	TGGACGAGCTGTACAAGTAAtaccttttcacaacgaacc	dl lowercase; used with LH dl R
	dl-mCherry-BLID	3x Gly linker lowercase
dl-mCh-BLID 1 R	AAGAAacccccaccCTTGTACAGCTCGTCCATGC	BLID, mCh uppercase; with LH dl F

dl-mCh-BLID 2 F ACAAGggtgggggtTTCTTGGCTACTACACTTGAACG mCh, BLID uppercase; with LH dl R

HDR Right Homology (RH) Primers

RH F	ATTtagatctTTTGTTAATACTGTTATAAAGATCC	BglII lowercase
RH R	ATTctcgagCAAAGGCCAAAGATTAGGAAA	XhoI lowercase

Sequencing Primers

F RH	TCACTGCATTCTAGTTGTGGT	in pHD-DsRed
R RH	CGCCCTTGAAC TCGATTGAC	in pHD-DsRed
F LH	GATGGTAGTGTGGGGACTCC	in pHD-DsRed
F1 dl LH	CCCACCAACAACAATGCCAA	in dl
R LH	GCCTCTATTTATACTCCGGCG	in pHD-DsRed
R BLID	TCTGGCAATCTTGGGTCAGT	in BLID
F2 dl LH	GCCATCGAGCAACTACAACC	in dl
R mCh	CATGTTATCCTCCTCGCCCT	in mCh

Primers for Probe Synthesis

sog int1 F	ATCTATTGCGCTCGTTGCTT
sog int1 R	AAITTAATACGACTCACTATAGGGTTGCACAAAATGCCACAAAT
NetA int F	CCATCCTTCGCGTCCATCCC
NetA int R	AAITTAATACGACTCACTATAGGGCCAAAACCAAGCGAACGCC

dpp F	ccagaactagaaaaccggaagc
dpp R	gaaatTAATACGACTCACTATAgggCGCCTGTGCTAAAGACCCTG
sog ex1 F	TCAGGTTCAGTCGCTCTTGA
sog ex1 R	AATTTAATACGACTCACTATAGGGGTGTCGGACTCCTCGAACAT

---

### III. SUPPLEMENTAL MOVIE LEGENDS

**MOVIE S1. Comparison of Dl-mCherry and Dl-mCherry-BLID imaging in nc14 embryo under blue laser illumination demonstrates Dl-mCherry-BLID decreases in signal.** Related to Figure 1J,J',L,L'. 488nm blue laser with high power (40%) was applied while mCherry signal was also imaged in *dl-mCherry* (left) and *dl-mCherry-BLID* (right) embryos from onset of nc14. Max projection of scans shown in this movie and all others.

**MOVIE S2. H2A-BFP imaging in *dl-BLID* embryo from onset of nc14 to gastrulation (control).** Related to Figure 2C. 405nm blue laser with low power (0.8%) was applied in order to support BFP signal imaging, while keeping *dl-BLID* blue-light induced degradation to a minimum.

**MOVIE S3. H2A-BFP imaging in *dl-BLID* embryo after blue laser illumination at nc14a (early timepoint) reveals a gastrulation defect.** Related to Figure 2D. After 20 min of 488nm blue laser with high power (40%) at nc14a, 405nm blue laser at low power (0.8%) was applied in order to support BFP signal imaging.

**MOVIE S4. H2A-BFP imaging in *dl-BLID* embryo after blue laser illumination at nc14c (late timepoint) demonstrates gastrulation proceeds.** Related to Figure 2E. After 20 min of 488nm blue laser with 40% power (high power) at nc14c, 405nm blue laser at low power (0.8%) was applied in order to support BFP signal imaging.

**MOVIE S5. *sna.wt* MS2-MCP.GFP signal in *dl-BLID* embryo when illuminated with blue laser at nc14a (early timepoint).** Related to Figure 3B. Blue laser illumination with intermediate power (5%) was applied between time 0 and 3 min showing baseline MS2-MCP GFP+ signal (white dots); followed by blue laser illumination with high power (15%) applied between 3 min and 7 min; embryo was allowed to rest from 19 min to 46 min; and followed with blue laser with intermediate power (5%) to facilitate detection of resulting MS2-MCP GFP+ signal (white dots). For details of imaging strategy see Supplementary Fig. S3A mLE and supplemental methods.

**MOVIE S6. *sna.Aprox* MS2-MCP.GFP and *sna.Δdis* MS2-MCP.GFP signals in *dl-BLID* embryo when illuminated with blue laser at nc14a (early timepoint).** Related to Figure 3C,D. Imaging conditions equivalent to Movie S5, but embryo contained reporter variant: *sna.Aprox* (left) or *sna.Δdis* (right).

**MOVIE S7. *sna.wt* MS2-MCP.GFP signal in *dl-BLID* embryo when illuminated with blue laser at nc14c (late timepoint).** Related to Figure 3E. Blue laser illumination with intermediate power (5%) was applied between time 0 and 3 min showing baseline MS2-MCP GFP+ signal (white dots); followed by blue laser illumination with high power (15%) applied between 3 min and 7 min; and then returned to blue laser illumination with intermediate power (5%) to facilitate detection of resulting MS2-MCP GFP+ signal (white dots). For the experimental details, see Supplementary Fig. S3A mLL and methods.

**MOVIE S8. *sna.Aprox* MS2-MCP.GFP and *sna.Δdis* MS2-MCP.GFP signal in *dl-BLID* embryo when illuminated with blue laser at nc14c (late timepoint).** Related to Figure

3F,G. Imaging conditions equivalent to Movie S7, but embryo contained reporter variant: *sna.Δprox* (left) or *sna.Δdis* (right).

**MOVIE S9. mCherry signal reveals Twi-mChLlamaTag protein expression live in *dl-BLID* embryo from onset of nc14 to gastrulation (control).** Related to Figure 4D. In this movie as well as those below, mCherry signals were imaged over time using the 555 nm laser from the onset of nc14a to gastrulation.

**MOVIE S10. mCherry signal reveals Twi-mChLlamaTag protein expression live in *dl-Blid* embryo from onset of nc14 to gastrulation when also illuminated with high power blue laser at nc14a (“LE”, early timepoint) or nc14c (“LL”, late timepoint).** Related to Figure 4E,F. While acquiring mCherry signals over time using the 555 nm laser, additionally, 488 nm blue laser with high power (40%) was applied to the embryo at nc14a (early timepoint, left) or nc14c (late timepoint, right) for 20 min to degrade D1-BLID.

## C. SUPPLEMENTARY MATERIALS FOR CHAPTER 4

**SUPPLEMENTAL INFORMATION TITLES AND LEGENDS****Supplemental Figures and Legends**

**Figure S1.** DL-LEXY can be reversibly, and repeatedly, exported from the nucleus.

Related to Figure 1.

**Figure S2.** A small number of embryos exhibit different phenotypes in *sna-MS2*

dynamics when applying blue light at particular time windows. Related to Figure 3.

**Figure S3.** Mutating serine residues to alanine in the C-terminal NES causes a reduction

in peak Dorsal levels in ventral regions but does not affect overall levels. Related to

Figure 4.

**Movie legends**

**Movie S1.** Blue light-induced export of DL-mCherry-LEXY is rapid and reversible.

Related to Figure 1.

**Movie S2.** *sna-MS2* in *dl-LEXY* and *dl-BLID* in the dark, with 10 min of blue light, and

with 20 min of blue light. Related to Figure 2.

**Movie S3.** *twi-MS2* and *vnd-MS2* in the dark and with 10 min of blue light. Related to

Figure 2.

**Movie S4.** *sna-MS2* in *dl-LEXY* in the dark, with blue light at nc13, and with light at nc12

and early nc14. Related to Figure 3.

**Movie S5.** *sog-MS2* in *dl-LEXY* and *dl-BLID* in the dark and with blue light

throughout nc13 and 14. Related to Figure 4.

**Movie S6.** *zen-MS2* in *dl-LEXY* and *dl-BLID* in the dark and with blue light throughout

nc13 and 14. Related to Figure 4.

Figure S1 related to Figure 1

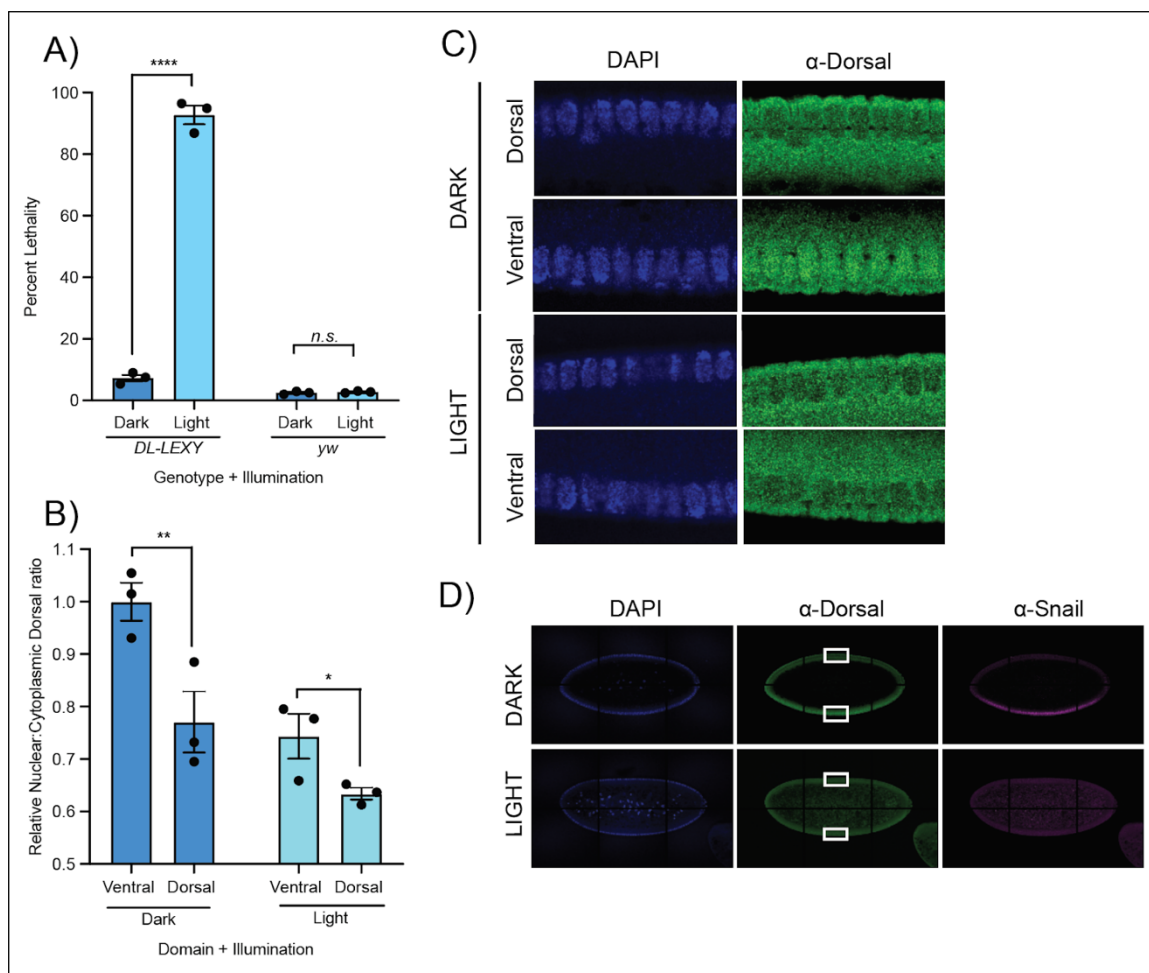


**Figure S1. DL-LEXY can be reversibly, and repeatedly, exported from the nucleus.**

(A) Quantification of hatching assay comparing dark vs light exposure for *dl-LEXY/dl-LEXY* and *yw* embryos. (mean  $\pm$  SEM, N = 3 independent experiments with n > 100 for each replicate and condition; \*\*\*\* p < 0.001 with Tukey's HSD). (B) Quantification of nuclear Dorsal levels during nc14 as demonstrated in C-C'. (mean  $\pm$  SEM, n=3; \* p < 0.05, \*\* p < 0.01 with Tukey's HSD). (C) *dl-LEXY/dl-LEXY* embryos showing nuclear Dorsal and Snail levels in dark or light exposure in both ventral and dorsal regions. (D) Whole mount embryos related to C (white boxes).

Figure S2 related to Figure 3

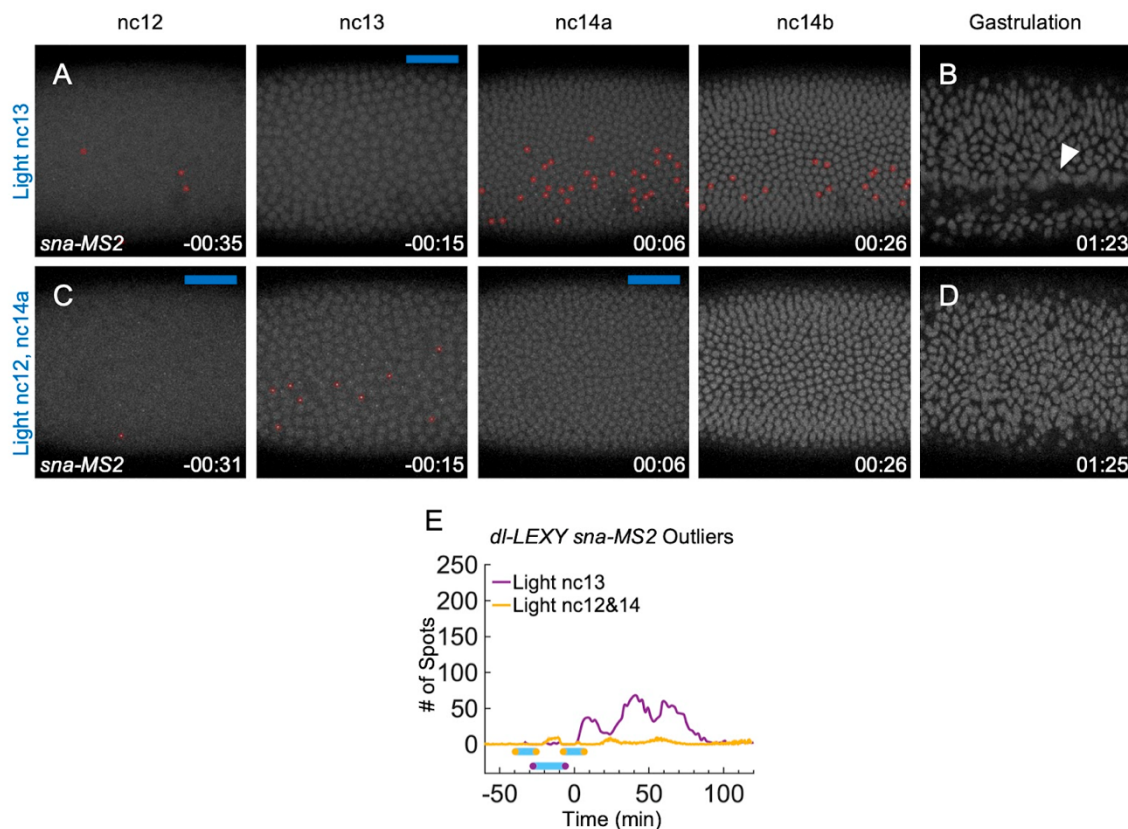


**Figure S2. A small number of embryos exhibit different phenotypes in *sna-MS2* dynamics when applying blue light at particular time windows.**

(A) *sna-MS2* in the single *dl-LEXY* embryo that exhibited recovery at nc14 when illuminated at nc13. (B) Gastrulation in the embryo from A. (C) *sna-MS2* in a representative *dl-LEXY* embryo (of three) that is unable to recover at any point when illuminated at nc12 and nc14a. (D) Lack of gastrulation in the embryo from C. (E) Quantification of *sna-MS2* in *dl-LEXY* for embryos represented by A and C that exhibited different phenotypes from Figure 3. Purple is light at nc13 (n=1/6, others shown in Figure 3L), and yellow is light at nc12 and early 14 (mean  $\pm$  SEM, n=3/8, others shown in

Figure 3L). For all images, foci are circled in red (*sna*),  $t = 0$  is set as the beginning of nc14, blue bars represent frames under blue light, white arrowheads point to mesoderm invagination, and time stamps are hours:minutes.

Figure S3 related to Figure 4

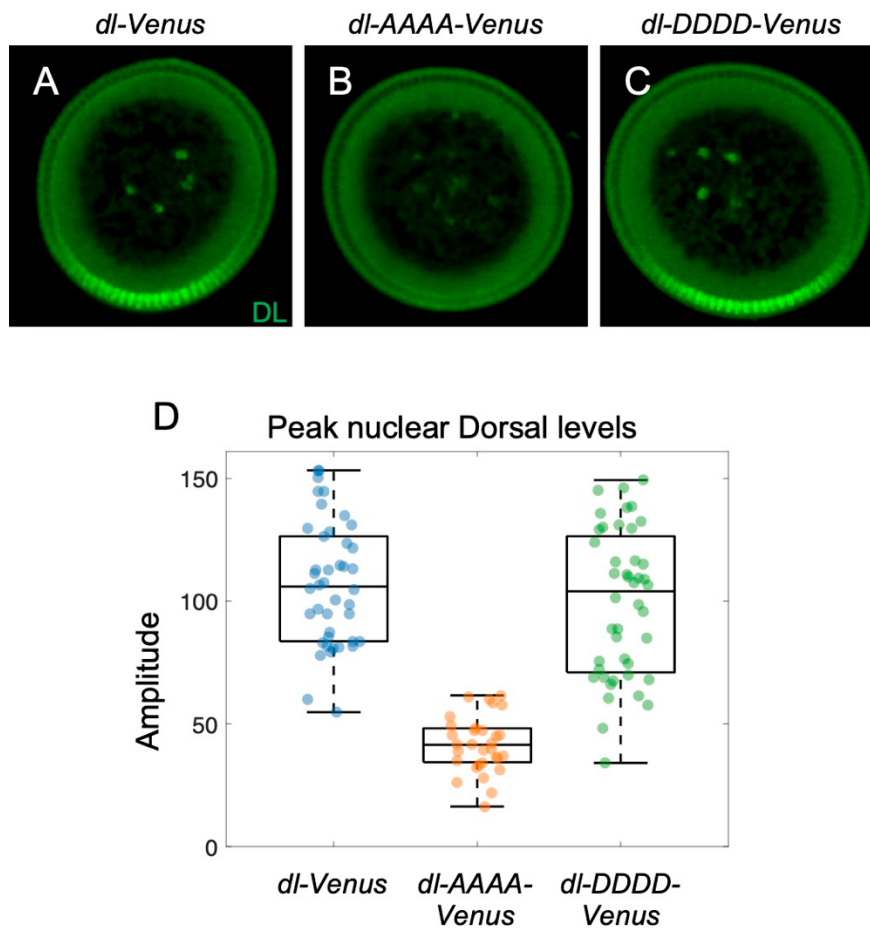


**Figure S3. Mutating serine residues to alanine in the C-terminal NES causes a reduction in peak Dorsal levels in ventral regions but does not affect overall levels.** (A-C) Antibody staining for Dorsal in a manually sectioned embryo in *dl-Venus* (A), *dl-AAAA-Venus* (B), and *dl-DDDD-Venus* (C). (D) Quantification of the peak levels of nuclear Dorsal in sectioned embryos associated with the indicated genotypes as in (A-C).